


MODELING OF THE INDUCED STRAIN ACTUATION OF SHELL STRUCTURES


by

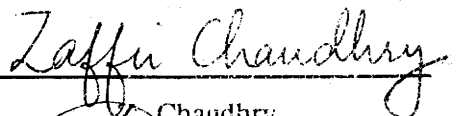
Frederic Lalande

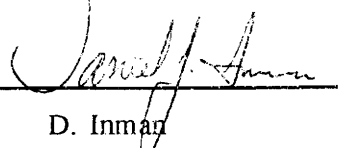
Dissertation submitted to the faculty of the
Virginia Polytechnic Institute and State University
in partial fulfillment of the requirements for the degree of
Doctor of Philosophy
in Mechanical Engineering


APPROVED:


C.A. Rogers, Chairman


O.H. Griffin


Z. Chaudhry


D. Inman


W. Saunders

April 1995
Blacksburg, VA

C.2

LD
5655
V856
1995
L358
C.2

MODELING OF THE INDUCED STRAIN ACTUATION OF SHELL STRUCTURES

by

Frederic Lalande

Committee Chairman: Dr. Craig A. Rogers

Mechanical Engineering

(ABSTRACT)

When discrete piezoelectric actuator patches bonded on structures are used for active shape, vibration, and acoustic control, the desired deformation field in the structure is obtained through the application of localized line forces and moments generated by expanding or contracting bonded piezoelectric actuators. An impedance-based model to predict the dynamic response of cylindrical shells subjected to excitation from surface-bonded induced strain actuators is presented. The essence of the impedance approach is to include the actuator/structure impedance ratio in the calculations of the actuator forces applied to the structure, which will retain the dynamic characteristics of the actuators.

The appropriate representation of the loading due to in-phase and out-of-phase actuation is discussed. Due to the curvature of the shell, the representation of the in-phase actuation with an equivalent in-plane line force applied along the edge of the actuator results in the application of erroneous rigid-body transverse force. To avoid these rigid body forces, the action of the actuator needs to be represented by an equivalent in-plane force and a transverse distributed pressure applied in the region of the actuator patch to maintain the structure self-equilibrium.

A full derivation of the impedance model is included, taking great care in the structural and actuator impedance definition. It is found that the actuator's output dynamic force in the axial and tangential direction are not equal. Various case studies of a cylindrical thin shell are performed to illustrate the capabilities of the developed impedance model. The in-phase and out-of-phase actuation authority of induced strain actuators bonded to the surface of a shell is compared. It is shown that out-of-phase actuation has better authority in

exciting the lower order bending modes, while in-phase actuation has better authority in exciting the higher order circumferential modes.

Dynamic finite element analysis has been performed using piezoelectric elements available in ANSYS 5.0. The good correlation between the finite element results and the impedance model confirms the analytical solution. Experimental data of a circular ring actuated in-phase and out-of-phase by a piezoelectric material (PZT) were also compared to the derived impedance model.

Acknowledgments

I would firstly like to acknowledge Dr. Rogers and all my committee members for their help, advice and time, with a special appreciation to Dr. Chaudhry whose door was always open for his valuable suggestions, comments and guidance.

I would also like to thank all the people at CIMSS that made my work so enjoyable, particularly, Ann Hardell, Tom Kiesling, Tony Ackerman, Jen Goodreau, and Eric Flint.

A special thank to all my friends in Blacksburg: Robert Bennett, Mike Pastor, Jim Dolan, Robert Smith, and Yannick Fierling. You all made life so enjoyable that I wish I could stay in Blacksburg forever.

I would also like to gratefully acknowledge the funding support of the Office of Naval Research, the National Science Foundation and the Air Force Office of Scientific Research.

But above all, thank you Diane.

Table of Contents

Chapter 1

Introduction	1
1.1 Motivation.....	1
1.2 Objectives.....	2
1.3 Dissertation Organization.....	3

Chapter 2

Review of the Mechanics of Induced Strain Actuation of Intelligent Structures

2.1 Introduction to Intelligent Structures	4
2.1.1 Intelligent Structures Definition.....	5
2.1.2 Intelligent Structures Components	5
2.2 Induced Strain Actuators	6
2.3 Static Models of Induced Strain Actuators Coupled with Simple Structures	7
2.3.1 Beam and Plate Analytical Models.....	8
2.3.2 Shell Structures.....	15
2.3.2.1 Layered Shells.....	15
2.3.2.2 Discrete Patch Actuation of Shells	17
2.3.3 Other Structural Applications.....	18
2.3.4 Finite Element Models.....	19
2.4 Actuator/Structure Interaction.....	21
2.4.1 Bonding Layer Effect.....	22
2.4.2 Edge Effects.....	25
2.4.3 External Loading Effects.....	28
2.5 Models Including the Dynamic Interaction of the Actuators and the Structure.....	29
2.5.1 Dynamic Modeling Approach	30
2.5.2 Impedance Modeling Approach	30
26 Summary.....	31

Chapter 3

Special Considerations for the Equivalent Loading of Induced Strain

Actuation of Shell Structures.....33

3.1 Introduction33

3.2 Model Formulation.....35

3.3 Finite Element Modeling and Verification.....40

3.4 Conclusions.....44

Chapter 4

Static Modeling of In-Phase Actuation of Actuators Bonded on Ring

Structures45

4.1 Introduction45

4.2 Shell Equivalent Loading Model.....47

4.3 Derivation of Governing Equations.....48

4.4 Derivation of the In-Phase Actuation Response Model50

4.5 Finite Element Verification.....53

4.6 Conclusions.....58

Chapter 5

Impedance Modeling of Out-of-Phase Actuation of Actuators Bonded on

Ring Structures59

5.1 Introduction59

5.2 Out-of-Phase Equivalent Loading61

5.3 Impedance Model Derivation.....63

5.3.1 System Dynamic Modeling.....63

5.3.2 Determination of the Structural Impedance.....64

5.3.2.1 Structural Impedance Based on the Raleigh-Ritz Method65

5.3.2.2 Structural Impedance Based on Modal Expansion66

5.4 Theoretical Results.....68

5.5 Finite Element Verification.....73

5.6 Conclusions.....76

Chapter 6

Impedance Modeling of In-Phase Actuation of Actuators Bonded on Ring Structures77

6.1 Introduction77

6.2 In-Phase Equivalent Loading.....78

6.3 Impedance Model Derivation.....81

6.3.1 System Dynamic Modeling.....82

6.3.2 Determination of the Structural Impedance.....84

6.4 Theoretical Results.....85

6.5 Finite Element Verification.....89

6.6 Conclusions.....92

Chapter 7

An Experimental Study of the Actuation Authority of Rings and Shells.....93

7.1 Introduction93

7.2 Impedance Models95

7.3 Comparison of In-Phase and Out-of-Phase Actuation97

7.4 Bonding of Piezoceramic Actuators on Curved Surfaces.....100

7.5 Experimental Verification.....102

7.6 Actuator Response Superposition.....105

7.7 Conclusions.....107

Chapter 8

Impedance-Based Modeling of Actuators Bonded to Shell Structures.....108

8.1 Introduction108

8.2 Impedance Model Derivation.....110

8.2.1 Determination of the Structural Impedance.....112

8.2.2 Determination of the Actuator Impedance116

8.2.3 Structural/Actuator Dynamic Interaction.....118

8.2.4 Shell Response Calculations.....119

8.3 Theoretical Results.....120

8.4 Finite Element Verification.....127

8.5 Conclusions.....131

Chapter 9

Conclusions and Recommendations.....132

9.1 Conclusions.....132

9.2 Recommendations134

Bibliography.....136

Appendix A

List of Publications150

Vita152

List of Figures

Figure 2.1	Definition of intelligent material structures	6
Figure 2.2	Effect of the thickness ratio on the three basic beam models for out-of-phase actuation.....	9
Figure 2.3	Assumed strain distribution through the thickness of the actuators and the structure for out-of-phase actuation.	10
Figure 2.4	Comparison of the effective bending moment obtained from various models.....	12
Figure 2.5	The linear shear stress variation models more accurately the effective forces near the actuator ends.....	14
Figure 2.6	Effect of the shear lag parameter on the actuator and structure strains ...	22
Figure 2.7	Effective curves illustrating the influence of the bonding layer thickness on the optimal piezoactuator thickness.	24
Figure 2.8	Reduced effective moment near the ends of the actuator when a bonding layer is considered.....	25
Figure 2.9	Reduced interfacial and peeling stresses with inactive actuator edges.....	27
Figure 3.1	Non-equilibrium of discrete tangential forces in shell structures.....	35
Figure 3.2	Thin circular cylindrical shell coordinate system.....	36
Figure 3.3	Adequate equivalent loading to maintain equilibrium.	40
Figure 3.4	Finite element models used to verify the theoretical model.....	41
Figure 3.5	Comparison of the displacements predicted by the proposed self-equilibrating equivalent forces, the plane stress finite element model and the tangential force alone (no pressure).....	42
Figure 3.6	Deformed shape of the ring using the self-equilibrium loading and the plane stress elements.....	42
Figure 3.7	Radial stress distribution through the thickness in the actuator region. ...	43
Figure 4.1	Non-equilibrium of discrete tangential forces in shell structures.....	47

Figure 4.2	Adequate equivalent loading to maintain equilibrium.	47
Figure 4.3	Adequate equivalent actuator loading on the ring.	51
Figure 4.4	Beam finite element model.	54
Figure 4.5	Match of displacements between the analytical model and the beam finite element model.	54
Figure 4.6	Deformed shape of the ring with and without self-equilibrium loading. .	55
Figure 4.7	Plane stress finite element model.	56
Figure 4.8	Match of displacements between the analytical model and the plane stress finite element model.	57
Figure 4.9	Deformed shape of the ring using the self-equilibrium loading and the plane stress elements.	57
Figure 5.1	One-dimensional ring with bonded PZT actuators actuated out-of- phase.	61
Figure 5.2	Different representations of the moment loading.	63
Figure 5.3	Structural impedance of the two impedance models. (10° patch).....	69
Figure 5.4	Only the actuator output force of the impedance model including shear stress converges to the static model at all frequencies. (10° patch).....	69
Figure 5.5	Impedance and finite element models frequency response at 30° from the actuators. (10° patch).....	71
Figure 5.6	Impedance and finite element models frequency response at 90° from the actuators. (10° patch).....	71
Figure 5.7	Frequency response at 90° from the actuators with larger actuators. (30° patch)	72
Figure 5.8	Frequency response at 90° from the actuators with larger shell radius. (10° patch)	72
Figure 5.9	Finite Element Model.	73
Figure 5.10	Impedance models and finite element displacements under dynamic loading at 5 Hz.	74
Figure 5.11	Dynamic deformed shape of the impedance models and the finite element model at 5 Hz.	74

Figure 5.12	Impedance models and finite element displacements under dynamic loading at 500 Hz.....	75
Figure 5.13	Dynamic deformed shape of the impedance models and the finite element model at 500 Hz.....	75
Figure 6.1	Equivalent loading to maintain self-equilibrium of the shell structure.	79
Figure 6.2	Different representations of the loading.....	81
Figure 6.3	One-dimensional ring with bonded pzt actuators actuated in-phase.....	82
Figure 6.4	Structural and actuator impedance.....	87
Figure 6.5	Actuator output forces based on the impedance and static models.....	87
Figure 6.6	Radial displacement frequency response at 30° from the actuator.....	88
Figure 6.7	Radial displacement frequency response at 90° from the actuator.	88
Figure 6.8	Finite element models without and with actuators.....	89
Figure 6.9	Impedance, static and finite element models radial displacement under dynamic loading at 5 Hz.....	90
Figure 6.10	Impedance, static and finite element models tangential displacement under dynamic loading at 5 Hz.....	90
Figure 6.11	Impedance and finite element models radial displacement under dynamic loading at 500 Hz.....	91
Figure 6.12	Impedance and finite element models tangential displacement under dynamic loading at 500 Hz.....	91
Figure 7.1	One-dimensional ring with bonded PZT actuators actuated in-phase or out-of-phase. The force applied by the actuators at the edge are shown.....	95
Figure 7.2	Structural impedance for in-phase and out-of-phase actuation.....	98
Figure 7.3	Authority comparison of in-phase and out-of-phase actuation for a one-dimensional ring.....	99
Figure 7.4	Authority comparison of in-phase and out-of-phase actuation for a two-dimensional shell.....	100
Figure 7.5	Methods for bonding flat actuators on curved structures.....	101

Figure 7.6	Non uniform adhesive layer to accommodate a flat PZT on a curved structure.....	101
Figure 7.7	Experimental setup used to measure the out-of-plane velocities of the structure.....	102
Figure 7.8	Experimental and impedance model ring response to out-of-phase actuation.....	103
Figure 7.9	Experimental and impedance model ring response to in-phase actuation.....	104
Figure 7.10	Experimental structural response to actuators bonded on the inside and on the outside of the ring.....	104
Figure 7.11	Finite element model using PZT elements.....	105
Figure 7.12	Structural response at 30° from the actuators bonded on the inside and on the outside of the ring, using finite element analysis.....	106
Figure 8.1	Simply supported thin shell with surface bonded actuators.....	110
Figure 8.2	Unsymmetric actuation created by electrically insulating the actuators from the structure.....	111
Figure 8.3	Transfer of the actuator's forces to the shell midplane.....	114
Figure 8.4	Dynamic interaction between the piezoelectric patch and the shell structure represented by mechanical impedance.	119
Figure 8.5	Structural admittance for in-phase actuation. Cross admittances are not equal when two dimensional admittance definition is used.	121
Figure 8.6	Structural cross admittances for in-phase actuation are equal when three dimensional admittance definition is used.....	121
Figure 8.7	Structural admittance for out-of-phase actuation. Slight difference in the cross admittances due to the transverse shear stress included in the equations.....	122
Figure 8.8	Dynamic equivalent forces produced by pure in-phase actuation on the structure are not equal in the axial and tangential directions.....	124
Figure 8.9	Dynamic equivalent moments produced by pure out-of-phase actuation on the structure are not equal in the axial and tangential directions.....	124

Figure 8.10 The comparison of the structural response between in-phase and out-of-phase actuation shows greater authority for out-of-phase actuation at ($x=0.09, \theta=90^\circ$).126

Figure 8.11 Even for thin shells, the structural response to single side actuation (inside and outside patches) is not equal at ($x=0.09, \theta=90^\circ$).126

Figure 8.12 Structural response to static in-phase actuation based on finite element analysis.....127

Figure 8.13 Structural response to static out-of-phase actuation based on finite element analysis.....128

Figure 8.14 Comparison of the displacements of the static finite element model and the impedance model at 5 Hz for out-of-phase actuation at $x=0.09$130

Figure 8.15 Comparison of the displacements of the static finite element model and the impedance model at 5 Hz for in-phase actuation at $x=0.09$130

List of Tables

Table 2.1 Comparison of the equivalent actuator force and moment of surface
bonded actuators.13

Table 5.1 Material and geometric properties of the PZT actuator and the
aluminum ring.....68

Table 6.1 Material and geometric properties of the PZT actuator and the
aluminum ring.....86

Table 7.1 Material and geometric properties of the PZT actuator and the steel
ring.....97

Table 8.1 Material and geometric properties of the PZT actuator and the aluminum
shell.....120

Nomenclature

$[A], [B], [D]$	Classical lamination theory stiffness matrices
A, B, C, D	Integration constants
C_1, C_2, C_3	Integration constants
C_θ	$\cos n\theta_1 - \cos n\theta_2$
C_x	$\cos \alpha x_1 - \cos \alpha x_2$
d_{32}	Piezoelectric constant
D	Bending stiffness
E	Applied electrical field on actuator
E_L	External loading potential energy
F_n, F_k	Forcing function
F_θ	Tangential actuator force
F_x	Axial actuator force
$H(\cdot, \cdot)$	Heaviside function
H	One dimensional admittance
H_{xx}	Axial direct admittance
$H_{\theta\theta}$	Tangential direct admittance
$H_{x\theta}, H_{\theta x}$	Cross admittance
i	Imaginary number
k	Wave number
K	Extensional stiffness
l_a	Length of the actuator in the axial direction
$L_i(u^o, v^o, w^o)$	Love operators
m_x	Actuator induced tangential moment
m_θ	Actuator induced axial moment
m_x^*	Actuator external equivalent tangential moment
m_θ^*	Actuator external equivalent axial moment
M	Bending forces vector in CLT
M_Λ	Equivalent induced strain bending forces vector in CLT
M_θ	Tangential moment magnitude
M_x	Axial moment magnitude
M_{xx}	Bending moment in x direction

$M_{\theta\theta}$	Bending moment in q direction
$M_{x\theta}$	Bending twisting moment
n_x	Discrete actuator induced tangential force
n_θ	Discrete actuator induced axial force
n_x^*	Actuator external equivalent tangential force
n_θ^*	Actuator external equivalent axial force
N	Membrane forces vector in CLT
N_{mnp}	See equation (8.13)
N_A	Equivalent induced strain membrane forces vector in CLT
N_θ	Tangential force magnitude
N_x	Axial force magnitude
N_{xx}	Membrane force in x direction
$N_{\theta\theta}$	Membrane force in q direction
$N_{x\theta}$	Membrane shearing force
p_n, p_k	Modal participation factor
p_r	Equivalent transverse pressure
p_r^*	Actuator equivalent external transverse pressure
q	Loading term
$Q_{\theta r}$	Transverse shear force resultant
$[\bar{Q}]$	Stiffness matrix
R	Radius
R_a	Length of the actuator in the tangential direction
S_θ	$\sin n\theta_1 - \sin n\theta_2$
t	Thickness
T	Thickness ratio
u	Axial displacement
v	Tangential displacement
V	Applied voltage on actuator
V_n	Rayleigh-Ritz tangential displacement coefficient
w	Radial displacement
W_n	Rayleigh-Ritz radial displacement coefficient
x	Axial coordinate
x_1, x_2	Axial coordinates of the actuator
Y	Young's modulus

z	Radial coordinate
Z	One dimensional impedance
Z_{xx}	Axial direct impedance
$Z_{\theta\theta}$	Tangential direct impedance
$Z_{x\theta}, Z_{\theta x}$	Cross impedance
α	$\frac{m\pi}{l}$
β	Rotational displacement
χ_{in}	See equation (8.19a)
χ_{out}	See equation (8.19b)
$\delta(\cdot, \cdot)$	Dirac function
δK	Variational kinetic energy
$\delta(U-E_b-E_L)$	Total variational potential energy
ε_x	Axial extensional strain
ε_θ	Tangential extensional strain
$\gamma_{x\theta}$	Shearing strain
κ_x	Axial bending strain
κ_θ	Tangential bending strain
$\kappa_{x\theta}$	Twisting strain
Λ	Free induced strain
ν	Poisson's ratio
ϑ	See equation (8.16a)
θ	Tangential coordinate
θ_p	Actuator half size in tangential direction
θ_1, θ_2	Tangential coordinates of the actuator
ρ	Density
ξ^i	In-phase weighting factor
ξ^o	Out-of-phase weighting factor
ω	Angular velocity
$\omega_n, \omega_{mnp}, \omega_k$	Structural natural frequencies
ψ	$\frac{Y_s t_s}{Y_a t_a}$

Superscripts

\cdot	Velocity
$\ddot{}$	Acceleration
$'$	First derivative
E	Zero electrical field
o	Neutral axis coordinate

Subscripts

a	Actuator
s	Structure

Chapter 1

Introduction

1.1 Motivation

In any mechanical system with moving parts, special attention must be given to reduce vibrations and accompanying noise. If the system cannot be balanced or is subjected to random vibrations, passive or active control of the structure can be considered to reduce vibrations. One way to perform active control is to use shaker type actuators, but this involves many moving parts external to the base structure. Induced strain actuators, like piezoelectric materials and shape memory alloys, can also be used in vibration and acoustic control. What distinguishes induced strain actuators from conventional hydraulic and electrical actuators, and makes them especially attractive for smart structures, is their ability to change their dimensions and properties without utilizing any moving parts. The absence of mechanical parts allows the induced strain actuators to be easily integrated (either through embedding or through surface-bonding) into the base structure. When integrated, the induced strain actuators apply localized strains and directly influence the extensional and bending responses of the structural elements. Efficient structural control can then be obtained by applying forces directly on the structure at critical locations, which will eliminate the undesirable dynamic effects due to changes in the apparent structural impedance. Also, the integration within the structure ensures an overall force equilibrium between the forcing actuator and the deforming structure, thus precluding any rigid body forces and torques.

Since this concept for vibration and acoustic control was introduced, numerous efforts have been made to analytically model the induced strain actuation of structures to further understand the mechanisms involved in the strain and stress transfer between the actuators and the structure. In the earlier analytical models, the actuator was subjected to a constant voltage and the actuator output force is computed from static considerations (i.e. local actuator/structural geometric and material properties), which resulted in frequency independent equivalent actuator forces and moments. For dynamic analysis of intelligent structures, the statically determined actuator forces and moments were simply assumed to

be constant over the whole frequency range of interest and were then introduced in the equations of motion. This static-based approach to dynamic analysis of intelligent structures shows important shortcomings in the accuracy of the calculated dynamic structural response because it neglects all the dynamic interactions between the actuators and the structures. In vibration control, the dynamic issues are present and should be considered in the modeling. Furthermore, these models did not take account of the different stiffnesses of the structure in different directions, which will mistakenly result in equal actuator output forces in both directions.

In shell structures, the in-plane and out-of-plane displacements are coupled and the equations of motion can not be solved independently. Models have been developed based on layered shell theory, i.e., the analytical model assumes that the induced strain actuator material comprises a total, distinct layer of the shell. However, layered actuators are only of theoretical interest, since typical piezoceramic actuators can not be implemented on curved surfaces due to their brittle properties. Discrete actuator patches bonded on thin shell structures can be implemented in practical applications but only few models adapted from plate theory were proposed. At first sight, this adaptation seems perfectly reasonable because the shell is thin. However, even for thin shells, the displacement coupling is important enough to introduce important errors when such plate adaptations to shells are made.

Impedance models based on the dynamic properties of the actuators and the structure have also been proposed. The essence of the impedance approach is to include the actuator/structure impedance ratio in the calculations of the actuator forces applied to the structure, which will retain the dynamic characteristics of the actuators. Thus far, work has been done on beams and plates. Impedance models were also derived for shells, but lack in accuracy and only applied to out-of-phase actuation.

1.2 Objectives

In this dissertation, the principal objective is to develop an accurate model for shell structures excited harmonically with induced strain actuator surface bonded patches. The impedance modeling approach, which is an effective method in modeling the dynamic interaction between the induced strain actuators and the structure, will be used. The impedance model will strengthen all the weaknesses of the previous analytical models; such

as actuator forces' independence to frequency, actuator forces' equality in the axial and tangential directions, model based on plate equations neglecting curvature effects, and omission of the actuator/structure dynamic interaction. The derived model is to be comprehensive, being developed for two dimensional cylindrical shells excited in-phase, out-of-phase, or unsymmetrically. Case studies of rings and shells are to be compared to dynamic finite element analysis and experimental data.

1.3 Dissertation Organization

This dissertation is a collection of papers presented at various conferences focusing on intelligent material systems and structures. Because of this organization, the reader might find some repetition in each chapter, but each chapter has the advantage of being independent. A detailed list of the paper references can be found in Appendix A.

The dissertation begins with a literature review on the mechanics of induced strain actuation of intelligent structures. The review will concentrate on the static and dynamic analytical modeling of beams, plates, and shells, on the finite element modeling, and on the actuator/structure interaction. To help the reader locate the present work in the literature, all chapters of the dissertation are included in the review.

Preliminary work to understand the difficulties created by the in-plane/out-of-plane coupling proper to curved structures is presented in Chapter 3. The special considerations needed for the in-phase actuation of shells are discussed. Based on these considerations, a closed form model for a ring statically actuated in-phase is presented in Chapter 4. The core of the dissertation comes with the impedance modeling presented in Chapters 5, 6, and 8. The model derivation of a one dimensional circular ring harmonically actuated out-of-phase and in-phase are presented in Chapters 5 and 6, respectively. An extended model for two dimensional circular shells harmonically actuated in-phase, out-of-phase, or unsymmetrically is presented in Chapter 8. All the derived models are compared with finite element analysis throughout the dissertation, along with an experimental verification presented in Chapter 7. Finally, in the final chapter, conclusions and recommendations for continuing research are presented.

Chapter 2

Review of the Mechanics of Induced Strain Actuation of Intelligent Structures

Abstract

For more than ten years, intelligent systems and structures have created great interest in the research community, both in the academia and in the industry, because of their enormous possibilities in vibration and acoustic control, shape control, and health monitoring. Intelligent structures consist of a full integration of its sensing, processing and actuation capabilities within the base structure. This review will focus on the actuation part of intelligent systems, particularly on the mechanics of induced strain actuators. Analytical models for beams, plates, and shells are first presented. Two types of models are considered: *static*; the action of the actuators is based on the static response of the intelligent structures, and *dynamic*; the full dynamic interaction between the induced strain actuators and the structure is considered. A discussion on the finite element modeling of intelligent structures is then presented. Finally, the actuator/structure interaction is discussed, concentrating on the bonding layer effects, the actuator edge effects, and the external loading effects.

2.1 Introduction to Intelligent Structures

In the design of space, aeronautic, and automotive structures, new technologies are needed to create high performance structures that are light, energy efficient, and autonomous. One of these new technologies is intelligent material systems and structures. Many names have been given to intelligent material systems and structures: smart, sense-able, multi-functional, and adaptive. The concept of intelligent materials is fairly new, only appearing in the eighties. Nevertheless, tremendous research efforts have been done in this new engineering discipline because many believe that it will bring the current state of technology to a higher level. The birth of intelligent materials systems and structures was made possible by three great technological advancements made since the 1960's. The three technologies'

combination that lead to the development of intelligent structures are: (i) laminated materials which allow the incorporation of active elements, (ii) usage of off-block diagonal terms in the material constitutive equations which allows the coupling of the mechanical, electromagnetic, thermal, and physical properties, and (iii) development of the microelectronics, bus architectures, switching circuitry, and fiber optics which allows the necessary processing, control, and artificial intelligence (Crawley, 1993). With the extended research done on intelligent material systems and structures during the last decade, a review of the current literature would give some perspective on what has been done thus far, and which path future research should take.

In this chapter, a review of the mechanics of induced strain actuation of intelligent structures is presented. But first, a brief introduction to intelligent structures will show the great possibilities of this new idea, followed by a comparison of various induced strain materials. The heart of the chapter will come when numerous static structural response models of induced strain actuation are reviewed. Then, a closer look at the structural/actuator interaction is made to verify the validity of the popular perfect bonding assumption and its consequences. The chapter concludes with the review of dynamic models which have the advantage of including the dynamic interaction between the structure and the actuators.

2.1.1 Intelligent Structures Definition

Various definitions have been given to intelligent structures, and no consensus has been reached thus far. Some authors argue that the intelligent structures' definition should be based on biological analogy (Davidson, 1990; Rogers, 1992), while others have more technical definitions. The five-step technical definition presented by Wada, Fanson and Crawley (1990) is presented in Figure 2.1. Although the different views are somewhat different, they all reduce to the same idea: intelligent systems and structures are highly integrated structures capable of adapting themselves to their environment.

2.1.2 Intelligent Structures Components

With the intelligent material systems and structures definition established, a short discussion of their three principal components (actuators, sensors, and electronic controls) will now be presented. Based on the biological definition of intelligent structures, the actuators can be seen as the artificial muscle, the sensors as the artificial nerves, and the electronic

controls as the brain. More extended discussions of the intelligent structure components can be found in other references (Crawley 1993).

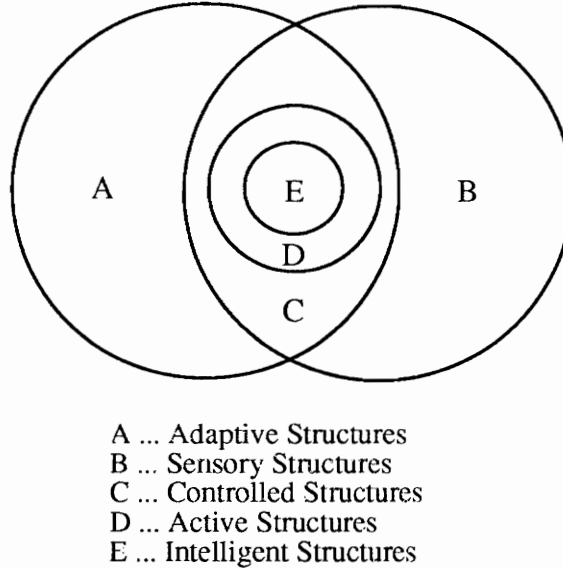


Figure 2.1 Definition of intelligent structures. (Wada et al., 1990)

2.2 Induced Strain Actuators

Actuator systems can be divided into two broad categories. In the first category, the actuators are applied to the surface or are embedded within the structure itself. In the second category are actuators used in truss-like structures where they replace some of the truss elements of the structure (Wada, Fanson and Crawley, 1990). The actuators in the first category are almost invariably induced strain actuators such as piezoelectric actuators, whereas in the second category the active truss members can be conventional displacement actuators (screwjacks), where the length of the member is controlled, or force actuators (voice coil), where the load in the member is controlled. This second category of actuators is widely used in active trusses. Deployable space structures will make use of such active trusses not only for deployment, but also for making fine resolution adjustments of the structural surfaces (Natori et al., 1988).

Induced strain actuators develop strains, through a change in their physical properties, in response to an external non-mechanical stimulus such as electric fields, temperature gradient or magnetic fields. These developed strains, capable of controlling

material/structural geometrical configurations, mechanical properties, and internal stress-strain characteristics, can be used to apply controlled forces to the structure. The most commonly used induced strain actuators in the first category, which includes shape memory alloys, electrorheological fluids, piezoelectrics, electrostrictors, and magnetostrictors.

2.3 Static Models of Induced Strain Actuators Coupled with Intelligent Structures

The interaction between induced strain actuators and intelligent structures has been modeled a number of times thus far, and a review of the most common models will now be presented. When integrated into a structure (either through embedding or surface-bonding), induced strain actuators apply localized strains that directly influence the extensional and bending responses of the structure. It has been demonstrated that induced strain actuators generate a set of forces concentrated close to the edges of the actuator and their action can be represented by line forces or moments applied along the periphery of the actuator (Liang and Rogers, 1989). The induced strain actuators are often used in pairs, bonded on opposite sides of the structure. By controlling the voltage applied on each actuator it is possible to drive the actuators in-phase (both actuators expanding or contracting together), which creates an extensional deformation of the middle surface or out-of-phase (one actuator expands while the other contracts), which creates bending deformation of the middle surface. Between these two extreme cases, unequal voltage application will create a combination of extension and bending. An actuator bonded only on one side of the structure is the most common case of unsymmetric actuation. The general objective in the modeling of induced strain actuators is to establish an equation that will convert the primary variable (electrical voltage applied to the actuator) to an equivalent loading that can be applied to the structure to represent accurately the action of the induced strain actuator.

In this section theoretical models in which the actuator output force is obtained from static considerations (i.e., local actuator/structural geometric and material properties) are presented. If vibrational control or dynamic analysis is desired, the static fixed amplitude actuator forces are simply applied over the whole frequency range of interest. For models including dynamic interaction between the actuator and the structure, the reader is referred to section 2.5. Also, only models assuming perfect bonding between the actuator and the

structure and no external loading will be discussed for the moment. Various models relaxing these restrictions will be presented in section 2.4.

2.3.1 Beam and Plate Analytical Models

Analytical models involving flat structures, i.e., one-dimensional beams and two-dimensional plates, will be the first type of intelligent structure presented. The models have been derived based on theory of elasticity, Bernoulli-Euler beam theory, or classical plate theory. The analytical models that have been derived thus far can be separated into three different groups. The first group contains the earlier models developed for beam structures and is often referred as the pin-force models. In the pin-force models, the actuators and the structure are considered to be separate elastic bodies and forces are transferred from the actuators to the structure by “pins” at the edges of the actuators. The first pin-force model was developed for a cantilever beam with a layer of PVDF bonded on one side only (Bailey and Hubbard, 1985). The modeling was based on a force equilibrium between the actuator and the beam, and a constant actuator force output proportional to the applied voltage was obtained. Another early model for out-of-phase actuation was developed by Fanson and Caughey (1987). In this case, the equivalent moment loading on the structure was simply given by the free induced strain multiplied by the extensional stiffness of the actuator: $M = (t_a + t_s)E_a t_a \Lambda$. This equation assumes a free expansion of the actuator, even though the structure to which it is bonded will not allow such free expansion.

A more extensive model was then proposed by Crawley and de Luis (1987) to model in-phase and out-of-phase actuation of beam structures. This model allows discrete patches of induced strain actuator to be bonded or embedded within the structure, with considerations for the bonding layer and preexisting strains in the structure (see section 2.4). When the actuators are surface bonded, the strain distribution in the structure (Fig 2.3a) is assumed to be uniform in the actuator and vary linearly across the structure, with a strain compatibility at the interface. The equivalent actuator force and moment to be applied to the structure are presented in Table 2.1. With the assumed strain distribution, the pin-force model will accurately predict the in-phase deformation of the beam but will incorrectly predict the out-of-phase deformation of the beam for relatively thick actuators. This can be attributed to the assumed uniform strain distribution in the actuators, which allow the actuators to bend. Additionally, the actuator flexural stiffness is not included in the modeling as it should be (Chaudhry and Rogers, 1994). For the embedded actuator case, the strain distribution is

assumed to vary linearly across the actuators and the structure, to satisfy strain compatibility between the structural layers and the actuator layers (Fig. 2.3b). The difficulties experienced in out-of-phase actuation of surface bonded actuators modeling will therefore not occur.

A generalization of the pin-force model to two-dimensional plates has been done by Hagood et al. (1989). Using the same strain distribution in the actuator (Fig. 2.3a), similar equivalent force and moment are found (only different in the $(1-\nu)$ term). The forces and moments in the x and y directions are equal in magnitude, and no twisting moment will be present in isotropic plates.

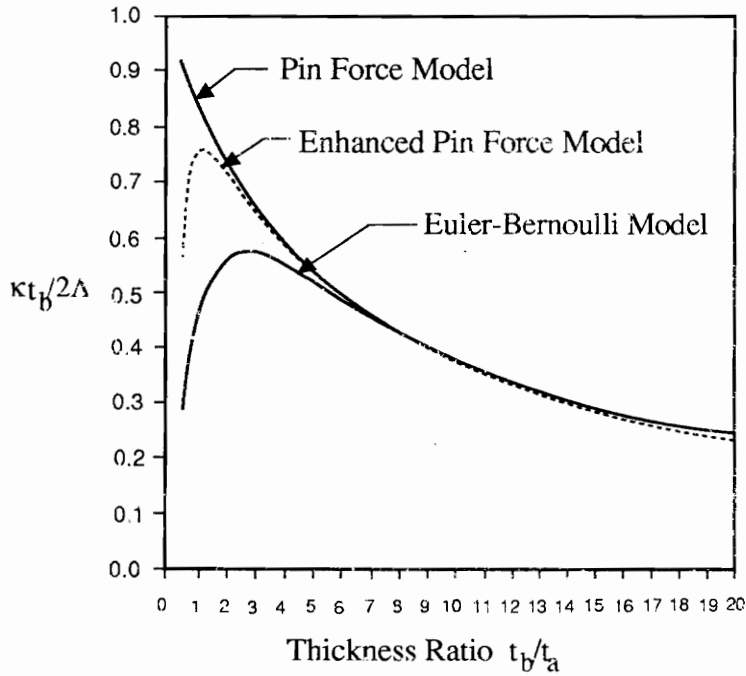


Figure 2.2 Effect of the thickness ratio on the three basic beam models for out-of-phase actuation. (Chaudhry and Rogers, 1994)

Modifications have been made to the pin-force model to enhance its ability to accurately describe the structural response (Chaudhry and Rogers, 1994). In this “enhanced pin-force model,” the actuators and the structure are still treated as separate entities, but the actuator flexural stiffness is included in the structural moment-curvature equations. In this new model, the structural surface strains will not approach the actuation strains for relatively thick actuators (see Fig. 2.2) and will not predict the structural response as accurately as the Bernoulli-Euler model that will be discussed next.

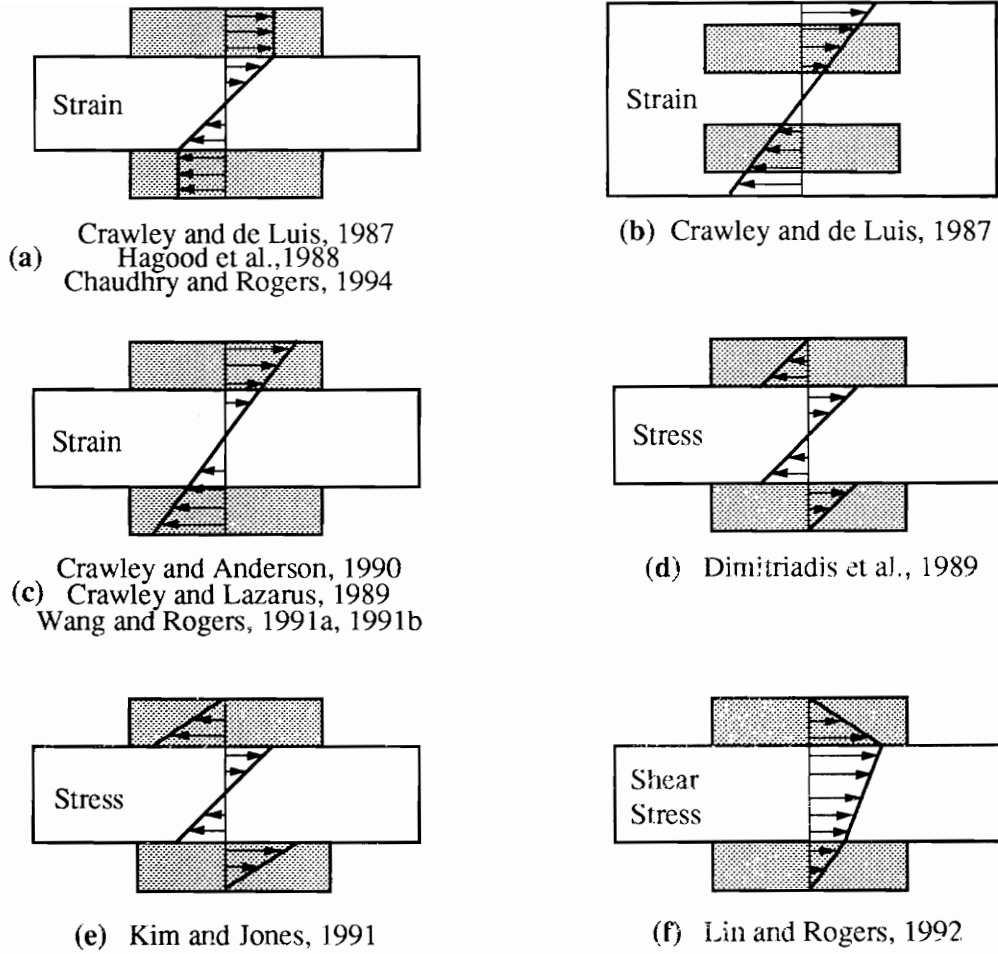


Figure 2.3 Assumed strain distribution through the thickness of the actuators and the structure for out-of-phase actuation.

The second group of static analytical models will now be presented. In this group, the modeling is based on a more accurate assumed strain distribution through the thickness of the structure and the actuators. All models assume a linear strain distribution through the thickness of the structure and the actuators (Fig 2.3c). The first model using this improved strain distribution was presented by Crawley and Anderson (1990) for the actuation of beams. This model was developed for embedded and surface bonded actuators and is often called the “Bernoulli-Euler” or “consistent strain” model. For out-of-phase actuation, the curvature strain is directly dependent on the structure/actuator thickness ratio due to the inclusion of the actuator bending stiffness. When compared to a finite element analysis, the Bernoulli-Euler model was found to give a more accurate prediction of the structural response. For in-phase actuation, there is no difference between the pin-force and the Bernoulli-Euler models since

the assumed strain distribution are the same in both cases. For embedded actuators, the strain relation for out-of-phase actuation is different from the one obtained by Crawley and de Luis (1987) even though the assumed strain distributions are the same. The difference can be attributed to the simplification made by Crawley and de Luis (1987) which included the actuator and beam stiffnesses at the actuator location.

A consistent plate model was developed by Crawley and Lazarus (1989). This model is a simple extension from the one-dimensional beam model to a two-dimensional plate model. This closed form model is once again applied to plates with free boundary conditions and no external loading. For more complicated boundary conditions and geometry with external loading, an approximate solution based on the Ritz formulation was proposed.

A model assuming a linear stress variation through the thickness of the actuators and the structure was developed by Dimitriadis et al. (1991). In this spherical pure bending model, the equivalent moment to out-of-phase actuation is based on the moment equilibrium about the neutral axis. However, it should be pointed out that the stress slopes across the structure and the actuators were assumed to be uniform through the thickness in this modeling effort (Fig. 2.3d). Since the elastic properties of the actuators and the structure are usually different, the stress slopes should be different in each layer, given a linear strain variation through the thickness.

Kim and Jones (1991a) modified the Dimitriadis et al. (1991) model to take account of the different elastic properties in the actuators and the structure, which will have the effect of varying the stress slopes through the thickness (see Fig. 2.3e). This analytical model including a bonding layer is developed based on the shear lag theory, but first, a reduced model assuming perfect bonding will be discussed. The reader is referred to section 2.4.1 for more details on the bonding layer effect. It can be seen from Table 2.1 that the equivalent moment is the same as the one obtained from the consistent plate theory (Crawley and Lazarus, 1989). Shown in Fig. 2.4 is a comparison of the equivalent moment based on the pin-force, the consistent plate, and the Dimitriadis et al. (1991) models. Based on the finite element analysis that was performed by various authors (Chaudhry and Rogers, 1994; Crawley and Anderson, 1990), the consistent plate model or the Kim and Jones (1991a) model gives the most accurate results. The same authors also demonstrated that the effective moment will be nearly identical whether static analysis or Love's equation of motion are used for actuators bonded on composite structures (Kim and Jones, 1991b). The non-linear

theory of composite beams was also used to model the actuators action on the structure (Kim and Jones, 1991c).

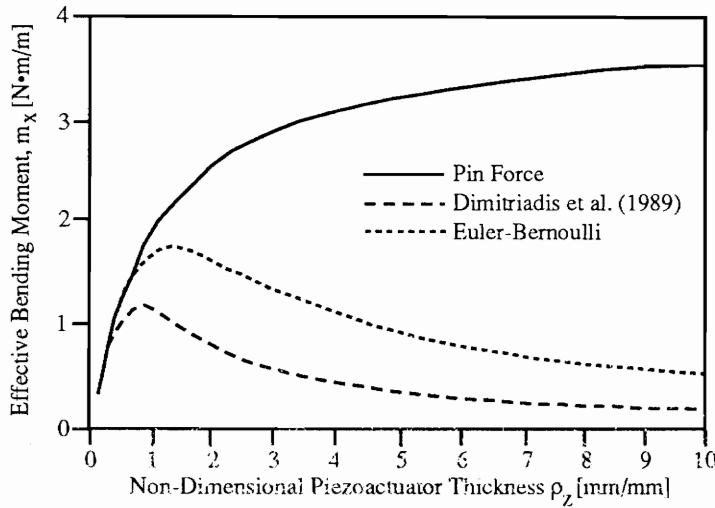


Figure 2.4 Comparison of the effective bending moment obtained from various models. (Kim and Jones, 1991a)

Using the same stress distribution through the thickness as Kim and Jones (1991a), Masters and Jones (1993) derived an analytical model for actuators embedded within the structure. An equation for the equivalent moment directly dependent on the actuator thickness and location was derived. This equation can be reduce to the Kim and Jones (1991a) model if the actuators are surface bonded.

Various optimization studies of the actuator thickness, stiffness, and location were performed. It was shown that the optimal actuator thickness is primarily dependent on the actuator and structural elastic properties. If the Young's modulus of the actuator was 3-5 times less than the Young's modulus of the structure, surface bonded actuators were shown to be the most efficient. However, if the Young's modulus of the actuator is increased, the actuator location is within the structure. (Masters and Jones, 1993). For given actuator properties, the influence of the location of the actuator in the laminate was also considered (Masters and Jones, 1991). It was shown that for thin structures, the optimal location is on the surface, while for thick structures it is within the composite.

A conservation of strain energy model was developed by equating the applied moment on the cross section of the edges of actuators to determine the induced linear strain distribution and the equivalent axial force and bending moment induced by the actuators

Table 2.1 Comparison of the equivalent actuator force and moment of surface bonded actuators.

Analytical Model	Equivalent Force	Equivalent Moment
Beams		
Crawley and de Luis (1987)	$2 \frac{E_s t_s}{2 + \psi} \Lambda$	$\frac{E_s t_s^2}{6 + \psi} \Lambda$
Chaudhry and Rogers (1994)	$2 \frac{E_s t_s}{2 + \psi} \Lambda$	$\frac{E_s t_s^2}{6 + \psi + \frac{2}{T^2}} \Lambda$
Crawley and Anderson (1990)	$2 \frac{E_s t_s}{2 + \psi} \Lambda$	$\frac{E_s t_s^2 \left(1 + \frac{1}{T}\right)}{6 + \psi + \frac{12}{T} + \frac{8}{T^2}} \Lambda$
Wang and Rogers (1991a)	$2 \frac{E_s t_s}{6 + \psi} \Lambda$	$(t_a + t_s) \frac{E_s t_s}{6 + \psi} \Lambda$
Plates		
Hagood et al. (1989)	$\frac{E_s t_s}{1 - \nu} \frac{2}{2 + \psi} \Lambda$	$\frac{E_s t_s^2}{1 - \nu} \frac{\Lambda}{6 + \psi}$
Crawley and Lazarus (1989)	$\frac{E_s t_s}{1 - \nu} \frac{2}{2 + \psi} \Lambda$	$\frac{E_s t_s^2 \Lambda}{1 - \nu} \frac{1 + \frac{1}{T}}{6 + \psi + \frac{12}{T} + \frac{8}{T^2}}$
Dimitriadis et al. (1991)	N/A	$\frac{E_s t_s^2 \Lambda}{(1 - \nu)} \frac{\left(1 + \frac{1}{T}\right)}{6 \left(1 + \frac{1}{T}\right) + \psi \left(1 + \frac{8}{T^3} + \frac{6}{T^2}\right)}$
Kim and Jones (1991)	N/A	$\frac{E_s t_s^2 \Lambda}{1 - \nu} \frac{1 + \frac{1}{T}}{6 + \psi + \frac{12}{T} + \frac{8}{T^2}}$
Wang and Rogers (1991a)	$2 \frac{E_s t_s}{(1 - \nu)(6 + \psi)} \Lambda$	$\frac{E_s t_s^2 \left(1 + \frac{1}{T}\right)}{(1 - \nu)(6 + \psi)} \Lambda$
Wang and Rogers (1991b)	$2 \frac{E_a t_a}{1 - \nu} \Lambda$	$\frac{E_a t_a^2}{1 - \nu} (1 + T) \Lambda$
Lin and Rogers (1992)	$\frac{\psi E_a^2 t_a^2 h \Lambda}{K_1} \left(K_{10} + K_{11} \frac{\cosh \eta_1 x}{\cosh \eta_1 l} \right)$	$\frac{\psi E_a^2 t_a^2 h \Lambda}{6 K_0} \left(K_8 + K_9 \frac{\cosh \eta_2 x}{\cosh \eta_2 l} \right)$

where $T = \frac{t_s}{t_a}$, $\psi = \frac{E_s t_s}{E_a t_a}$

(Wang and Rogers, 1991a). Like the pin-force model, the strain energy model overestimates the structural response for low thickness ratios.

The classical laminate plate theory was used to model the action of discrete induced strain actuator patches (Wang and Rogers, 1991b). Their work provided a theoretical basis for general application of induced strain actuators, but the equivalent force and moment were based on the free expansion of the actuators. The theoretical results have indicated that this approach is most accurate for high actuator thickness to plate thickness ratios and overestimates the force and moment induced by actuators for thin laminates. Lee (1990) also applied the classical laminate plate theory to the design of piezoelectric laminate for bending and torsional modal control.

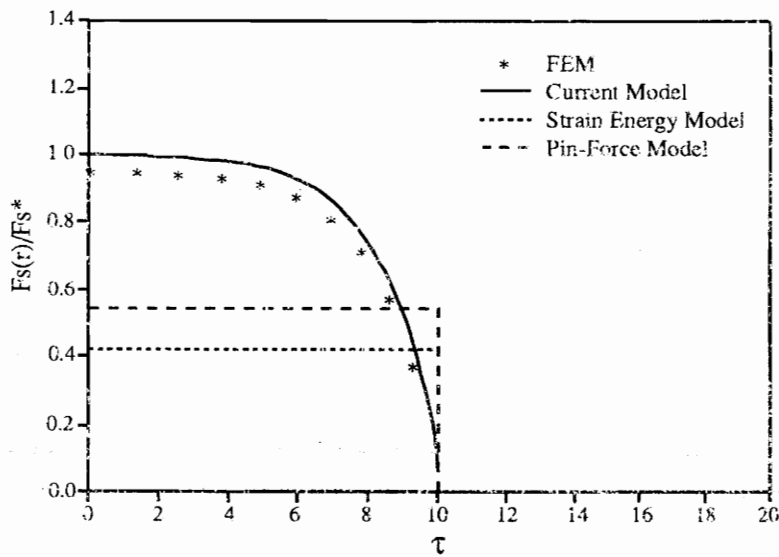


Figure 2.5 The linear shear stress variation models more accurately the effective forces near the actuator ends. (Lin and Rogers, 1992b)

The last model group contains more accurate and relatively complex analysis that accounts for transverse shear effects that were neglected in all the previous models. Among them is the nonlinear model proposed by Pai et al. (1992a, 1992b) in which piezoelectric plate response to large rotations and small strains was investigated. Another nonlinear analytical model for distributed control of beam structures was derived by Zhuang and Baras (1992) using the Timoshenko beam theory which includes the shear effect and rotational inertia. Also, a linear shear stress variation model based on an approximate through-the-thickness linear shear stress field was proposed by Lin and Rogers (1992). The advantage of

this model is that it captures the physics of induced stress field in a closed form solution. Indeed, the actuator impetus exerted internally in integrated actuator/structure system will be different from the response obtained from an externally applied equivalent loading. Furthermore, the structural response cannot be described properly based on a conventional theory of structural mechanics. Based on this more accurate formulation, the variation of the equivalent force and moment along the axial direction can be described more accurately (Fig. 2.5). This modeling effort has the advantage of eliminating the discontinuity at the actuator boundary, as opposed to the pin-force and consistent models which predict a constant force and moment over the entire length of the actuator.

2.3.2 Shell Structures

The coupling between the in-plane and the out-of-plane displacements found in curved structures needs to be considered in the study of structural response to induced strain actuation. This coupling adds complexity to the governing equations, which can no longer be solved independently. For such structures with curvatures such as rings and shells, analytical models based on layered shell theory, plate theory, and shell governing equations have been proposed.

2.3.2.1 Layered Shells

Layered shell models in which a distributed induced strain actuator comprises a total and distinct layer will now be presented. The implementation of the actuator layers is only possible for polymer piezoelectric material, which has very limited actuation capabilities. Induced strain actuator patches bonded on the surface of the shell or embedded within the shell will only be discussed in the "Discrete Patch Actuation Of Shells" section 2.3.2.2. Extensive work on layered shells has been done at the University of Kentucky by Tzou and co-workers. An analytical model for multi-layered thin shells with distributed piezoelectric actuators was proposed by Tzou and Gadre (1989). In this work, the theoretical development is based on Love's thin shell theory in which the transverse shear deformations and rotary inertias are neglected, and the governing equations are based on Hamilton's principle. The action of the piezoelectric actuators is included in the governing equations through the resultant forces and moments, which are based on the summation of the original strains and the actuator induced strains. The vibration control of layered thin shells has been proved to be possible and efficient. In Tzou and Tseng (1990), the model was extended to include the

coupling between sensor and actuator layers. The sensor voltage from the direct piezoelectric effect of the shell was derived using Maxwell's theory and induced strain equivalent loading was proposed for open-loop control and for closed-loop feedback control. Experimental work was done on a beam to verify the theoretical model simplified to beams (Tzou and Zhong, 1991). An analytical model for thick composite piezoelectric shells was proposed by Tzou and Bao (1993). In thick shells some assumptions made in the derivation of the thin shell models can no longer be made, such as the transverse deformations and rotary inertias that must now be included. Based on a triclinic anisotropic piezoelectric material, the electromechanical equations for thick shells were derived. To include geometrical nonlinearities due to large deformations, a piezothermoelastic nonlinear model was derived (Tzou et al., 1994). The von Karman assumptions which neglect the nonlinear effects due to large in-plane deflections and keep the nonlinear effects of transverse deflections were used in model derivation. The transverse shear deformations and rotary inertias are again neglected in this model. It is found that the transverse equilibrium equation is greatly influenced by the nonlinear terms. Finally, to increase the control of the actuators on the structure, a segmentation of the distributed active layer was proposed (Tzou and Fu, 1994a, 1994b).

A model based on the general thin laminate shell theory was proposed by Jia and Rogers (1990). The shell governing equations were derived in a similar fashion as in Tzou and Gadre (1989), but the transverse distance is not neglected compared to the radii of the shell, i.e., $1 + z/R \neq 1$. The derived forcing terms are functions of the actuation forces and moments, which are directly dependent on the applied voltage.

An axisymmetric composite cylinder with surface bonded or embedded PVDF induced strain actuator layer was studied by Mitchell and Reddy (1993). The analytical model is based on the Navier equations of elasticity for axisymmetric geometries and requires only the governing equations and constitutive model to be linear. No assumptions are made concerning the stresses and strains, but the shearing stresses and strains $\epsilon_{r\theta} = \epsilon_{z\theta} = \sigma_{r\theta} = \sigma_{z\theta}$ are zero due to the axisymmetry of the specially orthotropic cylinder considered. An elasticity solution of an axisymmetric composite cylinder statically loaded with embedded piezoelectric laminae was also derived (Mitchell, 1992).

A theoretical model based on Reissner's shell theory which does not neglect the transverse shear deformation and rotatory inertia was proposed by Larson and Vinson

(1993a). The shell governing equations were developed using Hamilton's principle and considered shell anisotropy. The derived model was shown to be identical to the classical shell theory model if the transverse shear deformation is neglected. This theoretical model has been applied to curved beams and rings (Larson and Vinson, 1993b).

2.3.2.2 Discrete Patch Actuation of Shells

The first category of analytical shell models for discrete induced strain actuator patches is based on a direct adaptation of the plate theory. The equivalent actuator force and/or moment obtained from plate models are directly applied to the shell governing equations, with no considerations of the shell curvatures. In Sonti and Jones (1991), work on active vibration control of thin shells was done and an important assumption was made: small piezoelectric actuators. This assumption allows one to neglect the added mass and stiffness of the actuators and, most importantly, to neglect the coupling between the in-plane and out-of-plane displacements. Other work on piezoelectrically actuated shell structures was proposed by Lester and Lefebvre (1991). Again, the shell model is adapted from the plate model, in which the curvatures of the shell are neglected. The basis of such assumptions was that the small size of the actuators compared to the shell radius will not introduce important error in the shell response calculations, even though the curvature effects were omitted.

Models for discrete actuator patches have also been derived based on the shell governing equations. Using Love's thin shell theory, Sonti and Jones (1993) derived the equations of motion of a composite thin shell and obtained approximate expressions for the equivalent actuator forces and moments to be applied to the edges of the actuator. When actuated in-phase, a uniform pressure over the actuator footprint was found in the equivalent loading. Chaudhry et al. (1994) looked more closely at this uniform pressure created by in-phase actuation (Chapter 3). Based on the thin shell Donnell theory, expressions for the equivalent forces and moments that represent the action of the actuator patches have been developed. The main conclusion of this work was that, due to the curvature of the shell, the representation of the in-phase actuation with only an equivalent in-plane line force applied along the edge of the actuator results in the application of erroneous transverse rigid-body forces. To avoid these rigid body forces, a uniform transverse pressure over the footprint of the actuator must be applied to maintain the self-equilibration of the shell. Using this concept, the in-phase actuation of a one-dimensional ring was modeled and the structural response was obtained in a closed form (Chapter 4).

2.3.3 Other Structural Applications

In this section, a brief review of various papers on the modeling of induced strain actuation of intelligent structures is presented. Not all papers that fall into this category are presented here, but those presented will give an overview of the application possibilities of intelligent structures.

Various analytical models for the induced strain actuation of more complex plate structures were developed. The modeling of laminated plates containing nonlinear actuators undergoing small strains using the equations of elasticity and Maxwell's governing equation was performed by Carman and Reichik (1994). The shape control of elastic plates using multiple embedded piezoelectric actuator patches was studied analytically by Agarwal et al. (1994). Sun (1993) presented a theoretical model for composite laminates consisting of piezoelectric materials and behaving with flexible deformation properties. An analytical model of a geometrically nonlinear composite plate with piezoelectric stiffeners was presented by Birman (1992). The actuation of clamped elliptic piezoelectric laminates was modeled by Lee (1994) using the classical lamination theory. Moiré interferometry experiments were conducted to investigate the induced strain actuation of surface bonded and embedded actuators (Mollenhauer, 1992).

Twist, shear, and torsion can be applied to a structure with induced strain actuators. An integrated theory was used to model the bending/twisting/shearing actuation of laminated beams (Lee and Sun, 1994). The torsion and bending actuation of structures with piezopolymer was explored by Lee (1989). Numerous papers were dedicated to the study of torsional control using piezoelectric actuators (Kawiecki and Smith, 1994; Park and Chopra, 1994, Park et al., 1993; Smith and Kawiecki, 1992; Sung et al., 1990). A Piezoceramic/polymer matrix composite which provides high stiffness and orthotropic symmetry for bending and twisting was developed by Wetherhold and Wang (1994). Also, theoretical models of the nonuniform surface deformation of piezoelectric ceramic-polymer composites with 2-2 connectivity (Cao et al., 1993) and with 1-3 connectivity (Cao et al., 1992) were presented. This work was extended to include surface plates and are added to the composite to improve the deformation uniformity (Cao, 1993).

Several ideas to improve the induced strain actuation of intelligent structures have been studied. The interdigitated surface electrodes idea was presented by Hagood et al. (1993) to improve the transverse actuation of piezoceramics. The effect of shaped

piezoceramic actuators on the excitation of beams was studied experimentally by Kim et al. (1993) and analytically by Diehl and Cudney (1994). The enhancement of the structural control using discretely attached induced strain actuators was studied by Chaudhry and Rogers (1992). A development of piezoelectric fiber composites for structural actuation was proposed by Hagood and Bent (1993). A linear piezoelectric motor prototype with light weight, large force and velocities, and micro and macro positioning characteristics was built at Vanderbilt University (Newton et al., 1994). Many other piezoelectric motor designs have also been under study (Fleischer et al., 1989; Goto and Sasaoka, 1988; Kumada, 1985; Kurosawa and Ueha, 1991; Kurosawa et al., 1988; Niedermann et al., 1988; Ohnishi et al., 1989; Schadegrodt and Salomon, 1990).

2.3.4 Finite Element Models

The analytical models that have been presented are generally applicable to simple structures such as beams, plates, and shells, with boundary conditions that can be easily modeled. For more complex structures, analytical modeling becomes strenuous, and numerical methods, such as finite element analysis, should be considered to resolve such problems. A simple way to perform finite element analysis of integrated structures is to use the analogous thermal expansion to model the induced strain actuators. This approach is helpful in the static analysis of integrated structures in that it gives the structural deformation response and stress distribution but does not include the electromechanical coupling effects. Following next is a review of the work done on the integration of the piezoelectric effect in the finite element method.

A finite element model based on the theory of elasticity and the Maxwell's electrical theory of piezoelectrics has been developed by Ha and Chang (1990) using the variational principle. An eight-node, 32 degrees of freedom (three normal displacements and one electrical per node), three-dimensional composite brick element was used to model the mechanical and electrical response of piezoelectric actuators integrated in a laminated composite. An important conclusion from this work was that the inclusion of the three-dimensional incompatible modes, which take account of the large bending in the structural response, is necessary to obtain accurate results. Static and dynamic simulations were performed on beams and plates (Ha et al., 1991, 1992) and compared to experimental data to verify the proposed finite element model. A different finite element model for two-dimensional plates was also proposed by Hwang and Park (1993). A four-node element with

a single electrical degree of freedom per element and three degrees of freedom per node (one normal displacement and two rotations) was developed. The equation derivation was based on Hamilton's principle and the classical lamination theory.

A finite element model was also proposed to model integrated actuators to shell structures (Tzou and Ye, 1994). The layerwise constant shear angle theory is used to develop a laminated quadratic C^0 piezoelectric triangular shell finite element. This element (quadratic in-plane and linear transverse) has twelve nodes with four degrees of freedom per node (three displacements and one electrical). The model is applied to two cases: bimorph and semi-circular shell.

Models for two-dimensional plates based on the first order shear deformation plate theory were developed by various authors. In all of following models, no electrical degree of freedom is included since the induced strain loading is being applied as external loading. The direct electromechanical coupling is therefore not available. First, Chandrashenkara and Agarwal (1993) proposed a nine-node isoparametric quadrilateral element with five degrees of freedom per node (three displacements and two rotations). The piezoelectric constitutive equations are included in this finite element model and the actuator moment loading is applied to the element boundaries after discretization of the mesh. The use of the shear theory only requires a C^0 element, as opposed to the C^1 element necessitated by the classical plate laminate theory. Similar work on nine-noded isoparametric quadrilateral element with five degrees of freedom per node was proposed by Shah et al. (1993a, 1993b). In this later work, it is shown that the stress field is strongly influenced by the shape of actuators and that actuators with sharp corners should be avoided. Another formulation based on the first order shear deformation laminated plate theory was proposed by Detwiler et al. (1994). The variational principle is used to derive quadrilateral isoparametric element with 20 degrees of freedom.

Finite element models using the concept of global/local response have also been applied to piezoelectric material. First, an eigenstrain formulation was used to model the local effects of embedded induced strain actuators or sensors and then was combined to a finite element method for the global structural response (Accorsi, 1993). An important feature of this method is the reduced time of computation achieved by performing only once a global finite element analysis of the structure without integrated induced strain actuators. Then, for various shapes, sizes, and locations of the actuators, only a solution of the eigenstrain is

necessary. This method is more flexible for the design of integrated structures. Another global/local finite element procedure was proposed by Robbins and Reddy (1993). In this work, laminated composite plates with embedded or surface bonded induced strain actuators were analyzed by dividing the structure into subregions, which has the capability of determining the three-dimensional effects. This proposed finite element model combines the variable kinematic finite elements and the finite element mesh superposition.

Work on the magnetostrictive effect has been studied on a smaller scale than the piezoelectric effect. Nevertheless, a finite element model for embedded magnetostrictive devices was proposed by Kannan and Dasgupta (1994a). The structural response to applied magnetic fields was obtained using a two-dimensional, coupled, linear finite element model (Kannan and Dasgupta, 1994a, 1994b). The magnetomechanical interactions were fully integrated in this model. Work on the direct effect of magnetostrictive sensors was also performed by the same authors (Kannan and Dasgupta, 1994c).

Finally, piezoelectric elements are now available in commercial finite element codes: ANSYS 5.0 by Swanson Analysis and ABAQUS by HKS. A short review of the capabilities of both packages is presented in Lin et al. (1994).

2.4 Actuator/Structure Interaction

To implement the induced-strain actuators on the structure, an adhesive is necessary to transfer the strain from the actuator to the structure. The quality of the bonding layer that is used will have an important impact on the response of the structure. In most of the static-based models presented in the previous section, an important simplification was made: a perfect bond between the actuator and the structure was assumed with a full transfer of the shear stresses exactly at the edges of the actuator. Such a simplification will define the structure at the edges of the actuator as the critical region. This removes the critical region from the bonding layer, which is most likely to fail in operation. Issues such as the thickness and compliance of the bonding layer and the intensive shear and peeling stresses at the actuators edges must be taken into consideration if a complete understanding of the actuator/structure interaction is desired. A review of more extensive studies of the bonding layer and the free-edge effects on the structure is presented next.

2.4.1 Bonding Layer Effect

Different bonding techniques such as adhesive bonding, diffusion bonding, silicate brazing, and metal brazing can be used to join piezoceramic actuators to metallic structures. Adhesive joints are the most convenient way to bond the actuators since they may be cured at room temperature, have small residual stresses, and distribute stresses during service (Cawley, 1991).

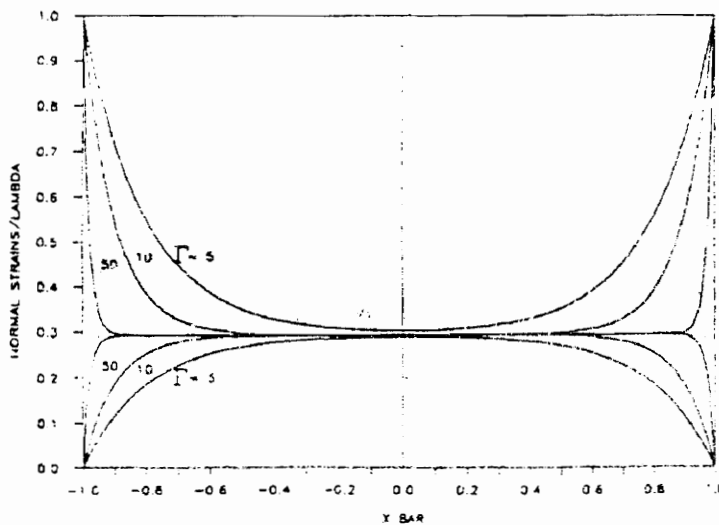


Figure 2.6 Effect of the shear lag parameter on the actuator and structure strains. (Crawley and de Luis, 1987)

The first analytical model which considers the bonding layer in the actuator/structure interaction was based on the classic shear lag theory, which assumes an elastic bonding layer of a finite thickness (Crawley and de Luis, 1987). The strain between the actuator and the structure is transferred through the shear stress present in the bonding layer. The work was performed on a simple beam submitted to out-of-phase actuation. The theoretical model was based on four assumptions: (i) only in-plane constant shear stress through the thickness of the bonding layer, (ii) uniform strain distribution through the thickness of the actuators, (iii) linear strain distribution through the thickness of the beam, (iv) only external forces causing pure bending can be applied to the beam. In this analysis, the principal conclusion concerning the bonding layer was that the shear stress in the bonding layer is only present over a small distance from the edges of the actuator, with no shear stress at the middle of the actuator (See Fig. 2.6). It was also found that, to obtain good shear transfer between the actuator and the structure, a large shear lag parameter which is primarily dependent on the

stiffness and thickness of the bonding layer is needed. The shear lag parameter is essentially a means of quantifying the “quality” of the bonding layer between the actuator and the structure. For the perfectly bonded case in which the shear lag parameter approaches infinity, the induced strain is transferred between the actuator and the structure over an infinitesimal distance at the edges of the actuator. In typical engineering applications, the perfect bonding assumption is acceptable for shear lag values larger than 30.

A refinement of the Crawley and de Luis (1987) model was proposed by Crawley and Anderson (1991). In this work, the Euler-Bernoulli beam theory was used to predict the response of a beam to in-phase and out-of-phase actuation. The difference between the two models is in the assumed strain distribution through the thickness (see section 2.3.1.1) that was considered in the modeling of the bonding layer. The pure shear in the bonding layer and the absence external loading of the structure assumptions were, however, maintained. In general, one can draw the same conclusions concerning the effect of the bonding layer as for the model developed by Crawley and de Luis (1987), but with more accurate results.

Another model also based on the shear lag theory for the out-of-phase actuation of beam structures, was derived by Kim and Jones (1991) under the assumption of composite plates. Again, a continuous linear strain distribution across the plate thickness is assumed, with the linear stress distribution depending on the material properties of each of the layers (actuator, adhesive and structure). Based on this different stress distribution, the effective bending moments were derived taking into consideration the influence of the bonding layer. Similar conclusions to Crawley and de Luis (1987) were obtained. For example, a thicker layer will reduce the effectiveness of the strain transfer (Fig. 2.7). A study of the optimal actuator thickness for maximizing the effective moment induced to the structure was performed. It was found that the influence of the bonding layer stiffness is not significant when compared to the influence of the piezoelectric actuator stiffness in the determination of the optimal actuator thickness.

Under cyclic loading, delamination of the bonding layer is likely to occur and will decrease the strain transfer effectiveness. It was shown that edge delamination significantly will reduce the structural coupling between the actuator and the structure, while inner delamination will have only a small effect (Kim and Jones, 1992). The edge delamination will also reduce the authority of the actuators at low frequencies (Kim and Jones, 1991d).

The dynamic response and natural frequency alterations due to delamination in composites with embedded actuators was also investigated by Babu and Hanagud (1990).

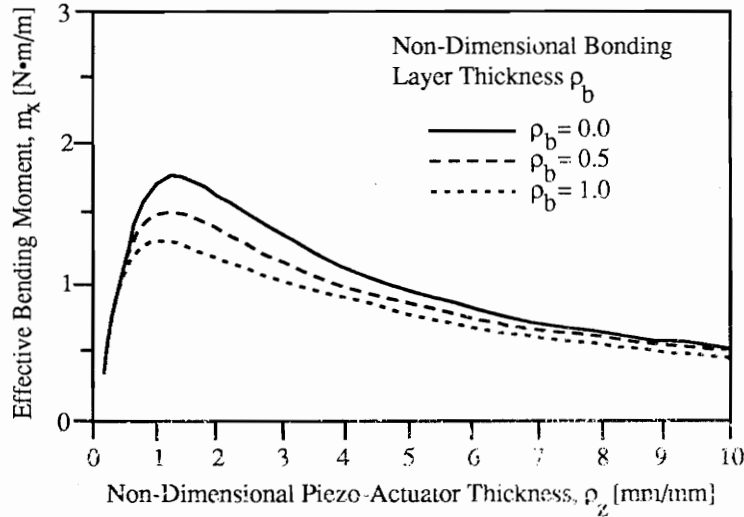


Figure 2.7 Effective curves illustrating the influence of the bonding layer thickness on the optimal piezoactuator thickness. (Kim and Jones, 1991a)

A static-based model was developed by Im and Alturi (1989) for a beam subjected to general loading, having less assumptions than the model proposed by Crawley and de Luis (1987). The shear stress distributions in both the top and bottom bonding layers were considered, with a possible application of unsymmetric induced strains to the actuators bonded on the beam structure. In this model the effects of the transverse shear and axial forces, in addition to a bending moment on the beam, was included in the formulation of the governing equilibrium equations. Based on this study, it was found that the shear stress transmitted through the bonding layer is greatly influenced by the externally applied axial and shear forces. The shear stress distribution over the length of the actuator is still concentrated at its ends, but the magnitude at both ends of the actuator can be significantly different.

A model based on the theory of elasticity and solved approximately by the principle of complementary energy was derived by Lin and Rogers (1994a). The analytical model is applied to the in-phase and out-of-phase actuation of a beam structure. The axial normal, shear, and transverse normal stresses were all included in the modeling of the bonding layer. The results of this approach were compared to the models based on the shear lag theory. When compared to the present elasticity model, the shear lag theory over-predicts the

effective force and moment near the actuator edges because the bonding layer is incapable of carrying normal and shear loads (see Fig. 2.8). Parametric studies showed that a relatively thick and/or compliant bonding layer will cause non-negligible reduction in the transfer of the actuation mechanism, particularly close to the edges of the actuator.

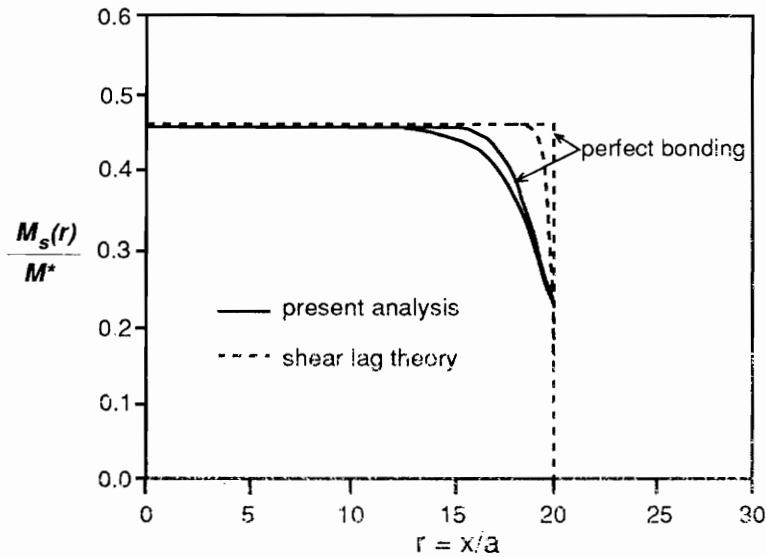


Figure 2.8 Reduced effective moment near the ends of the actuator when a bonding layer is considered. (Lin and Rogers, 1994a)

Finite element analysis has also been used to study the effect of the bonding layer (Robbins and Reddy, 1991). Using the generalized plate theory, a finite element formulation is applied to a beam structure including a bonding layer. This approach satisfies all the boundary conditions without using a large number of elements. This finite element formulation, however, restricts the thickness of the bonding layer to be the same order of magnitude as the structure and the actuator and involves heavy computations.

An experimental investigation to determine the optimum adhesive layer parameters using Taguchi methods has been performed by Onders and Naganathan (1994). Different types of adhesive, bond layer thickness, and type of base metal were considered in order to maximize the strain transfer of the system.

2.4.2 Edge Effects

The interaction mechanisms between the actuator and the structure have been theoretically modeled based on various theories such as shear lag, elasticity, and linear shear

stress field. According to these models, a high interfacial shear stress state near the ends of the actuator was desirable to obtain a good structure/actuator interaction, i.e., effective strain transfer from the actuator to the structure. Such conclusions were reached because issues such as interfacial shear and peeling stresses were not considered, although the low strength interfacial bond is most likely to be the weakest structural component. Such models are thus valid only in a distance approximately four actuator thicknesses away from the actuator edges (Liang and Rogers,1989). Another neglected aspect is the excessive stress gradients in the bonding layer which can be present and are able to initiate debonding of the actuator from the structure.

A theoretical model capable of predicting the interfacial shear and peeling stresses has been developed by Lin and Rogers (1993). The refined model is based on an approximate through-the-thickness second order axial normal stress field, solved using the principle of complementary energy after converting the induced strain actuation problem to a boundary value problem. The solutions of the whole field stress distribution are obtained for in-phase and out-of-phase actuation for actuators perfectly bonded to the structure (no bonding layer present in the modeling). It was found that the effective actuator force attenuates near the ends of the actuators, which reduces the discontinuities at the actuator edges. The interfacial shear stress vanishes at the ends of the actuator, with a peak at one actuator thickness from the edges. The interfacial peeling stresses peak at the edge and then decrease with increasing distance from the actuator edge.

An extended model to include the bonding layer was later proposed by the same authors (Lin and Rogers, 1994a). This model has already been discussed in section 2.4.1. It was pointed out that thick and/or compliant bonding layer causes noticeable losses in the transfer of the actuation mechanism. Nevertheless, the bonding layer yields low interfacial shear and peeling stresses, which is beneficial to the structural integrity.

A finite element analysis of embedded and surface bonded induced strain actuators was performed to study the stress distribution in the proximity of the actuators (Shah et al., 1993c). In their work, it was concluded that the stress concentration at the edges of the actuators are sufficient to initiate cracks at the edges and that stress concentrations are lesser for the embedded case. A quasi-three-dimensional finite element analysis was also used to study the interfacial stress distribution in composites with embedded piezoelectric layers (Shah et al., 1990). The principal conclusions were that the maximum interlaminar stress is not

affected by the location of the piezoelectric layer and that an addition of a glass layer will reduce the stress levels.

Some modifications in the implementation design of piezoceramic patches have been proposed to reduce the high stress gradients present in the localized regions near the ends of the actuator. These modifications consisted of employing partial electrodes to the actuator surfaces instead of fully electroding the surfaces, examining actuators with chamfered ends, and using structural caps to reduce the stress concentrations in the bonding layer (Walker et al., 1993). Based on a finite element analysis, axial and normal stress reduction of the order of 80% were obtained with a 60% reduction of the shear stress, for typical cases of in-phase and out-of-phase actuation. The two best arrangements in reducing the stress levels were found to be the partial electrode and the edge cap configurations.

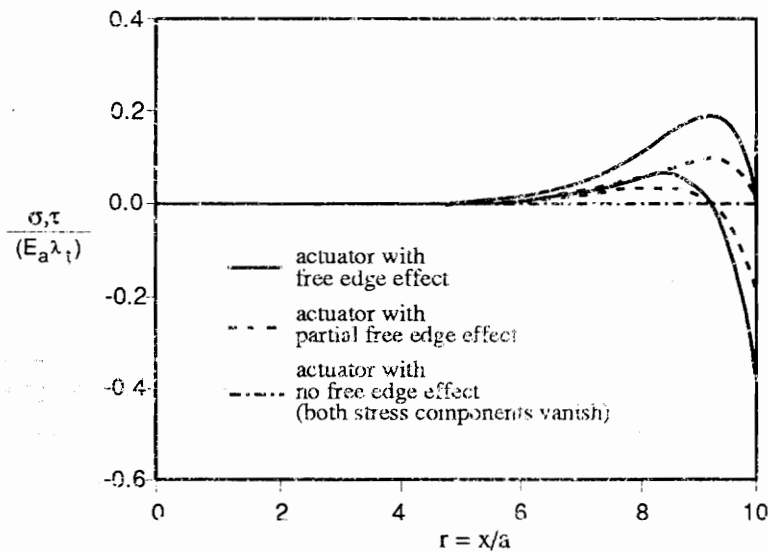


Figure 2.9 *Reduced interfacial and peeling stresses with inactive actuator edges.*
(Lin and Rogers, 1994b)

A more extensive analytical study of partial electroding was performed by Lin and Rogers (1994b). When the partial electroding technique is used, the interfacial shear stress is reduced because the actuation force is now not only transferred by the interfacial shear force, but also by the normal force on the inactivated ends of the actuator. This will significantly reduce the interfacial and peeling stresses (see Fig. 2.9). The strain transfer from the actuator to the structure will increase slightly near the ends of the actuator, with an improved

performance for stiffer inactive edges. To minimize the free edge effect, it was found that an inactive edge with a length of two actuator thicknesses is optimum for better performance.

Special attention has also been given to embedded piezoelectric actuators in composite materials. Various studies showed that the structural integrity will be affected by presence of embedded actuators. Crawley and de Luis (1987) reported a reduction of 20% in the ultimate strength of glass/epoxy laminates. Because of the presence of inert implants in the composite laminate, discontinuities will be created and will increase the interlaminar stresses at these locations. A solution was proposed by Singh and Vizzini (1993) to reduce the negative effects created by embedded actuators: interlaced piezoceramic actuators. Such a technique reduces the maximum interlaminar shear stress by 25% and the maximum interlaminar normal stress by 35% and moves the initial delamination location away from the interface between the actuator and the composite.

2.4.3 External Loading Effects

Thus far, very few of the analytical models discussed considered the boundary conditions of the structure. It was generally assumed that the structure had free boundary conditions and was not subjected to any external loading. However, some studies showed that the boundary conditions can have an important impact on the structural response and should therefore be considered for more accurate theoretical modeling.

In the pin-force model developed by Crawley and de Luis (1987), the equations for the equivalent force and moment were included. Strains due to external loading or deformations that are not caused by the actuation of the induced strain actuators themselves can be included in the structure at the ends of the actuator. The preexisting strains in the structure at the ends of the actuators must be known in advance. No case study was presented.

Chaudhry and Rogers (1993) presented an analysis of the effect of externally applied moments on a beam actuated out-of-phase with various boundary conditions. It was shown that boundary conditions which prevent the free actuation of the structure have the same effect as external loading. The authors concluded that, if the actuators are replaced with a set of equivalent moments on the structure without considering the effect of external loading and/or constrained boundary conditions, a large error in the structural response is found. An optimization study for maximizing the strain induced in the structure showed that the

optimum thickness ratio changes with the external load and also with the electric field applied across the actuator. This behavior was reported to be caused by the external load that the actuators must work against in addition to working against the structural stiffness.

A model based on the theory of elasticity, including external loading, was derived by Lin and Rogers (1994c). This model is a simple extension of the model discussed earlier (Lin and Rogers, 1993). Including the effect of external loading, the effective force and moment due to in-phase and out-of-phase actuation, respectively, showed an excellent match with the finite element analysis performed. In this analysis, it was also demonstrated that the interfacial shear stress distribution is altered with external loads, and the maximum interfacial shear and peeling stresses are a linear function of the external loads. The model proposed by Im and Alturi (1989), presented earlier, included the effects of externally applied transverse shear and axial normal forces. It was also shown that the external loads have noticeable effects on the magnitude of the interfacial shear stresses. Because this model is based on the shear lag theory, it lacks quantitative accuracy.

A nonlinear theory of laminated piezoelectric plates was proposed by Pai et al. (1992). In this work, in addition to the actuator induced loads, external loading was considered in the model formulation.

2.5 Models Including the Dynamic Interaction of the Actuators and the Structure

All of the analytical models presented in section 2.3 neglected the dynamic properties of the actuator. The modeling efforts were based only on static considerations, which resulted in frequency independent equivalent actuator forces and moments. For dynamic analysis of intelligent structures, the statically determined actuator force and moment were simply assumed to be constant over the whole frequency range of interest and were then introduced in the equations of motion. This static-based approach to dynamic analysis of intelligent structures shows important shortcomings in the accuracy of the calculated dynamic structural response. In this section, models that includes the dynamic characteristics of the actuator and the structure will be presented.

2.5.1 Dynamic Modeling Approach

Issues associated with coupling the piezoelectric actuator dynamics to mechanical system dynamics were discussed by Hagood et al. (1990). Based on Rayleigh-Ritz energy formulation, the equations of motion for piezoelectrically coupled electromechanical systems were derived. This model includes dynamic coupling between the structure and the electrical network through the piezoelectric effect. In this dynamic model, the governing equations of the electroelastic system (Eq. 2.1) includes the mass and stiffness of the integrated PZT patch.

$$(M + M_p)\ddot{r} + (K + K_p)r - \Theta v = B_f f \quad 2.1$$

where r and v represent the generalized displacement and voltage coordinates. Θ denotes electromechanical coupling matrix and B_f is the forcing matrix. f is the vector of external point forces. Case studies of a cantilevered beam with surface bonded induced strain actuators with direct voltage-driven electrodes and direct charge-driven electrodes were presented. The actively controlled cantilevered beam was tested and favorable results were obtained. However, actuator force loading is not explicitly expressed as a function of the actuator input impedance and the host structural mechanical impedance. As the active control force needs to be calculated, the blocking force was used so that the induced force loading is still independent of the dynamics of the host structure and frequency.

Inman (1990) investigated the phenomenon of the control/structure interaction (CSI) for the lumped dynamic system. It was assumed that the actuators used for control have second-order dynamics. The effects of added actuator dynamics to the state feedback in vibration suppression problems were considered in the modeling. The stability of the integrated control system was specifically discussed.

2.5.2 Impedance Modeling Approach

An impedance model based on the dynamic properties of the actuators and the structure has been proposed by Liang et al. (1993a). This analytical model is able to model the dynamic response of the intelligent structure accurately by including the dynamic interaction between the actuators and the structure. The essence of the impedance approach is to match the actuator impedance to the structural impedance along the edges of the actuators. This modeling approach includes the actuator stiffness and damping, but not the actuator mass loading. Based on the structural impedance, the induced strain actuator force

output will be frequency-dependent, and this will result in a more accurate prediction of the dynamic response. The impedance model has been shown to be more accurate than static-based models for the calculation of the dynamic structural response of intelligent structures.

The impedance modeling approach has been applied to numerous cases. An impedance model for a beam under out-of-phase actuation was proposed by Liang et al. (1993b) and then extended to two dimensional plates (Zhou et al., 1994a). The impedance approach was also applied to curved structures, such as out-of-phase actuated rings (Rossi et al. 1993). Extended models for rings structures including the transverse shear resultant were proposed for out-of-phase actuation (Chapter 5) and in-phase actuation (Chapter 6). Two-dimensional shell model for out-of-phase actuation (Zhou et al. 1993) and for general actuator loading (Chapter 8) completed the work on this dynamic modelization approach.

Experimental work on plates (Zhou et al., 1994a) and rings (Rossi et al., 1993; Chapter 7) was performed to verify the impedance models. A computer implementation of the impedance model for Euler-Bernoulli beams with various boundary conditions, loading conditions, structural damping, and stiffness and mass loading was performed by Subramaniam et al. (1993).

Using the impedance approach, the coupled electro-mechanical analysis of induced strain actuators can be easily integrated to determine the power consumption and energy transfer in the electro-mechanical system (Liang et al., 1992, 1993c). An extended thermo-electro-mechanical study was proposed by Zhou et al. (1994b) to estimate the temperature and thermal stress distribution in the actuators.

2.6 Summary

In this chapter, a review of the mechanics of induced strain actuation of intelligent structures was presented. A discussion of the intelligent material systems and structures concluded with the enormous possibilities of such intelligent systems. An overview of the principal induced strain actuation materials showed that no material has a large advantage over the others, each material being appropriate in its own field of application. The variety of static models of induced strain actuators coupled with intelligent structures showed various levels of performance in the structural response modeling. The most common Euler-Bernoulli model showed better performance than the pin-force model due to the more

accurate assumed strain distribution through the structure and the actuators. A drawback of the static models is the impossibility of including the dynamic characteristics of the intelligent system. The actuator/structural interaction was shown to have an important impact on the structural response. The bonding layer decreases the strain transfer from the actuator to the structure, the edge effects can create peeling and interfacial stresses reaching the ultimate strength, and the external loads greatly affect the response of the system. The impedance modeling approach, which includes the actuator and structural dynamic characteristics, was reported to give better results over the static models for the dynamic response cases. Although this review consisted only of a brief overview of the current status of the research conducted on the induced strain actuation of smart structures, it gives an insight on the importance of pursuing the research, development, and design of this promising field of intelligent material systems and structures.

Chapter 3

Special Considerations for the Equivalent Loading of Induced Strain Actuation of Shell Structures

Abstract

Based on the thin-shell Donnell theory, a model to represent the action of discrete induced strain actuator patches symmetrically bonded to the surface of a circular cylindrical shell has been developed. The model provides estimates of the bending curvatures due to the out-of-phase actuation and the in-plane strains due to the in-phase actuation of the bonded actuator patches. The magnitudes of the induced curvature and the in-plane strain are found to be identical to those of plates; however, due to the strain-displacement relations in cylindrical coordinates, the in-plane and out-of-plane displacements are coupled. Expressions for the equivalent forces and moments that represent the action of the actuator patches have been developed. Due to the curvature of the shell, the representation of the in-phase actuation with an equivalent in-plane line force applied along the edge of the actuator results in the application of erroneous rigid-body transverse forces. To avoid these rigid body forces, a method to represent the in-phase actuation with a system of self-equilibrating forces is proposed. The action of the actuator is then represented by an equivalent in-plane force and a transverse distributed pressure applied in the region of the actuator patch. Finite element verification of the proposed model is presented. The displacements due to the actual actuator actuation are compared with the proposed model, and very good agreement is found.

3.1 Introduction

In recent years there has been a great surge of interest in research on shape, vibration and acoustic control of structures with induced strain actuators like piezoelectric materials and shape memory alloys. What distinguishes induced strain actuators from conventional hydraulic and electrical actuators, and makes them especially attractive for smart structures, is their ability to change their dimensions and properties without utilizing any moving parts.

These actuator materials contract and expand just like the muscles in the human body. When integrated into a structure (either through embedding or through surface-bonding), they apply localized strains and directly influence the extensional and bending responses of the structural elements. Because of the absence of mechanical parts they can be easily integrated into the base structure. Integration within the structure ensures an overall force equilibrium between the forcing actuator and the deforming structure, thus precluding any rigid body forces and torques.

Induced strain actuators, like piezoelectric materials when bonded to the surface of a structure, generate a set of forces which are concentrated close to the edges of the actuator. Therefore, their action is often represented by line moments or forces applied along the periphery of the actuator. This representation simplifies analysis because the structure does not have to be discretized (to represent the non-uniform structural properties in the regions of the patches) and global structural equations can be solved with the actuator forces appearing as discretely applied external forces. This analysis method, although approximate (approximate because the actuator mass and stiffness are not represented and actuator forces derived from static and stress-free boundary conditions are used), gives reasonably accurate results for small and thin patches of actuators. Also, for the case of straight structural members like beams and plates, it does not pose any problems such as the equivalent actuator forces producing rigid-body motion. For shell-type structures, however, due to their curvature, this simple representation is not appropriate for the case of in-phase actuation. In-phase actuation refers to the case when the two actuators bonded to the top and bottom surface of the shell are activated to produce strains in the same direction. Because the circumferential forces used to represent the action of the actuator are not co-linear they produce rigid-body transverse forces on the shell. Thus, certain special modifications must be made to such a representation scheme to accommodate the special characteristics of the shell structures. The modification proposed and verified in this chapter is the application of a uniform transverse pressure across the footprint of the actuator.

To date, a number of models to represent the action of actuators on beams and plates have been proposed (Crawley and Lazarus, 1989; Lee, 1990; Crawley and Anderson, 1990; Wang and Rogers, 1991a; Dimitriadis, Fuller and Rogers, 1991). For shells, the only models that have been developed are based on layered shell theory, i.e., the analytical model assumes that the induced strain actuator material comprises a total, distinct layer of the shell (Tzou and Gadre, 1989; Jia and Rogers, 1990). In the work that has been reported on vibration and

acoustic control of shells using piezoelectric actuators, plate models are often adapted to shells (Sonti and Jones, 1991; Lester and Lefebvre, 1991). At first sight, this adaptation seems perfectly reasonable because the shell is thin and r/t_s is large. This does, however, pose a problem for the representation of in-phase actuation forces because the actuator forces are no longer co-linear as in the case of beams and plates, and as stated earlier, this results in a rigid-body force being applied to the shell (see Fig. 3.1). If this is not recognized, then the action of in-phase actuation of even a small actuator patch will result in an erroneous response and can lead to a totally wrong solution. In a recent model for curved piezoelectric actuators, Sonti and Jones (1993) also recognized this fact and showed the necessity of including a uniform transverse pressure, in addition to the axial and tangential forces, to correctly represent the action of in-phase actuation.

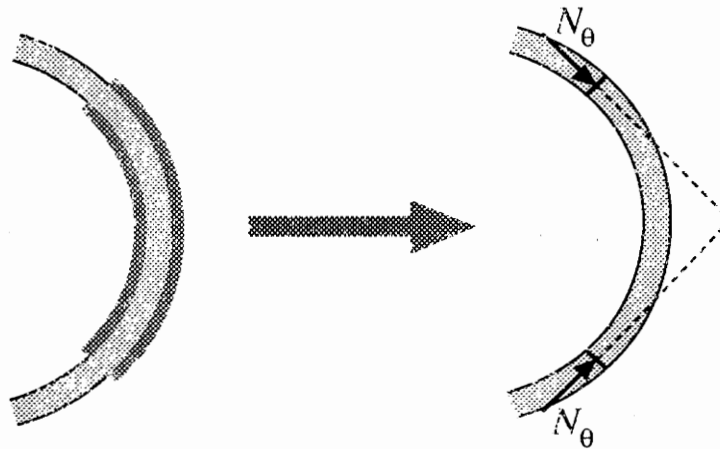


Figure 3.1 *Non-equilibrium of discrete tangential forces in shell structures.*

A model has been developed to compute the equivalent forces and moments applied by a pair of symmetrically-bonded actuator pairs, and is described here. This is followed by a discussion of the special considerations for shell-type structures. The development of the model is similar to the work of Crawley and Lazarus (1989) for plates, and relies on classical lamination theory (CLT).

3.2 Model Formulation

A model describing the interaction between surface-bonded actuators and a circular cylindrical shell has been developed based on Donnell's theory. For completeness a short

derivation of the accompanying equations of motion is also presented. Consider a thin circular cylindrical shell, as shown in Fig. 3.2. We start with the following Donnell's assumptions ($l + \frac{z}{R} = l$, $r \rightarrow R$) for the kinematics of deformation:

$$u(x, \theta, z) = u^o(x, \theta) - z \frac{\partial w^o}{\partial x}, \quad (3.1)$$

$$v(x, \theta, z) = v^o(x, \theta) - z \frac{\partial w^o}{R \partial \theta}, \quad (3.2)$$

$$w(x, \theta, z) = w^o(x, \theta). \quad (3.3)$$

In the above, z is the local thickness coordinate, measured from the middle surface of the shell. The superscript zero denotes displacements of the cylindrical panel's middle surface

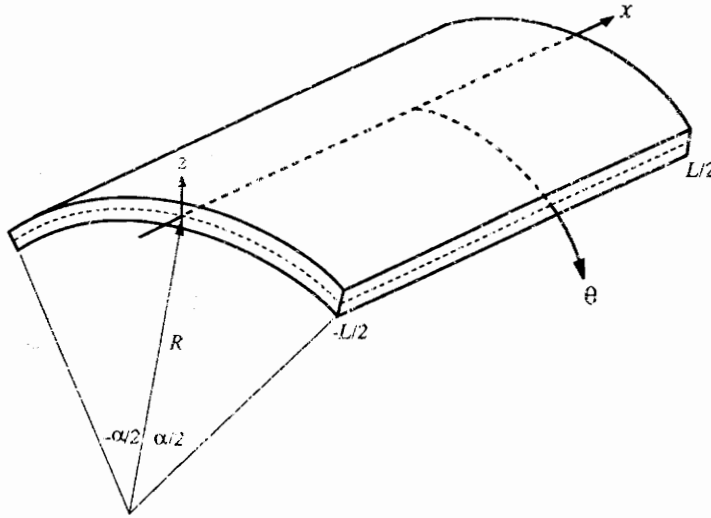


Figure 3.2 Thin circular cylindrical shell coordinate system.

The pertinent strain-displacement relations in cylindrical coordinates are:

$$\varepsilon_x = \frac{\partial u}{\partial x} = \varepsilon_x^o + z \kappa_x; \quad \varepsilon_x^o = \frac{\partial u^o}{\partial x}; \quad \kappa_x = -\frac{\partial^2 w^o}{\partial x^2}, \quad (3.4)$$

$$\varepsilon_\theta = \frac{\partial v}{R \partial \theta} + \frac{w}{R} = \varepsilon_\theta^o + z \kappa_\theta; \quad \varepsilon_\theta^o = \frac{\partial v^o}{R \partial \theta} + \frac{w^o}{R}; \quad \kappa_\theta = -\frac{\partial^2 w^o}{R^2 \partial \theta^2}, \quad (3.5)$$

and

$$\gamma_{x\theta} = \frac{\partial v}{\partial x} + \frac{\partial u}{R\partial\theta} = \gamma_{x\theta}^o + z\kappa_{x\theta}; \quad \gamma_{x\theta}^o = \frac{\partial v^o}{\partial x} + \frac{\partial u^o}{R\partial\theta}; \quad \kappa_{x\theta} = -2 \frac{\partial^2 w^o}{\partial x R \partial \theta}. \quad (3.6)$$

The resultant force-strain relations for a layered composite laminate are given by (Jones, 1975):

$$\begin{Bmatrix} N \\ M \end{Bmatrix} = \begin{bmatrix} A & B \\ B & D \end{bmatrix} \begin{Bmatrix} \varepsilon^o \\ \kappa \end{Bmatrix} - \begin{Bmatrix} N_\Lambda \\ M_\Lambda \end{Bmatrix} \quad (3.7)$$

where

$$\{N_\Lambda\} = \int [\bar{Q}] \{\Lambda\} dz \quad (3.8)$$

$$\{M_\Lambda\} = \int [\bar{Q}] \{\Lambda\} z dz \quad (3.9)$$

are the equivalent of thermal forces in CLT. Note that Λ is the free induced strain developed in the actuator in response to an applied voltage ($\Lambda_x = Ed_{3x} = Vd_{3x}/t_a$). The three governing equilibrium equations are:

$$\frac{\partial N_{xx}}{\partial x} + \frac{\partial N_{x\theta}}{R\partial\theta} - \rho_s t_s \ddot{u}^o = 0, \quad (3.10)$$

$$\frac{\partial N_{x\theta}}{\partial x} + \frac{\partial N_{\theta\theta}}{R\partial\theta} - \rho_s t_s \ddot{v}^o = 0, \quad (3.11)$$

and

$$\frac{\partial^2 M_{xx}}{\partial x^2} + 2 \frac{\partial^2 M_{x\theta}}{\partial x R \partial \theta} + \frac{\partial^2 M_{\theta\theta}}{R^2 \partial \theta^2} - \frac{N_\theta}{R} - \rho_s t_s \ddot{w}^o = q, \quad (3.12)$$

with boundary conditions at $x=\pm L/2$ and $\theta=\pm\alpha/2$. For an unconstrained symmetric panel with no externally applied forces or moments, i.e., $N, M=0$, Equation (3.7) reduces to:

$$\begin{Bmatrix} \varepsilon^o \\ \kappa \end{Bmatrix} = \begin{bmatrix} A & B \\ B & D \end{bmatrix}^{-1} \begin{Bmatrix} N_\Lambda \\ M_\Lambda \end{Bmatrix}. \quad (3.13)$$

For a symmetric shell ($B=0$), the above equations are uncoupled, and

$$\{\varepsilon^o\} = [A]^{-1} \{N_\Lambda\} \quad (3.14)$$

$$\{\kappa\} = [D]^{-1} \{M_\Lambda\}. \quad (3.15)$$

To obtain simplified expressions for the induced curvature, we assume that the shell is isotropic and has the same Poisson's ratio as the actuator. For such a case, the $[A]$ and $[D]$ matrices reduce to:

$$[A] = \frac{Y_s t_s + 2Y_a t_a}{(1-\nu^2)} \begin{bmatrix} 1 & \nu & 0 \\ \nu & 1 & 0 \\ 0 & 0 & \frac{1-\nu}{2} \end{bmatrix}, \quad (3.16)$$

$$[D] = \left\{ \frac{Y_s t_s^3}{12(1-\nu^2)} + \frac{2}{3} \frac{Y_a}{(1-\nu^2)} \left[\left(\frac{t_s}{2} + t_a \right)^3 - \left(\frac{t_s}{2} \right)^3 \right] \right\} \begin{bmatrix} 1 & \nu & 0 \\ \nu & 1 & 0 \\ 0 & 0 & \frac{1-\nu}{2} \end{bmatrix}. \quad (3.17)$$

Rewriting in a more convenient way,

$$[A] = \frac{Y_a t_a (2 + \psi)}{(1-\nu^2)} \begin{bmatrix} 1 & \nu & 0 \\ \nu & 1 & 0 \\ 0 & 0 & \frac{1-\nu}{2} \end{bmatrix}, \quad (3.18)$$

$$[D] = \frac{t_s^2}{12} \frac{Y_a t_a}{(1-\nu^2)} \left[6 + \psi + \frac{12}{T} + \frac{8}{T^2} \right] \begin{bmatrix} 1 & \nu & 0 \\ \nu & 1 & 0 \\ 0 & 0 & \frac{1-\nu}{2} \end{bmatrix}. \quad (3.19)$$

With these assumptions, the following expression for the induced bending strains due to the out-of-phase actuation is obtained from equation (3.15) (t_s = shell thickness, t_a = actuator thickness):

$$\begin{Bmatrix} \kappa_x \\ \kappa_\theta \\ \kappa_{x\theta} \end{Bmatrix} = \frac{6 \left(1 + \frac{1}{T} \right) \frac{2}{t_s}}{6 + \psi + \frac{8}{T^2} + \frac{12}{T}} \begin{Bmatrix} 1 \\ 1 \\ 0 \end{Bmatrix} \Lambda, \quad (3.20)$$

where

$$\psi = \frac{Y_s t_s}{Y_a t_a}, \quad T = \frac{t_s}{t_a}, \quad (3.21)$$

and for in-phase actuation, the following expression for induced middle-surface strains is obtained from equation (3.14):

$$\begin{Bmatrix} \varepsilon_x^o \\ \varepsilon_\theta^o \\ \varepsilon_{x\theta}^o \end{Bmatrix} = \frac{2}{2 + \psi} \begin{Bmatrix} 1 \\ 1 \\ 0 \end{Bmatrix} \Lambda . \quad (3.22)$$

The above expressions for the middle-surface strains for the case of in-phase actuation and the bending strains for the case of out-of-phase actuation are the same as those obtained for plates; however, the circumferential strain is now coupled with the out-of-plane displacement (equation (3.5)).

To solve a plate or a shell problem, an expression for a set of equivalent forces is often developed. These forces, when applied along the edges of the footprint of the actuator, on the structure result in the same degree of bending strains and in-plane middle-surface strains as those obtained from equations (3.20) and (3.22). The equivalent forces and moments are obtained by substituting the bending strains and the in-plane strains from equations (3.20) and (3.22) into equation (3.7), with N_A and M_A set to zero. For out-of-phase actuation, the equivalent moments are found to be:

$$\begin{Bmatrix} M_{xx} \\ M_{\theta\theta} \\ M_{x\theta} \end{Bmatrix}_{eq.} = \frac{Y_s t_s^2}{1 - \nu} \frac{\left(1 + \frac{1}{T}\right)}{6 + \psi + \frac{8}{T^2} + \frac{12}{T}} \begin{Bmatrix} 1 \\ 1 \\ 0 \end{Bmatrix} \Lambda . \quad (3.23)$$

and for in-phase actuation, the following expression for the equivalent axial and tangential force is obtained:

$$\begin{Bmatrix} N_{xx} \\ N_{\theta\theta} \\ N_{x\theta} \end{Bmatrix}_{eq.} = \frac{Y_s t_s}{1 - \nu} \frac{2}{2 + \psi} \begin{Bmatrix} 1 \\ 1 \\ 0 \end{Bmatrix} \Lambda . \quad (3.24)$$

The tangential force obtained from the above equation, when applied to the shell along the two circumferential edges of the actuator will not be co-linear, due to the curvature of the shell, and will have an erroneous component resulting in a rigid body mode. This situation has already been illustrated in Fig. 3.1. This occurs due to the simplifying assumptions in the above formulation. In actuality, a set of self-equilibrating stresses are developed between the shell and the bonded actuator, and there is no rigid body force developed.

To remedy this situation, we have proposed the application of an equilibrating uniform radial pressure applied across the footprint of the actuator. The magnitude of the uniform pressure is obtained from simple statics and is equal to $-N_\theta / R$ (Fig. 3.3). This set of forces, i.e., an equivalent tangential force given by equation (3.24) and a uniform radial pressure, now provide a convenient means of representing the action of surface-bonded actuators which are actuated in-phase. To verify whether this set of forces results approximately in the same displacement field as a true actuator bonded to a cylindrical shell a comparison with a finite element model is made.

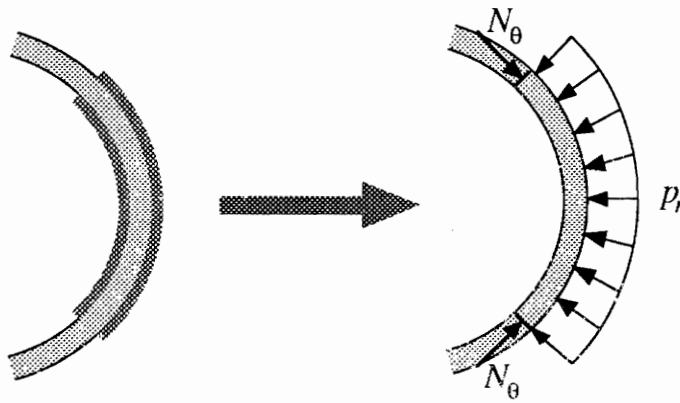


Figure 3.3 Adequate equivalent loading to maintain equilibrium.

3.3 Finite Element Modeling and Verification

Two finite element models have been constructed to verify the equivalent loading scheme. A 6" radius, 0.032" thick and 1" deep ring with piezoelectric actuators 1/6 of the ring thickness and covering an arc 10° long (α) have been used. Making use of symmetry, only the top half needs to be modeled. The first model, shown in Fig. 3.4a, consists of beam elements. First, the actuation is simulated by specifying a coefficient of thermal expansion for the elements in the actuator region and then applying a known temperature to the model. Second, an equivalent self-equilibrating load, i.e., pressure and tangential force, corresponding to the temperature, is applied (equations (3.23) and (3.24)). The radial and tangential displacements obtained from the above analysis are identical and therefore not shown. It must be noted that the pressure loading must be transformed to nodal forces only (lumped loading). The lumped loading is often better for flat elements representing a curved surface (De Salvo and Swanson, 1979).

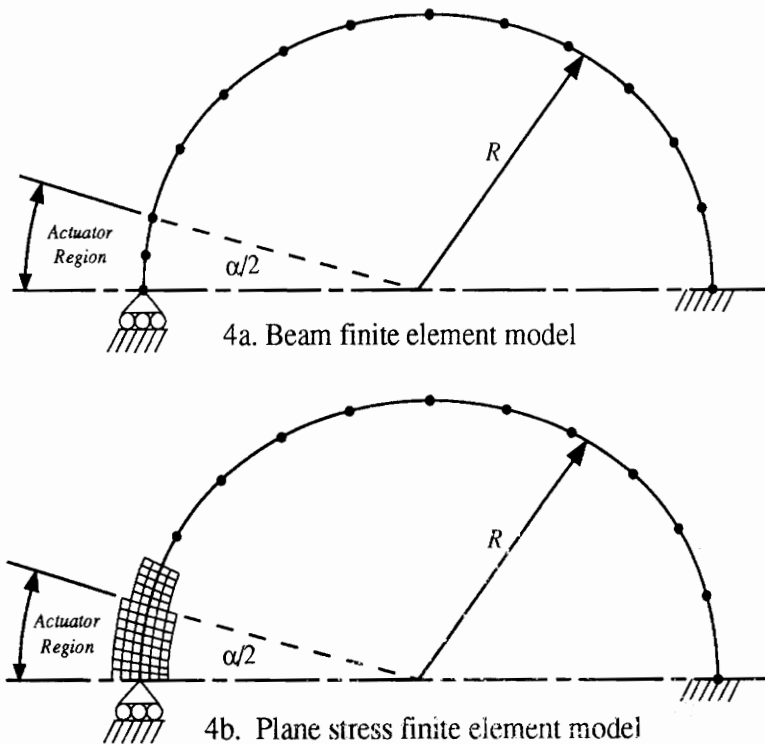


Figure 3.4 Finite element models used to verify the theoretical model.

The second finite element model uses plane stress elements in the actuator region to include the actuator's stiffness and uses beam elements for the rest of the shell (Fig. 3.4b). A rigid element connecting the five nodes at the end of the plane stress element region is introduced. A constraint equation is then used to ensure the continuity in the rotations between the beam and plane stress elements. Again, thermal expansion is used to simulate the static action of the actuators on the shell.

The radial and tangential displacements are shown in Fig. 3.5. Discrepancies between the equivalent loading model and the plane stress finite element model exist since no assumptions about the actuator stiffness or about the equivalent loading are made in the latter model. The differences are however greater in the actuator region due to the added structural stiffness of the actuators. Even though displacement differences are present, the plane stress finite element model validates the derived model since it gives results of the same order of magnitude with similar deformed shapes as opposed to when only point tangential forces (without a transverse pressure) are used. The deformed shape of the analytical model and the plane stress finite element model are shown in Fig. 3.6. Also shown in Fig. 3.5 are the

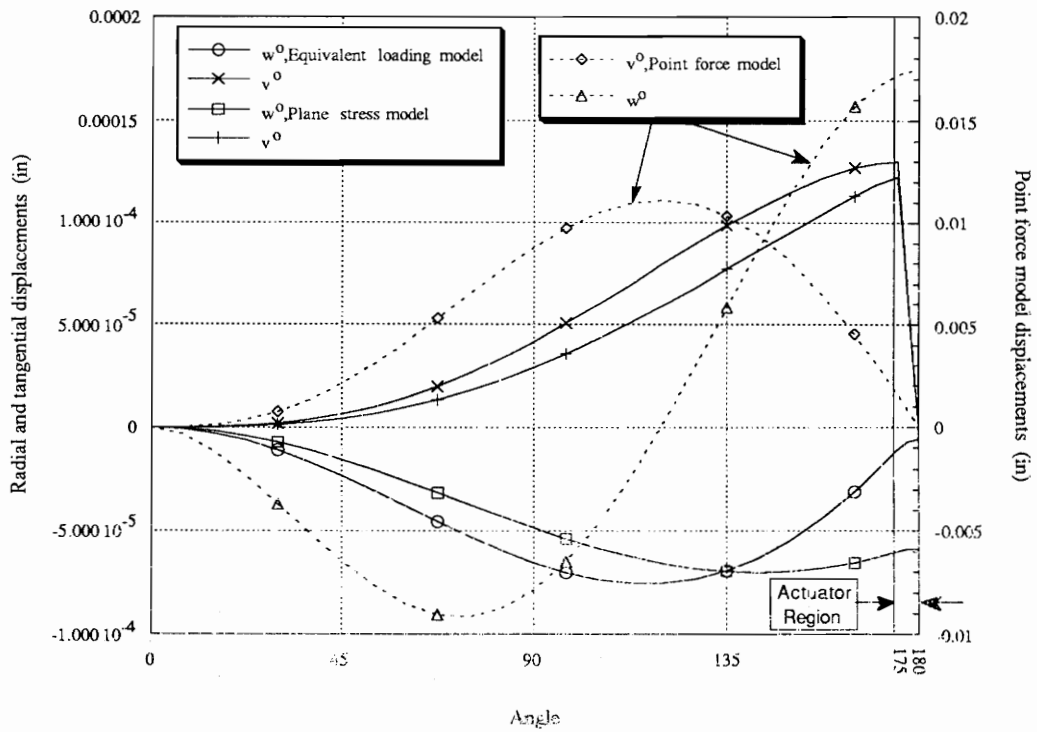


Figure 3.5 Comparison of the displacements predicted by the proposed self-equilibrating equivalent forces, the plane stress finite element model and the tangential force alone (no pressure).

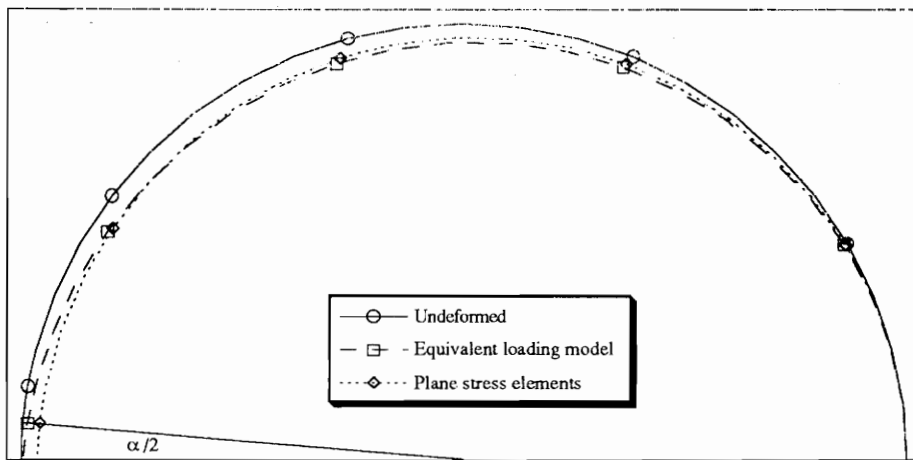


Figure 3.6 Deformed shape of the ring using the self-equilibrium loading and the plane stress elements.

displacements of the same ring if only discrete tangential forces are applied (without transverse pressure). This model using only tangential forces does not satisfy the ring's

self-equilibrium. Major displacement discrepancies between the proposed equivalent loading model and the case using only tangential forces are observed both in shape and magnitude. Using the tangential forces alone over predicts the displacements by a factor of up to 1000, as seen on the right vertical axis of Fig. 3.5 (note that the scales of the two vertical axis are different). Also, a reaction force in the x-direction at the clamped boundary is present if uniform pressure is not applied. This reaction force should not be present since the actual ring with bonded actuators is in self-equilibrium. Adequate equivalent loading did not show any reaction force in the x-direction at the clamped boundary.

From the finite plane stress element model shown in Fig. 4b, it is possible to justify the use of a uniform radial pressure on the actuator footprint to maintain the self-equilibrium of the ring. Figure 3.7 shows the radial stress distribution through the thickness of the actuator and the ring. This stress distribution is virtually constant over the whole actuator region, except at the ends of the actuator, which validates the use of a uniform radial pressure in the analytical model. With the actuators removed, an equilibrating radial pressure applied on both sides of the shell is necessary to produce the same stress distribution on the shell surface ($z/t_s = 1, -1$) shown in Fig. 3.7. Because the interest is in global shell deformations, the equilibrating pressure can be applied on one side only or on the shell midplane, since it will produce the same shell response.

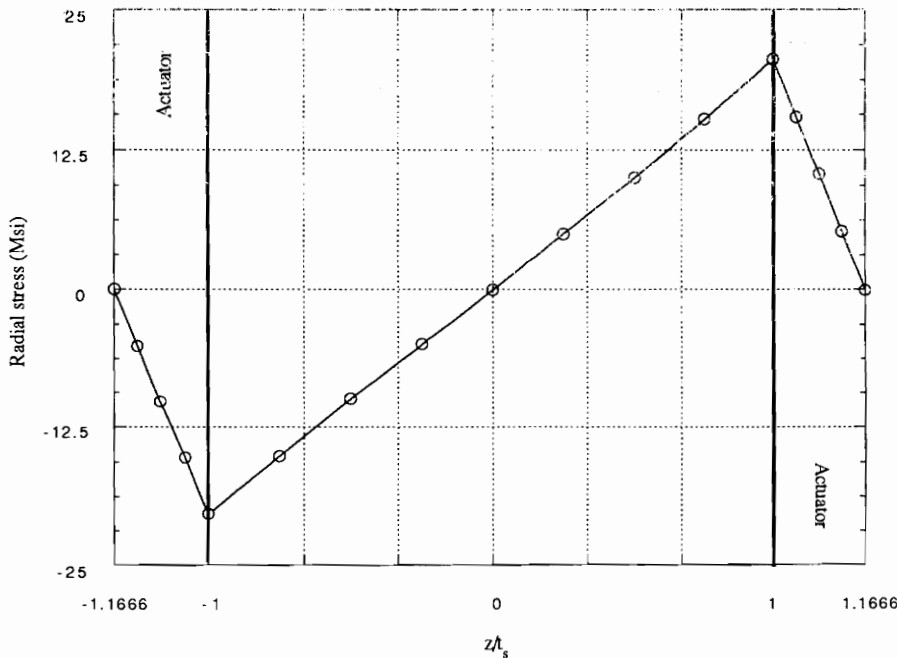


Figure 3.7 Radial stress distribution through the thickness in the actuator region.

3.4 Conclusions

In this chapter, a model to represent the action of discrete induced strain actuator patches bonded to the surface of a circular cylindrical shell is developed based on Donnell's theory. Expressions to represent the actuator forces and moments have been developed for shells and are found to be the same as those obtained for plates. However, this equivalent set of forces and moments produces a rigid body mode resulting from the non-colinearity of the tangential forces due to the shell curvature. To avoid this rigid body mode, uniform pressure is applied in the region of the actuator patch. This solution method is verified using finite element modeling and shows very good agreement.

Chapter 4

Static Modeling of In-Phase Actuation of Actuators Bonded on Ring Structures

Abstract

A closed-form model to represent the in-phase actuation of induced strain actuators bonded to the surface of a circular ring is developed. Due to the inherent shell curvature, the equivalent discrete tangential forces generally used to represent the in-phase actuation of the actuators (such as in pin-force models) are not co-linear and result in the application of rigid body forces on the shell. This non-equilibrium state violates the principle of self-equilibrium of fully integrated structures, such as piezoelectrically actuated shells. The solution to this non-equilibrium problem is to apply a uniform transverse pressure over the actuator region to maintain equilibrium. Using this adequate equivalent loading scheme for in-phase actuation, a response model for a circular ring is derived based on shell governing equations.

To verify the in-phase actuation response model, finite element analysis is performed. A perfect match between the in-phase actuation response model and the finite element results, when the actuator mass and stiffness are neglected, validates the derived analytical model. If the self-equilibrium is not maintained (point-force model), the predicted deformed shape is completely different from the actual shell response to in-phase actuation. Thus, by simply applying a uniform transverse pressure along with the discrete tangential forces in order to maintain the self-equilibrium of the shell, the shell response can be modeled accurately.

4.1 Introduction

Piezoelectric actuators have been used for active shape, vibration and acoustic control of structures because of their adaptability and light weight. Their ability to be easily integrated into structures makes them very attractive in structural control since all moving parts encountered with conventional actuators are eliminated. Structural control is obtained by simply embedding PZT

actuators in the structure or bonding them on the structure. In structural control, the desired deformation in the structure is obtained by the application of localized line forces and moments generated by the expanding or contracting bonded or embedded PZT actuators. In the case of vibration and acoustic control, the piezoelectric actuators, by the application of these line forces, will change the impedance of the structure to reduce the unwanted dynamic effects at given frequencies.

Previous research performed on PZT-actuated beam and plate structures has led to models describing their response (Crawley and de Luis, 1987; Crawley and Anderson, 1990; Dimitriadis, Fuller and Rogers, 1991; Liang, Sun, and Rogers, 1993; Wang and Rogers, 1991; Zhou, Liang and Rogers, 1994a). Simple but efficient models were proposed to describe the response of a plate structure to bonded/embedded piezoelectric actuators (Crawley and Lazarus, 1989). By simply replacing the PZT actuator with line forces and moments along its edges, very accurate results are produced even though this type of model is approximate since the mass and stiffness of the actuator is not considered. However, much less research has been done on structures with curvature. Some experimental work (Fuller et al., 1990) and adaptations of flat structure models to curved structures have been made (Lester and Lefebvre, 1991; Sonti and Jones, 1993). Some models based on shell equations have also been proposed (Larson and Vinson, 1993b; Rossi, Liang and Rogers, 1993b; Sonti and Jones, 1991; Zhou, Liang and Rogers, 1993).

In the previous chapter, the author considered the modeling of piezoelectric actuator patches on circular cylinders. When the piezoelectric actuators are actuated in-phase, it is found that the point force model used to represent the actuator creates a rigid body motion since the equivalent line forces are not collinear due to the curvature of the shell (Fig. 4.1). Since the PZT actuators are integrated within the structure, self-equilibrium must be satisfied. This equilibrium discrepancy between the actual structure and the equivalent loading scheme will produce serious errors when the shell response, based on the line force representation of the actuator, is calculated. Until now, no models take account of this non-equilibrium application of the equivalent line forces. The solution proposed to solve this problem is to apply a uniform transverse pressure over the actuator location to eliminate the rigid body mode. Good agreement between the equivalent loading model and the actual response of the piezoelectrically-actuated structure was found.

In this chapter, a model for in-phase actuation response of a piezoelectrically-actuated circular ring, which takes into account the non-collinear equivalent line forces, is proposed.

4.2 Shell Equivalent Loading Model

The first step in this paper is to repeat the conclusions established in the previous chapter. An equivalent loading scheme for shell structures was presented. It was shown that in the case of in-phase actuation, a rigid body mode was present due to the fact that the equivalent line forces N_θ are not collinear (Fig. 4.1).

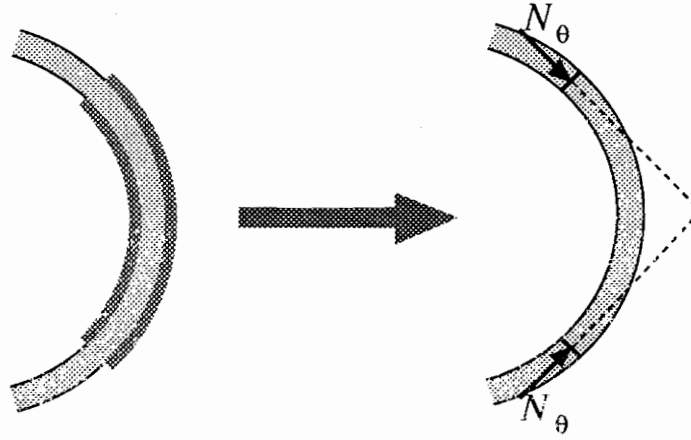


Figure 4.1 Non-equilibrium of discrete tangential forces in shell structures.

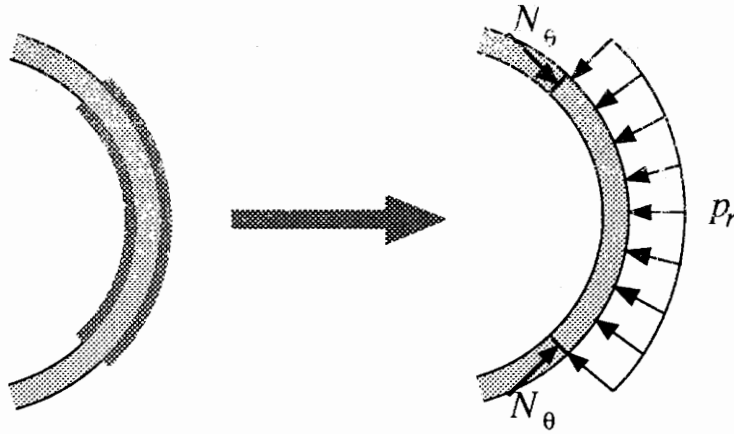


Figure 4.2 Adequate equivalent loading to maintain equilibrium.

To eliminate this non-equilibrium state of the structure, a transverse uniform pressure is added (Fig. 4.2). The magnitude of the transverse pressure from simple statics is then:

$$p_r = -\frac{N_\theta}{R}, \quad (4.1)$$

where

$$N_{\theta} = \frac{Y_s t_s}{1 - \nu} \frac{2}{2 + \psi} \Lambda \quad (4.2)$$

and

$$\psi = \frac{Y_s t_s}{Y_a t_a}, \quad (4.3)$$

when the Poisson's ratio of the shell and the piezoelectric actuator are assumed to be the same. Y , t , L and R are the Young's modulus, the thickness, the free induced strain and the radius of the ring, respectively, while the subscripts s and a stand for shell and actuator, respectively. If a circular ring is considered, the Poisson's effect disappears since there are no constraints in the axial direction. Thus, for the case of a ring, the Poisson's ratio in equation (4.2) is set to zero. Based on this equivalent loading scheme, a response model for a circular ring with two discrete tangential forces and a uniform radial pressure will be derived.

4.3 Derivation of Governing Equations

A brief overview of the governing equations of a thin ring subjected to radial pressure and discrete tangential loading will be presented (Soedel, 1981). In the case of a thin circular ring, only the in-plane stress resultants N_{θ} , M_{θ} and $Q_{\theta r}$ are present and a linear variation in the tangential direction and a constant radial displacement through the thickness are assumed (Kirchhoff's assumption, Soedel, 1981):

$$v = v^o + z\beta \quad (4.4a)$$

$$w = w^o \quad (4.4b)$$

$$\beta = \frac{1}{R} \left(v^o - \frac{\partial w^o}{\partial \theta} \right), \quad (4.4c)$$

where β is the rotational displacement and v^o and w^o are the neutral surface tangential and radial displacements, respectively.

Under those assumptions, the strain-displacement relation is:

$$\varepsilon_{\theta} = \frac{1}{R} \left(\frac{\partial v^o}{\partial \theta} + w^o \right) + \frac{z}{R^2} \left(\frac{\partial v^o}{\partial \theta} - \frac{\partial^2 w^o}{\partial \theta^2} \right) \quad (4.5)$$

The membrane force, bending moment and transverse shear force resultants are obtained by integrating the stress components through the thickness of the ring:

$$N_{\theta\theta} = \int_{-t_s/2}^{t_s/2} \sigma_{\theta} dz = \int_{-t_s/2}^{t_s/2} Y_s \varepsilon_{\theta} dz = \frac{K}{R} \left(\frac{\partial v^o}{\partial \theta} + w^o \right) \quad (4.6a)$$

$$M_{\theta\theta} = \int_{-t_s/2}^{t_s/2} \sigma_{\theta} z dz = \int_{-t_s/2}^{t_s/2} Y_s \varepsilon_{\theta} z dz = \frac{D}{R^2} \left(\frac{\partial v^o}{\partial \theta} - \frac{\partial^2 w^o}{\partial \theta^2} \right) \quad (4.6b)$$

$$Q_{\theta r} = \int_{-t_s/2}^{t_s/2} \sigma_{\theta r} dz, \quad (4.6c)$$

where the membrane and bending stiffnesses are:

$$K = Y_s t_s, \quad (4.7a)$$

$$D = \frac{Y_s t_s^3}{12}; \quad (4.7b)$$

respectively. It must be noted that the Poisson's ratio is not present in the stiffness expressions equation (4.7) since the ring is free to deform in the axial direction.

The equilibrium equations derivation is based on the energy method, using Hamilton's principle:

$$\int_{t_0}^{t_1} [\delta(U - E_b - E_L) - \delta K] dt = 0, \quad (4.8)$$

where $\delta(U - E_b - E_L)$ is the total variational potential energy and δK is the variational kinetic energy. Since the ring is subjected to static loading, the kinetic energy term is equal to zero. The Love ring equations for the equivalent loading scheme are found to be:

$$\frac{dN_{\theta\theta}}{R d\theta} + \frac{1}{R} \frac{dM_{\theta\theta}}{R d\theta} + \frac{N_{\theta}}{R} \delta(\theta - \theta_a) = 0, \quad (4.9a)$$

$$\frac{d^2 M_{\theta\theta}}{R^2 d\theta^2} - \frac{N_{\theta\theta}}{R} + p_r = 0. \quad (4.9b)$$

The derived equilibrium equations (equation (4.9)) are very similar to those obtained when a pressure loading is considered. The difference appears in the tangential line loading term $-\frac{N_\theta}{R} \delta(\theta - \theta_a)$ which replaces the $p_\theta(\theta)$ term when tangential pressure loading is considered in equation (4.9a).

Indeed, this difference occurs in the potential energy of the external line loading used in Hamilton's principle, which is given by:

$$E_L = \int_x N_\theta v^o dx. \quad (4.10)$$

Rewriting the previous equation under a double integral by introducing a Dirac function:

$$E_L = \iint_{x\theta} \left(\frac{N_\theta}{R} \delta(\theta - \theta_a) v^o \right) R d\theta dx, \quad (4.11)$$

where θ_a is the location of the applied line load. The loads are assumed to be applied on the neutral surface of the ring.

Finally, the necessary boundary conditions for the ring are:

$$N_{\theta\theta} = N_{\theta\theta}^* \text{ or } v^o = v^{o*}, \quad (4.12a)$$

$$M_{\theta\theta} = M_{\theta\theta}^* \text{ or } \beta = \beta^*, \quad (4.12b)$$

and

$$Q_\theta = Q_\theta^* \text{ or } w^o = w^{o*}. \quad (4.12c)$$

4.4 Derivation of The In-Phase Actuation Response Model

With the governing equations now derived, the next step is to apply them to the particular problem shown in Fig. 4.3. To simplify the analytical model derivation, the actuator stiffness will be neglected.

As established previously, the ring is subjected to discrete tangential forces at the end of the modeled actuator and to a uniform radial pressure of magnitude $(\frac{N_\theta}{R}$ equation (4.1)), to

ensure equilibrium of the ring. The loading of the ring is expressed using Dirac and Heaviside functions:

$$n_\theta = N_\theta [\delta^- - \delta^+] \quad (4.13)$$

$$p_r = -\frac{N_\theta}{R} [H^- - H^+], \quad (4.14)$$

where

$$\theta^- = \theta - (\pi - \theta_a) \quad (4.15a)$$

$$\theta^+ = \theta - (\pi + \theta_a) \quad (4.15b)$$

$$\delta^- = \delta[\theta^-] \quad (4.16a)$$

$$\delta^+ = \delta[\theta^+] \quad (4.16b)$$

$$H^- = H[\theta^-] \quad (4.17a)$$

$$H^+ = H[\theta^+] \quad (4.17b)$$

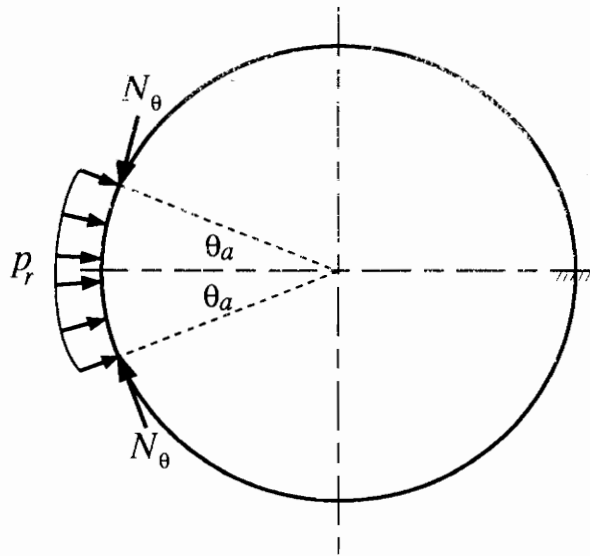


Figure 4.3 Adequate equivalent actuator loading on the ring.

The integration constants will be determined from the continuity conditions at $\theta = 0, 2\pi$:

$$w^o(0) = w^o(2\pi) \quad (4.18a)$$

$$v^o(0) = v^o(2\pi) \quad (4.18b)$$

$$\beta(0) = \beta(2\pi). \quad (4.18c)$$

From the rotational displacement expression equation (4.4c), it is possible to rewrite the continuity conditions of equation (4.18c), by making use of equation (4.18a), as:

$$w'^o(0) = w'^o(2\pi). \quad (4.18d)$$

Combining the equilibrium equations (4.9), the differential equation for the moment in the ring is obtained as follows:

$$\frac{d^3 M_{\theta\theta}}{d\theta^3} + \frac{dM_{\theta\theta}}{d\theta} = -R^2 \left[\frac{N_{\theta}}{R} + p'_r \right] = 0. \quad (4.19)$$

Substituting the loading expressions equations (4.13) and (4.14) in the previous equation (equation (4.19)), it can be seen that the right hand side of the equation will be zero. Solving the differential equation (equation (4.19)), an expression of the moment distribution in the ring is obtained:

$$M_{\theta\theta} = C_1 + C_2 \sin\theta + C_3 \cos\theta. \quad (4.20)$$

Combining the two stress-displacement equations (4.6), the following differential equation is obtained:

$$w^o(\theta) + \frac{d^2 w^o(\theta)}{d\theta^2} = \frac{R^2}{D} \left(\frac{N_{\theta\theta} D}{KR} - M_{\theta\theta} \right). \quad (4.21)$$

Rewriting the second equilibrium equation (Eq. (4.9b)):

$$N_{\theta\theta} = \frac{1}{R} \frac{d^2 M_{\theta\theta}}{d\theta^2} + R p_r. \quad (4.22)$$

Substituting the expression of the moment equation (4.20) and the tangential force equation (4.22) into equation (4.21), the following differential equation in $w^o(\theta)$ is obtained:

$$w^o(\theta) + \frac{d^2 w(\theta)}{d\theta^2} = -\frac{R^2}{D} \left[C_1 + C_2 \left(1 + \frac{D}{KR^2} \right) \sin\theta + C_3 \left(1 + \frac{D}{KR^2} \right) \cos\theta - \frac{D}{K} p_r \right]. \quad (4.23)$$

For thin rings, the $\frac{D}{KR^2}$ term is neglected since its value is much less than one. The radial displacement equation is obtained using Laplace transform:

$$w^o(\theta) = \frac{R^2}{D} \left[\begin{aligned} &C_1(1 - \cos\theta) + \frac{C_2}{2}(\sin\theta - \theta \cos\theta) + \frac{C_3}{2}(\theta \sin\theta) - \\ &\frac{DN_\theta}{KR} \left[(1 - \cos\theta^-)H^- - (1 - \cos\theta^+)H^+ \right] + w^o(0)\cos\theta + w^{o'}(0)\sin\theta \end{aligned} \right] \quad (4.24)$$

Introducing equation (4.24) in equation (4.6a), the tangential displacement differential equation is

$$\frac{dv^o(\theta)}{d\theta} = \frac{R^2}{D} \left\{ \begin{aligned} &-C_1(1 - \cos\theta) - \frac{C_2}{2}(\sin\theta - \theta \cos\theta) - \frac{C_3}{2}(\theta \sin\theta) - \\ &\frac{DN_\theta}{K} [\cos\theta^- H^- - \cos\theta^+ H^+] - w^o(0)\cos\theta - w^{o'}(0)\sin\theta \end{aligned} \right\} \quad (4.25)$$

Solving this equation using Laplace transformation and applying continuity conditions equation (4.18), the equations of the tangential and radial displacements are found to be:

$$v^o(\theta) = -\frac{RN_\theta}{K} \left\{ -\frac{\sin\theta_a}{\pi} (\sin\theta - \theta \cos\theta) + [\sin\theta^- H^- - \sin\theta^+ H^+] \right\}, \quad (4.26)$$

and

$$w^o(\theta) = -\frac{RN_\theta}{K} \left\{ \frac{\sin\theta_a}{\pi} \theta \sin\theta + [(1 - \cos\theta^-)H^- - (1 - \cos\theta^+)H^+] \right\}. \quad (4.27)$$

4.5 Finite Element Verification

The developed in-phase actuation response model is verified using finite element analysis. A ring of 6" radius, 0.032" thickness and 1" deep, and piezoelectric actuators 1/6 of the ring thickness and covering an arc 30° long ($2\theta_a$), are used. A Young modulus of 30Msi and 9.1Msi are used for the ring and the PZT actuators, respectively. Making use of symmetry, the finite element model consists of beam elements in the upper half of the ring only, as shown in Fig. 4.4. Two load cases are considered: i) temperature contraction equivalent to 1000 μ strain of the beam elements modeling the actuator region; and ii) equivalent discrete forces and uniform pressure loading from equations (4.1) and (4.2). The finite element analysis results are shown in Fig. 4.5, as well as the in-phase actuation response model results. A single curve can be observed

since the curves match perfectly. Also shown in Fig. 4.5 are the displacements of the same ring if only discrete tangential forces are applied (point force model). The point force model does not satisfy the ring's self-equilibrium. Major displacement discrepancies between the in-phase actuation response and the point force model occur both in shape and magnitude. The point force model overpredicts the displacements by a factor up to 1000. Fig. 4.6 shows the deformed shape of the self-equilibrium loading and the non-equilibrium loading with the displacements magnified

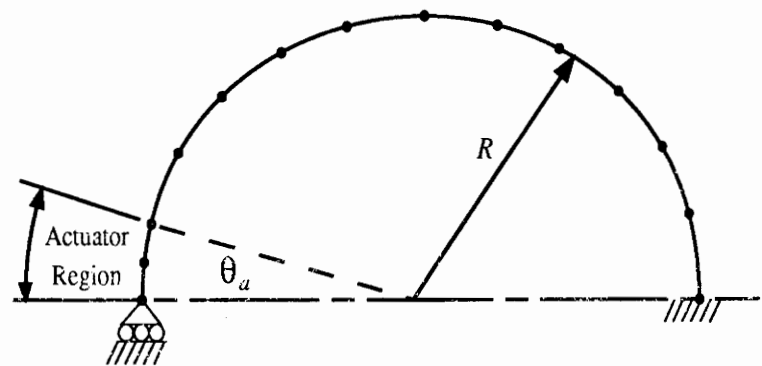


Figure 4.4 Beam finite element model.

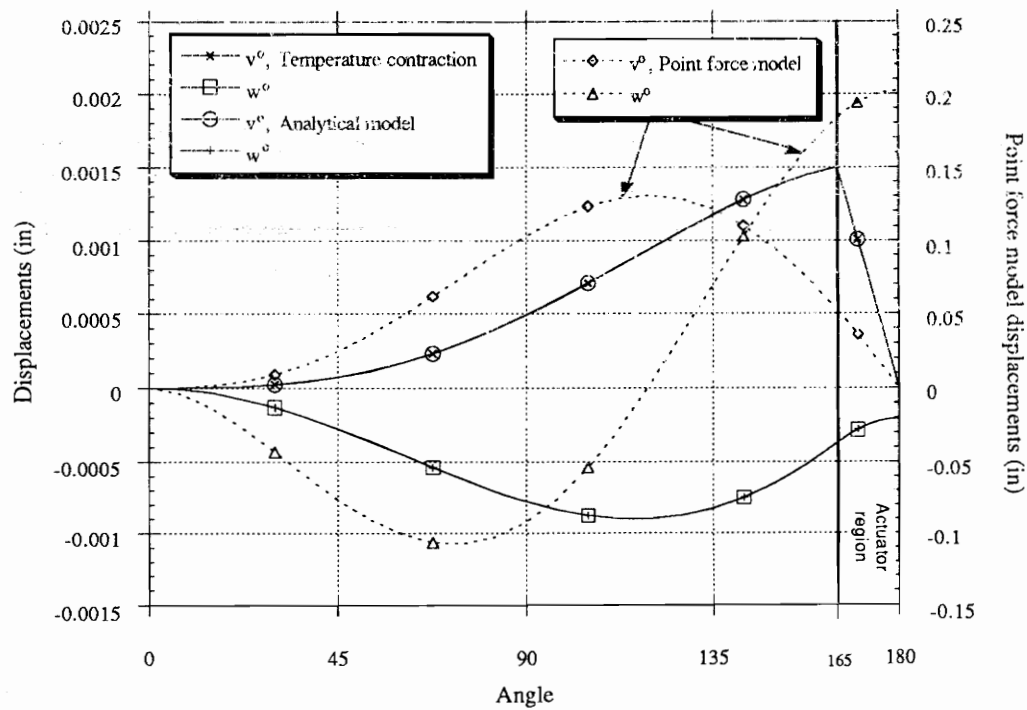


Figure 4.5 Match of displacements between the analytical model and the beam finite element model.

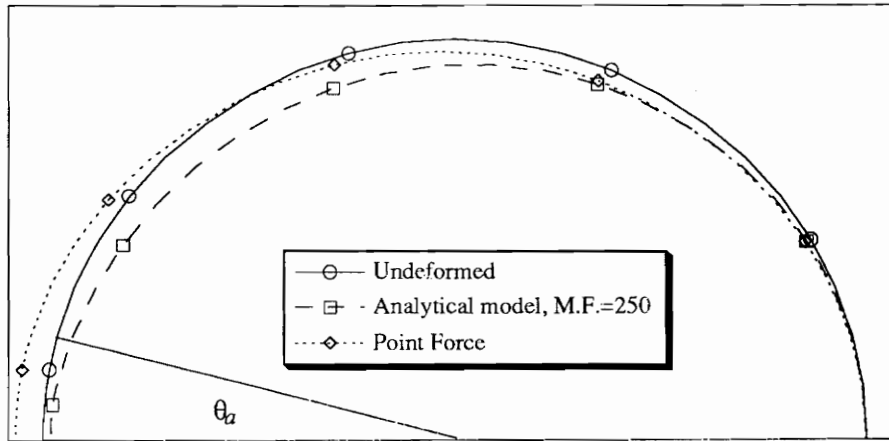


Figure 4.6 Deformed shape of the ring with and without self-equilibrium loading.

by a 250 and 1 factor, respectively. It can be seen again that when a uniform pressure is not applied to maintain equilibrium, the deformed shape is erroneous. Also, a reaction force in the x-direction at the clamped boundary condition is present if the uniform pressure is not applied. This reaction force should not be present since the actual ring with bonded actuators is in self-equilibrium. The adequate equivalent loading did not show any reaction force in the x-direction at the clamped boundary condition. The verification of the results also have been made with 10° and 60°-long piezoelectric patches, and the coincidence is still perfect between the in-phase actuation response model and the finite element analysis.

However, it must be mentioned that the response of the ring is very sensitive to the applied load in the finite element model. An error of 0.1% in the magnitude of the applied equivalent line force will completely change the response of the ring. This sensitivity of the nodal displacements is due to the low stiffness of the ring (0.032" thick only). The application of a tangential line force of 0.1% magnitude of the applied equivalent line force on the ring will produce nodal displacements of the same order as the self-equilibrium loading nodal displacements.

Also, the pressure loading must be transformed to nodal forces only (lumped loading). The lumped loading is often better for flat elements representing a curved surface (De Salvo and Swanson, 1979).

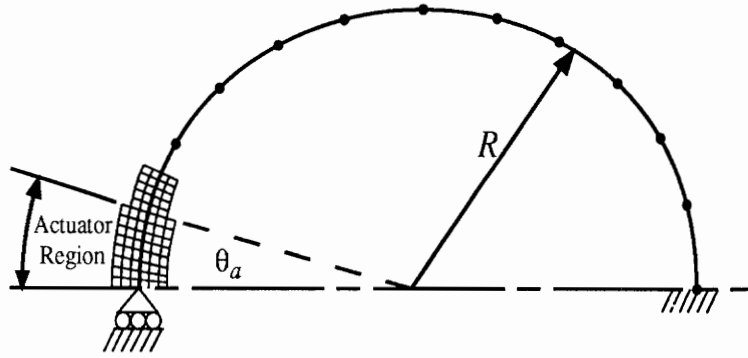


Figure 4.7 *Plane stress finite element model.*

Up to this point, the added stiffness of the actuators has been neglected both in the analytical model and the finite element analysis. A second finite element model, using plane stress elements in the actuator region to include the actuator's stiffness, is made to compare the actual behavior of the system to the derived analytical model (Fig. 4.7). To keep the FE model small, the actuator size is reduced to 10° ($2\theta_a$). The radial and tangential displacements are shown in Fig. 4.8. Disparities between the analytical model and the plane stress finite element model are present since the actuator stiffness is not neglected and no assumptions towards equivalent loading are made on the latter one. Increased actuator stiffness will further increase the disparities between the two solutions. But, it should be borne in mind that in typical applications, the actuator patches are small and add minimally to the baseline structural stiffness. Even though displacement differences are present, the plane stress finite element model validates the derived analytical model since it gives results of the same order of magnitude with similar deformed shapes as opposed to the point force model previously discussed. The deformed shape of the analytical model and the plane stress finite element model is shown in Fig. 4.9.

The discussion of in-phase actuation of induced strain actuators symmetrically bonded on shells can be extended to unsymmetric actuation. Unsymmetric actuation is obtained when the actuators on each side of the shell are submitted to voltages of different magnitudes, or when a single actuator is bonded on one side of the shell. Unsymmetric actuation is a combination of extension and bending of the shell and can be solved using simple superposition. Thus, for unsymmetric actuation, the equivalent loading will consist of discrete tangential forces and moments at the ends of the actuator(s) and a distributed transverse pressure over the actuator(s) footprint to maintain the self-equilibrium of the shell.

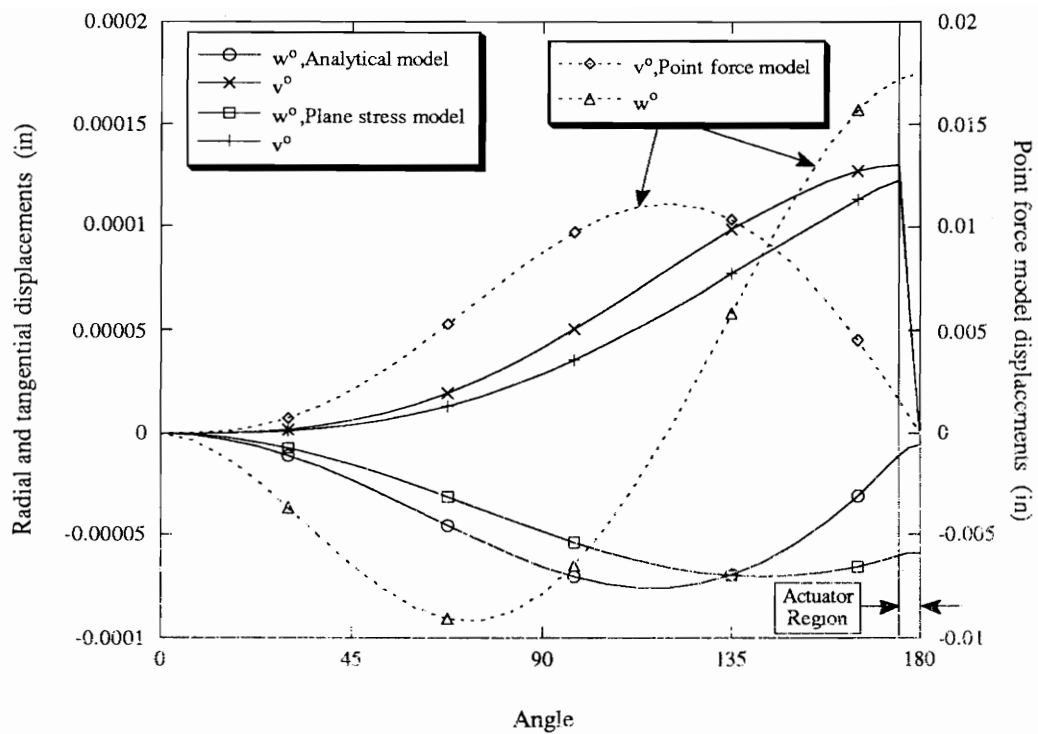


Figure 4.8 Match of displacements between the analytical model and the plane stress finite element model.

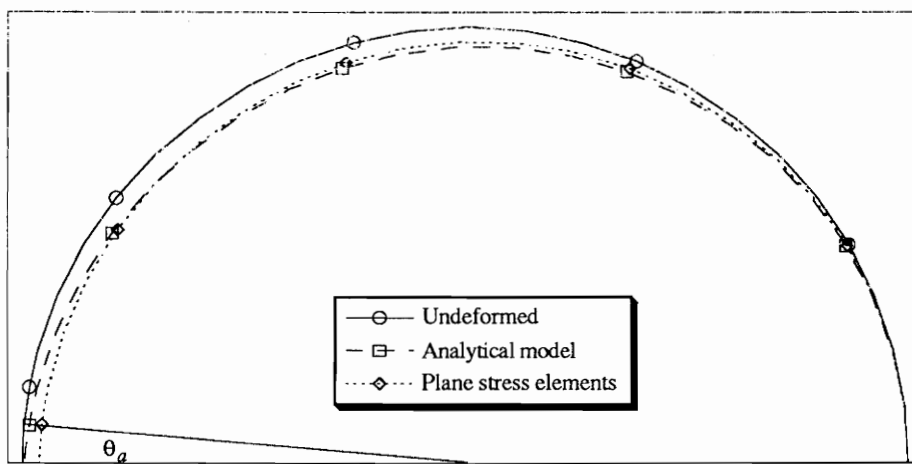


Figure 4.9 Deformed shape of the ring using the self-equilibrium loading and the plane stress elements.

4.6 Conclusions

In this chapter, a closed-form solution for a ring subjected to in-phase actuation of surface bonded strain actuators is presented. The loading used to represent the in-phase actuation consists of uniform transverse pressure and tangential line forces to maintain the self-equilibrium of the shell structure. The results of the in-phase actuation deformation model are in exact agreement with the finite element results when actuator stiffness is neglected. If the actuator stiffness is considered, the analytical model gives a good approximation of the shell's deformed shape. If the self-equilibrium is not maintained (point-force model), the predicted deformed shape is completely different from the actual shell response to in-phase actuation. Thus a uniform transverse pressure in addition to the tangential line loads is necessary to preclude rigid body motion and to obtain accurate displacement response.

Chapter 5

Impedance Modeling of Out-of-Phase Actuation of Actuators Bonded on Ring Structures

Abstract

Two impedance models representing out-of-phase actuation of induced strain actuators bonded to the surface of a circular ring are compared. The first impedance model includes the transverse shear stress, while the second model neglects it. But first, a discussion of the proper way to apply the equivalent loading due to the out-of-phase actuation is discussed. The loading due to actuation can be represented in the shell governing equations either as an induced uniform moment over the footprint of the actuators or as an external line moment at the ends of the actuators. A comparison between the impedance modeling and the more conventional static modeling approach is also made and shows convergence with the impedance models at low frequencies. A full derivation of the impedance models is included, taking great care in the structural impedance definition. A dynamic finite element analysis using piezoelectric elements available in ANSYS 5.0 is performed to verify the impedance models. The impedance model including the transverse shear stress shows an excellent match with the finite element results.

5.1 Introduction

The use of piezoelectric materials (PZT) within intelligent structures for active control of the shape and vibration has been under study for some time now. Great interest has been drawn to vibrational and acoustical control of cylindrical bodies, like aircraft fuselage and submarine hull, in the recent years. Bonding PZT actuators on the surface of the structure or embedding them within the structure will allow efficient structural control, by applying localized forces on the edges of the actuator or by changing the structural impedance. In order to simplify the analysis of piezoelectric actuated structures, models have been developed to further extend the understanding of this type of intelligent material systems. Numerous models for PZT-actuated beams and plates which describe the structural response have been proposed (Crawley and de

Luis, 1987; Crawley and Anderson, 1990; Wang and Rogers, 1991; Dimitriadis et al., 1991; Crawley and Lazarus, 1989). Adaptations of flat structure models to model curved structures (Sonti and Jones, 1991; Lester and Lefebvre, 1991) have been done. Models have also been developed using the shell governing equations (Sonti and Jones, 1993; Larson and Vinson, 1993b). All the previous models are based on the structural stiffness and do not include the dynamic effects of the system in the development of the equivalent actuator force output. An impedance model developed by Liang et al. (1993a, 1993c) includes these dynamic effects. Based on the structural impedance, the actuator force output will be frequency-dependent, and this will result in a more accurate prediction of the dynamic response. Models using the impedance approach have been proposed for beams (Liang et al., 1993b), plates (Zhou et al., 1994a) and shells (Rossi et al., 1993; Zhou et al., 1993). The essence of the impedance modeling approach is to match the actuator impedance with the structural impedance at the ends of the actuators. Based on this method, it is possible to replace the actuators with equivalent moments on the structure and not have to deal with the non-uniform structural properties. This facilitates greatly the solution of the global shell equations.

Zhou et al. (1993) studied the out-of-phase actuation of a circular cylinder with a discrete line moment applied along the edges of the actuator using modal expansion to determine the mechanical impedance and displacements. However, the transverse shear stress was neglected as a simplification. Rossi et al. (1993) studied the out-of-phase actuation of a circular ring using a uniform induced moment on the actuator footprint and the Rayleigh-Ritz method to model the mechanical impedance and displacements. However, the definition of the mechanical impedance of the structure was not appropriate in that paper: the mechanical impedance was defined as the tangential force divided by the tangential velocity at the end of the actuator bonded on the top surface of the ring only. This definition would be appropriate if a single actuator is bonded to the ring on the top surface. For out-of-phase actuation, the ring is subjected to a pure moment generated by forces applied on the ring by actuators bonded on the top and bottom surfaces of the ring. Since the forces are coupled, the force applied on the ring by the actuator on the bottom surface should also be included, since it will have an impact on the displacements on the top surface of the ring, and vice-versa (Fig. 5.1). Thus, the proper definition of the impedance based on the tangential force and the tangential velocity at the end of the actuator should be as follows:

$$\begin{Bmatrix} F_{top} \\ F_{bottom} \end{Bmatrix} = \begin{bmatrix} Z_{tt} & Z_{bt} \\ Z_{tb} & Z_{bb} \end{bmatrix} \begin{Bmatrix} \dot{v}_{top} \\ \dot{v}_{bottom} \end{Bmatrix}. \quad (5.1)$$

This equation can be simplified substituting $F_{top} = F_{bottom} = F$ for out-of-phase actuation. Also, the mechanical impedance can be defined as the moment divided by the rotational velocity at the ends of the actuator, as in Zhou et al. (1993). This latter approach will be used for its accuracy as well as its simplicity. Both impedance definitions can be shown to be equal through simple geometrical relations. Thus, corrections need to be made to the impedance model developed by Rossi et al. (1993).

In this chapter, the application of the out-of-phase actuation loading which can be included either as an induced moment distribution over the footprint of the actuator or as discrete external moments at the ends of the actuators will be discussed. Then, the impedance model derivation including the shear stress resultant will be presented and compared to the previous impedance model neglecting the shear stress resultant. The chapter will conclude with a finite element verification of the impedance models.

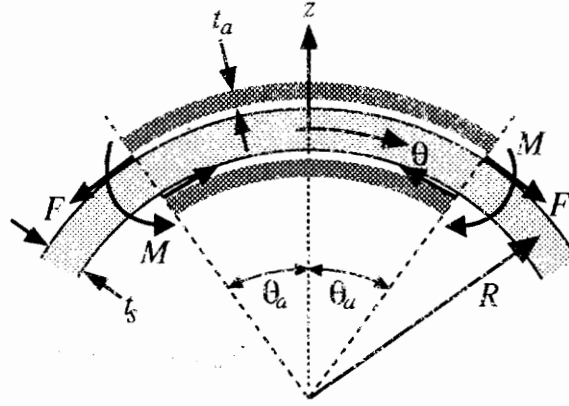


Figure 5.1 One-dimensional ring with bonded PZTactuators actuated out-of-phase.

5.2 Out-of-Phase Equivalent Loading

Before presenting the impedance model, a discussion of the appropriate method of applying the actuators loading to shell structures is required. The moment loading on the structure can be applied in two different fashions: i) induced uniform moment loading on the actuator footprint (Fig. 5.2a); ii) external line moment loading on the actuator edges (Fig. 5.2b).

Using the thin shell theory (Soedel, 1976), the equations of motion can be written in terms of the internal shell bending moment M_{xx} , $M_{x\theta}$, and $M_{\theta\theta}$, with both the actuator induced

uniform moment m_x and m_θ , and the external line moment m_x^* and m_θ^* simultaneously applied to illustrate the differences, as (note that from Soedel (1976), the external line moments, m_x^* and m_θ^* , appear on the right-hand side of the equation):

$$\frac{\partial N_{xx}}{\partial x} + \frac{\partial N_{x\theta}}{R\partial\theta} = \rho_s t_s \ddot{u}^o \quad (5.2a)$$

$$\frac{\partial N_{x\theta}}{\partial x} + \frac{\partial N_{\theta\theta}}{R\partial\theta} + \frac{I}{R} \left[\frac{\partial M_{x\theta}}{\partial x} + \frac{\partial (M_{\theta\theta} - m_\theta)}{R\partial\theta} \right] = \rho_s t_s \ddot{v}^o + \frac{m_\theta^*}{R^2} \quad (5.2b)$$

$$\frac{\partial^2 (M_{xx} - m_x)}{\partial x^2} + 2 \frac{\partial^2 M_{x\theta}}{\partial x R \partial \theta} + \frac{\partial^2 (M_{\theta\theta} - m_\theta)}{(R \partial \theta)^2} - \frac{N_{\theta\theta}}{R} = \rho_s t_s \ddot{w}^o + \frac{\partial m_x^*}{\partial x} + \frac{\partial m_\theta^*}{R^2 \partial \theta}, \quad (5.2c)$$

where the induced uniform moments can be written using Heaviside functions:

$$m_x = M_x [H(x - x_1) - H(x - x_2)] [H(\theta - \theta_1) - H(\theta - \theta_2)] \quad (5.3a)$$

$$m_\theta = M_\theta [H(x - x_1) - H(x - x_2)] [H(\theta - \theta_1) - H(\theta - \theta_2)], \quad (5.3b)$$

and the external line moments can be written using Dirac functions (Soedel, 1976):

$$m_x^* = M_x [\delta(x - x_1) - \delta(x - x_2)] [H(\theta - \theta_1) - H(\theta - \theta_2)] \quad (5.4a)$$

$$m_\theta^* = M_\theta [H(x - x_1) - H(x - x_2)] [\delta(\theta - \theta_1) - \delta(\theta - \theta_2)]. \quad (5.4b)$$

The induced uniform moments can be transferred to the right-hand side of the equations (5.2b and 5.2c), resulting in the following equations:

$$\frac{\partial N_{x\theta}}{\partial x} + \frac{\partial N_{\theta\theta}}{R\partial\theta} + \frac{I}{R} \left[\frac{\partial M_{x\theta}}{\partial x} + \frac{\partial M_{\theta\theta}}{R\partial\theta} \right] = \rho_s t_s \ddot{v}^o + \frac{I}{R} \frac{\partial m_\theta}{R\partial\theta} + \frac{m_\theta^*}{R^2} \quad (5.5b)$$

$$\frac{\partial^2 M_{xx}}{\partial x^2} + 2 \frac{\partial^2 M_{x\theta}}{\partial x R \partial \theta} + \frac{\partial^2 M_{\theta\theta}}{(R \partial \theta)^2} - \frac{N_{\theta\theta}}{R} = \rho_s t_s \ddot{w}^o + \frac{\partial^2 m_x}{\partial x^2} + \frac{\partial^2 m_\theta}{(R \partial \theta)^2} + \frac{\partial m_x^*}{\partial x} + \frac{\partial m_\theta^*}{R^2 \partial \theta}. \quad (5.5c)$$

From equation (5.5), it can be seen that whether the action of the actuators is modeled as an induced uniform moment or as an external line moment, the equations of motion are the same; the two last terms on the right hand side of the equations being equals. Thus, the moment applied by the actuators can be included in the governing equations either as induced uniform moment on the actuators footprint or as external line moments on the actuators edges.

The external line moment loading can be seen as the pin-force approach, since the

actuator is simply replaced by line moments of appropriate magnitude on the actuator edges using Dirac functions (Fig. 5.2a). For the induced uniform moment loading, the moment is not considered to be external and is included in the equilibrium equations as piezoelectricity induced loading. The moment will be uniform over the actuator footprint and is expressed using Heaviside functions (Fig. 5.2b).

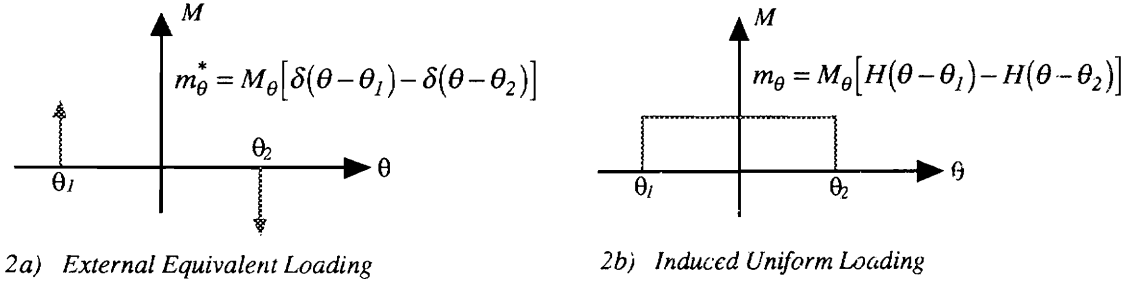


Figure 5.2 Different representations of the moment loading

In Zhou et al. (1993), the loading coming from the shear stress resultant, which is the $\frac{m_\theta^*}{R^2}$ term in equation (5.5b), is neglected compared to the tangential stress resultant. This approximation violates the static equilibrium of the system. For a thin shell, this approximation will have an increasing impact on the behavior of the structure with an increasing shell thickness. For greater accuracy and completeness, the equations including the transverse shear will be derived.

5.3 Impedance Model Derivation

In this section, a brief derivation of the impedance model based on two approaches, i.e. Rayleigh-Ritz and modal expansion, will be presented. The models will be derived for a thin circular ring with a pair piezoelectric actuators bonded on the top and bottom of the ring surface to create a pure bending moment (Fig. 5.1). The linear Love-Kirchhoff theory (Leissa, 1973; Soedel, 1981) is used since the ring is assumed to be thin. The symmetry of the system will be considered in the development of the impedance model.

5.3.1 System Dynamic Modeling

The first step in impedance modeling is to model the dynamic interaction between the actuators and the shell structure. Only the final equations are presented next (details can be found

in Rossi et al. (1993), Zhou et al. (1993) and Liang et al., (1993a)). The mechanical moment admittance is defined on the basis of the discrete applied moment and the rotational velocity at the end of the actuator (Fig. 5.1) :

$$H = -\frac{\dot{\theta}}{M_\theta} = -i\omega \frac{\theta}{M_\theta}. \quad (5.6)$$

where M_θ is the actuator output moment, which is frequency-dependent, and $\dot{\theta}$ is the rotational velocity. The minus sign indicates that the structural reactions are equal and opposite to the output force of the actuator. The induced moment created by the two actuators is simply given by (force times the distance between the actuators):

$$M_\theta = F_\theta(t_s + t_a). \quad (5.7)$$

The force output of the actuator is given by:

$$F_\theta = -\frac{Zd_{32}EY_a^E t_a}{Z + Z_a}, \quad (5.8)$$

and the short-circuit actuator mechanical impedance is:

$$Z_a = \frac{Y_a^E t_a}{i\omega} \frac{k}{\tan(kR\theta_a)}, \quad (5.9)$$

where Y_a^E is the actuator Young's modulus at constant field, d_{32} is the charge coefficient of the PZT actuator, E is the applied electrical field and k is the wave number. t_s and t_a are the structure and actuator thicknesses, respectively.

5.3.2 Determination of the Structural Impedance

The impedance calculation at the ends of the actuator can be done using two different methods: i) by solving the equations of motion by expanding the tangential and radial displacements with an appropriate assumed solutions (Rayleigh-Ritz); ii) by using the modal expansion technique (Zhou et al., 1993). The modal expansion technique leads to a formulation similar, but different, to that Rayleigh-Ritz technique. The Rayleigh-Ritz method uses trial functions which only needs to satisfy the all boundary conditions of the system. On the other hand, the modal expansion technique uses the eigenfunctions of the system which satisfies both all boundary conditions and the differential equations. If the eigenfunctions are used as trial

functions in the Rayleigh-Ritz method, the modal expansion technique and the Rayleigh-Ritz method will give the same results. When the eigenfunctions of the system are available, they should be used since they produce more accurate results. However, for complicated boundary conditions, the eigenfunctions of the system are not always available and the Rayleigh-Ritz method should be used. Brief derivations of the structural impedance for both the Rayleigh-Ritz and the modal expansion techniques are now presented. For simplicity, the equation will only be derived for a free-floating one-dimensional ring. Using the same guidelines, the structural impedance for general shells can be derived.

5.3.2.1 Structural Impedance Based on the Rayleigh-Ritz Method

The equation of motion for the ring can be written in matrix form (Soedel, 1981) as:

$$\begin{bmatrix} K \left[\frac{\partial^2}{R^2 \partial \theta^2} \right] + \frac{D}{R^2} \left[\frac{\partial^2}{R^2 \partial \theta^2} \right] & \frac{K}{R} \left[\frac{\partial}{R \partial \theta} \right] - \frac{D}{R} \left[\frac{\partial^3}{R^3 \partial \theta^3} \right] \\ -\frac{K}{R} \left[\frac{\partial}{R \partial \theta} \right] + \frac{D}{R} \left[\frac{\partial^3}{R^3 \partial \theta^3} \right] & -\frac{K}{R^2} - D \left[\frac{\partial^4}{R^4 \partial \theta^4} \right] \end{bmatrix} \begin{Bmatrix} v^o \\ w^o \end{Bmatrix} - \rho_s t_s \begin{Bmatrix} \ddot{v}^o \\ \ddot{w}^o \end{Bmatrix} = \begin{Bmatrix} \frac{m_\theta^*}{R^2} \\ \frac{1}{R} \left(\frac{\partial m_\theta^*}{R \partial \theta} \right) \end{Bmatrix}, \quad (5.10)$$

where the bending stiffness is:

$$D = \frac{Y_s t_s^3}{12} \quad (5.11a)$$

and the extensional stiffness is:

$$K = Y_s t_s. \quad (5.11b)$$

Y_s is the complex Young's modulus of the ring, and ρ_s is the density of the ring. The complex Young's modulus is used to include the damping through the structural damping factor. The Poisson's ratio is not present in the stiffness expressions due to the one-dimensional state of the ring. Taking into consideration the free floating boundary conditions of the ring, the tangential and radial neutral axes displacements, v^o and w^o , respectively, have the following assumed solutions

$$v^o(t, \theta) = \sum_{n=1}^{\infty} V_n \sin(n\theta) e^{i\alpha t} \quad (5.12a)$$

$$w^o(t, \theta) = \sum_{n=1}^{\infty} W_n \cos(n\theta) e^{i\alpha t}. \quad (5.12b)$$

Introducing the tangential and radial displacement expressions (equation 5.12) in the equation of motion (equation 5.10), a linear system of equations is obtained:

$$\begin{bmatrix} -\frac{D}{R^4}n^2 - \frac{K}{R^2}n^2 + \rho_s t_s \omega^2 & -\frac{D}{R^4}n^3 - \frac{K}{R^2}n \\ -\frac{D}{R^4}n^3 - \frac{K}{R^2}n & -\frac{D}{R^4}n^4 - \frac{K}{R^2} + \rho_s t_s \omega^2 \end{bmatrix} \begin{Bmatrix} V_n \\ W_n \end{Bmatrix} = \begin{Bmatrix} \frac{M_\theta \sin(n\theta_a)}{\pi R^2} \\ \frac{n M_\theta \sin(n\theta_a)}{\pi R^2} \end{Bmatrix}. \quad (5.13)$$

From equation 5.6, the mechanical moment admittance of the ring can be determined:

$$H = \frac{i\omega}{\pi R^3} \sum_{n=1}^{\infty} \left[\frac{\left[\frac{Kn}{R^2}(n^2 - 1) - \rho_s t_s \omega^2 \right] \sin^2(n\theta_a)}{\frac{DK}{R^6}(n^2 - 1)^2 - (n^2 + 1) \left(\frac{Dn^2}{R^4} + \frac{K}{R^2} \right) \rho_s t_s \omega^2 + (\rho_s t_s \omega^2)^2} \right]. \quad (5.14)$$

5.3.2.2 Structural Impedance Based on Modal Expansion

The structural impedance will now be calculated using the modal expansion technique. Since the ring is thin, only the dominant bending modes are used. The general solution of the response of a thin shell subjected to a uniform induced moment can be determined by solving the following Love equations (Soedel, 1976; Soedel, 1981).

$$L_2(v^o, w^o) - \rho_s t_s \ddot{v}^o = -\frac{m_\theta}{R^2} \quad (5.15a)$$

$$L_3(v^o, w^o) - \rho_s t_s \ddot{w}^o = -\frac{1}{R} \left(\frac{\partial m_\theta}{R \partial \theta} \right), \quad (5.15b)$$

where the modal expansion series solution for a free floating ring is:

$$v^o(t, \theta) = \sum_{n=2}^{\infty} p_n(t) V_n \sin(n\theta) \quad (5.16a)$$

$$w^o(t, \theta) = \sum_{n=2}^{\infty} p_n(t) W_n \cos(n\theta), \quad (5.16b)$$

where p_n is the modal participation factor. The first natural frequency ($n=1$), which is zero, corresponds to the rigid body motion mode and will not be included in the series. Making use of the eigenvalue analysis, the usual modal expansion technique yields:

$$\ddot{p}_n(t) + \omega_n^2 p_n(t) = F_n e^{i\omega t}, \quad (5.17)$$

where the forcing function F_n is:

$$F_n = \frac{1}{2\pi R \rho_s t_s} \int_0^\pi \left(\frac{1}{R} \left(\frac{\partial m_\theta^*}{R \partial \theta} \right) w^o(\theta) + \frac{m_\theta^*}{R^2} v^o(\theta) \right) R d\theta \quad (5.18)$$

The solution of the governing equation (equation (5.17)) is:

$$p_n(t) = \frac{F_n e^{i\omega t}}{\omega_n^2 - \omega^2}, \quad (5.19)$$

The radial and tangential displacements responses of the ring are thus obtained:

$$v^o(t, \theta) = -\frac{2M_\theta}{\rho_s t_s \pi R^2} \sum_{n=2}^{\infty} \left[\frac{\frac{V_n}{W_n} \left(\frac{V_n}{W_n} + n \right) \sin(n\theta_a) \sin(n\theta) e^{i\omega t}}{\left(\frac{V_n^2}{W_n^2} + 1 \right) (\omega_n^2 - \omega^2)} \right] \quad (5.21a)$$

$$w^o(t, \theta) = -\frac{2M_\theta}{\rho_s t_s \pi R^2} \sum_{n=2}^{\infty} \left[\frac{\left(\frac{V_n}{W_n} + n \right) \sin(n\theta_a) \cos(n\theta) e^{i\omega t}}{\left(\frac{V_n^2}{W_n^2} + 1 \right) (\omega_n^2 - \omega^2)} \right], \quad (5.21b)$$

where the $\frac{V_n}{W_n}$ ratio is obtained from the eigenfunction analysis of the system

$$\frac{V_n}{W_n} = \frac{\rho_s t_s \omega_n^2 - \frac{1}{R^2} \left(\frac{n^4 D}{R^2} + K \right)}{\frac{n^2}{R^2} \left(\frac{n^2 D}{R^2} + K \right)}. \quad (5.22)$$

From equation (5.6), the expression of the mechanical moment admittance is obtained:

$$H = -\frac{2i\omega}{\rho_s t_s \pi R^3} \sum_{n=2}^{\infty} \left[\frac{n \left(\frac{V_n}{W_n} + n \right) \sin^2(n\theta_a)}{\left(\frac{V_n^2}{W_n^2} + 1 \right) (\omega_n^2 - \omega^2)} \right]. \quad (5.23)$$

5.4 Theoretical Results

To verify and compare the impedance models, a case study of a circular aluminum ring with G1195 piezoelectric actuator patches bonded to its surface is made. The material and geometric properties of the system are shown in Table 5.1. Two actuator sizes of 10° and 30° arc length are used to consider the influence of the actuator size on the accuracy of the theoretical models. When the size of the PZT actuator is kept small and thin (compared to ring), the stiffness and mass loading of the actuators can be neglected in the analytical models. The results from the static approach will be compared to the impedance models.

Table 5.1 *Material and geometric properties of the PZT actuator and the aluminum ring.*

	Aluminum Ring	PZT Actuator
Young's Modulus, Pa	59.5×10^9	63×10^9
Density, kg/m^3	2647	7650
Loss factor	0.006	0.001
Piezo. Coefficient d_{32} , m/V	N/A	-166×10^{-12}
Applied electric field, V/m	N/A	2.625×10^5
Radius, cm Arc length, $^\circ$	12.475	10° and 30°
Thickness, mm	3	0.23

Figure 5.3 shows the structural impedance for the two impedance models and the actuator impedance. The lower peaks of the curves correspond to the natural frequencies of the original cylinder, as expected. Only small differences are found between the two impedance models, including or not the shear stress resultant. The impedance levels of the actuator and the structure are in the same order of magnitude at structural resonance, which indicates a good dynamic interaction between the piezoelectric actuators and the structure.

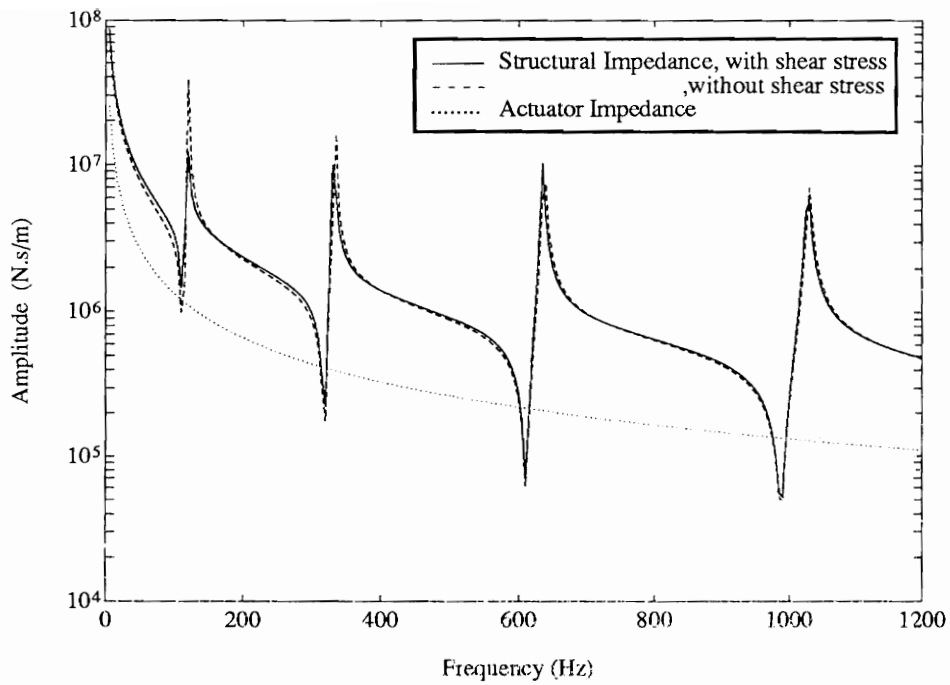


Figure 5.3 Structural impedance of the two impedance models. (10° patch)

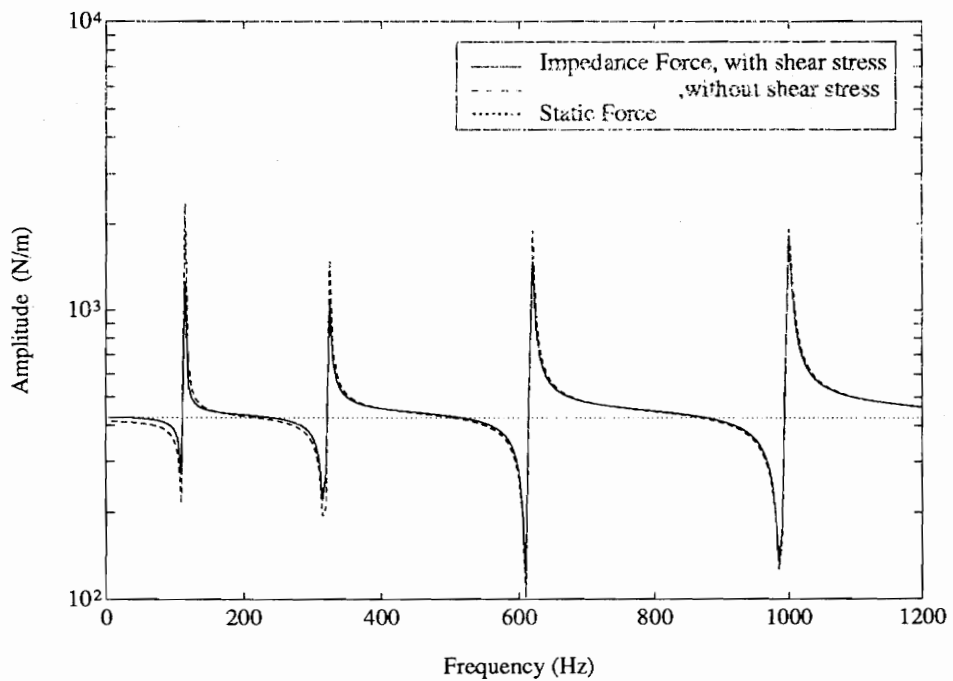


Figure 5.4 Only the actuator output force of the impedance model including shear stress converges to the static model at all frequencies. (10° patch)

The next figure (Fig. 5.4) shows the actuator output force based on the two impedance models. The dotted horizontal line is the actuator force output calculated with the static approach (Crawley and de Luis, 1988). Both models shows similar behavior, but only the impedance model including the shear stress resultant converge to the static force at low frequencies; as it should be. It can also be observed that the actuator force output is heavily dependent on the excitation frequency.

The four following figures show the radial displacement frequency response of the structure for different cases and locations. Figures 5.5 and 5.6 show the radial displacement of the ring at 30° and 90° from the actuator, respectively, for a 10° piezoceramic actuator patch. The displacements without the shear stress resultant are overestimated when compared to the case when the shear stress resultant is included in the second governing equation. At higher frequencies, the influence of the shear stress resultant is minimal, but significant at low frequencies. Thus, the inclusion of the shear stress resultant in the governing equations does not imply major complications and thus should be considered for greater accuracy. Figure 5.7 shows the radial displacement frequency response at 90° for a larger piezoceramic actuator patch (30°). The same conclusions can be drawn on the influence of the shear stress resultant. Finally, a case study of a larger radius ring is presented in Fig. 5.8. An increased radius or a reduced ring thickness will decrease the shear stress level in the structure. Once again, above the third resonant mode, the shear stress resultant have small impact on the structural response. At lower frequencies, the differences are still present but are smaller. The dotted lines are from the finite element analysis which will be discussed next.

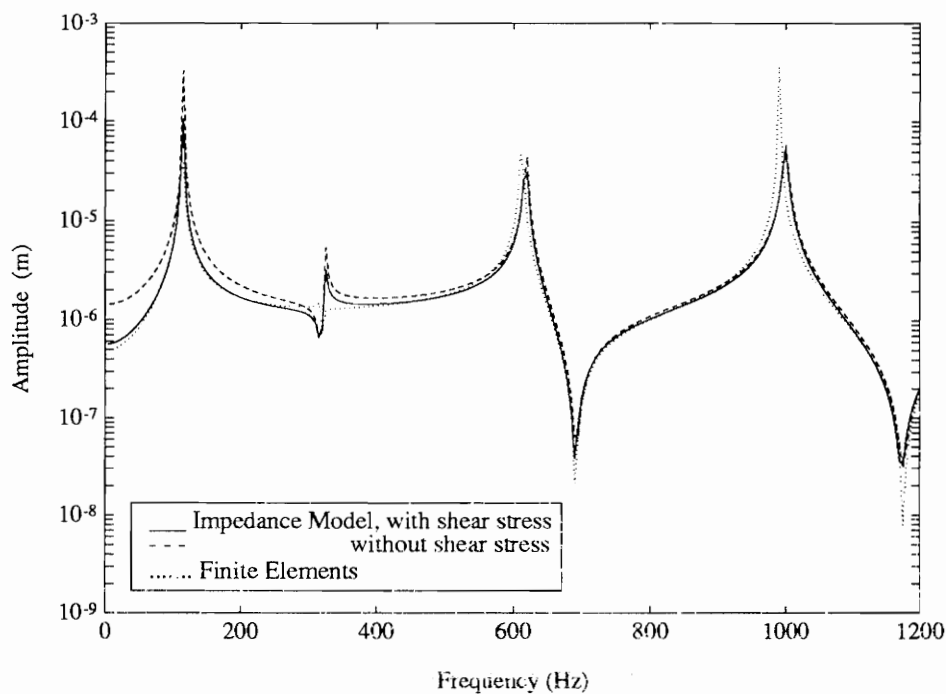


Figure 5.5 Impedance and finite element models frequency response at 30° from the actuators. (10° patch)

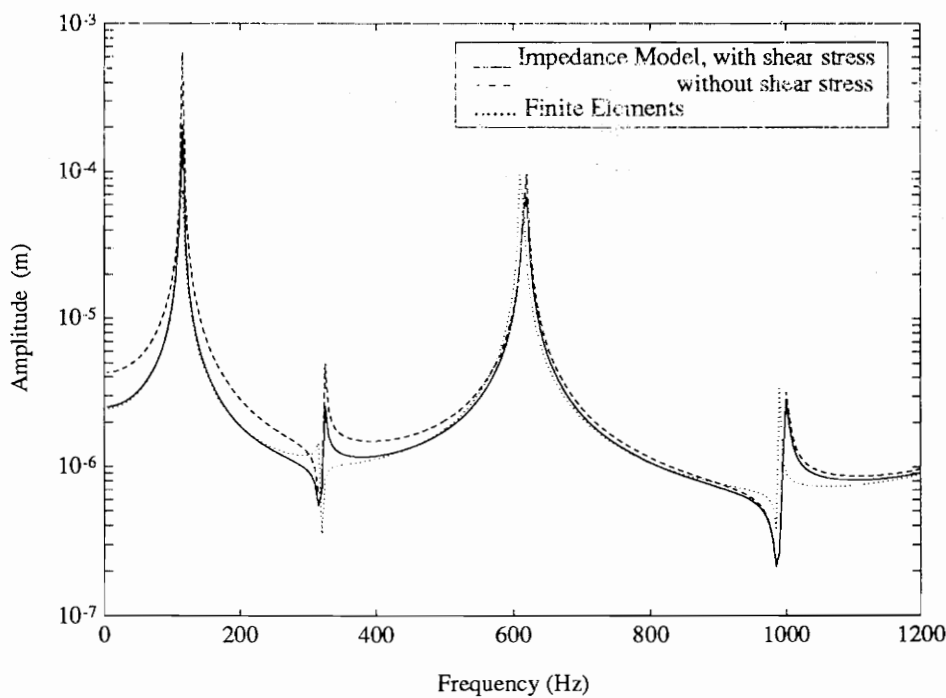


Figure 5.6 Impedance and finite element models frequency response at 90° from the actuators. (10° patch)

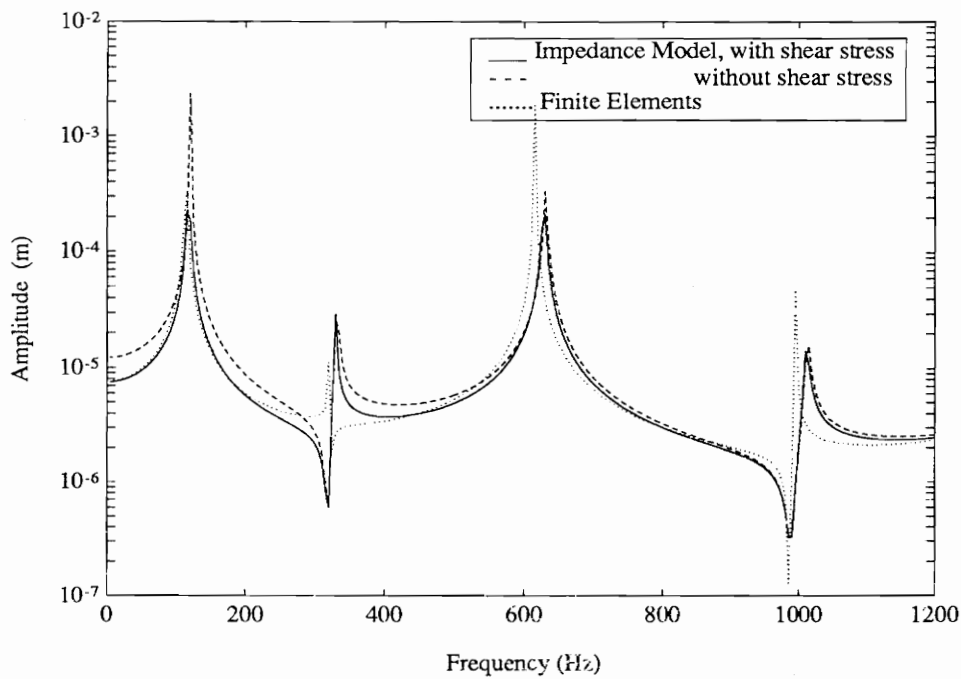


Figure 5.7 Frequency response at 90° from the actuators with larger actuators. (30° patch)

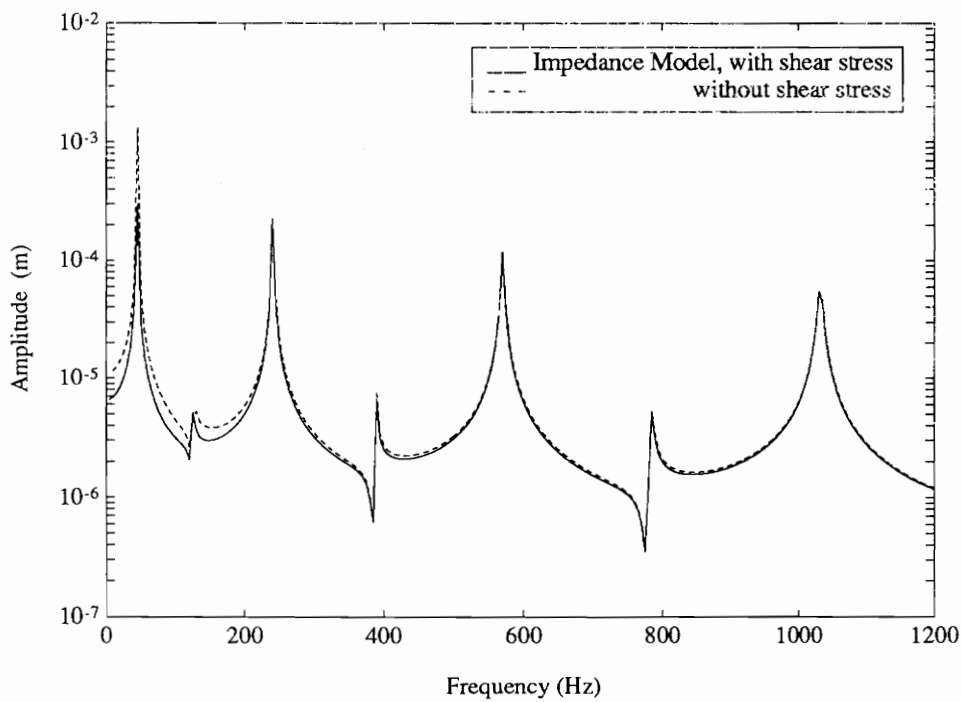


Figure 5.8 Frequency response at 90° from the actuators with larger shell radius. (10° patch)

5.5 Finite Element Verification

The impedance models developed have been verified using finite elements. A dynamic analysis was performed using piezoelectric elements available in ANSYS 5.0. Making use of symmetry, the finite element model consists of structural plane stress elements for the ring, and the actuator is modeled with plane stress piezoelectric elements (Fig. 5.9). The impedance models used free floating boundary conditions, as well as the dynamic finite element model. In the modeling of the piezoelectric elements, great care must be taken in the input of the piezoelectric material properties to obtain accurate results.

The frequency response of the ring using finite elements at 30° and 90° from the actuators are shown in Figs. 5.5 and 5.6 (dotted lines) along with the impedance models' frequency responses. Both at 30° and 90° , the frequency response of the impedance model match with great accuracy the dynamic finite element analysis. The finite element natural frequencies are a little lower than the ones obtained from the impedance models due to the increased stiffness provided by the actuators in the finite element model. With an increasing actuator size, this discrepancy increases too. For a larger piezoceramic actuator (Fig. 5.7), the match between the finite element analysis and the theoretical models is still very good, even though small discrepancies are present due to the increased mass and stiffness of the actuators and due to the assumptions made in the impedance modeling.

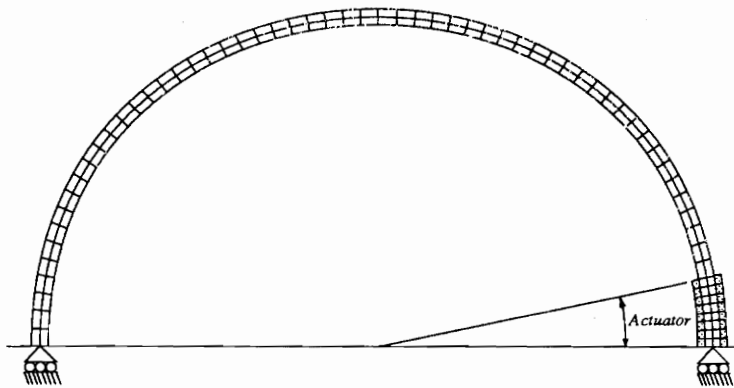


Figure 5.9 *Finite Element Model.*

The next step is to look at the structural response at low frequency (5 Hz) where the response of the ring will be similar to the static response. The radial and tangential displacement amplitudes are shown in Figure 5.10. The displacements predicted by the impedance models shows an excellent match with the finite element results. The deformed shape of the ring is

shown in Figure 5.11. As noted earlier, the impact of neglecting the shear stress resultant is significant. Differences of up to 75% in the displacements are obtained when the shear stress resultant is ignored. However, the difference only shows in magnitude, the deformed shape of the ring being the same.

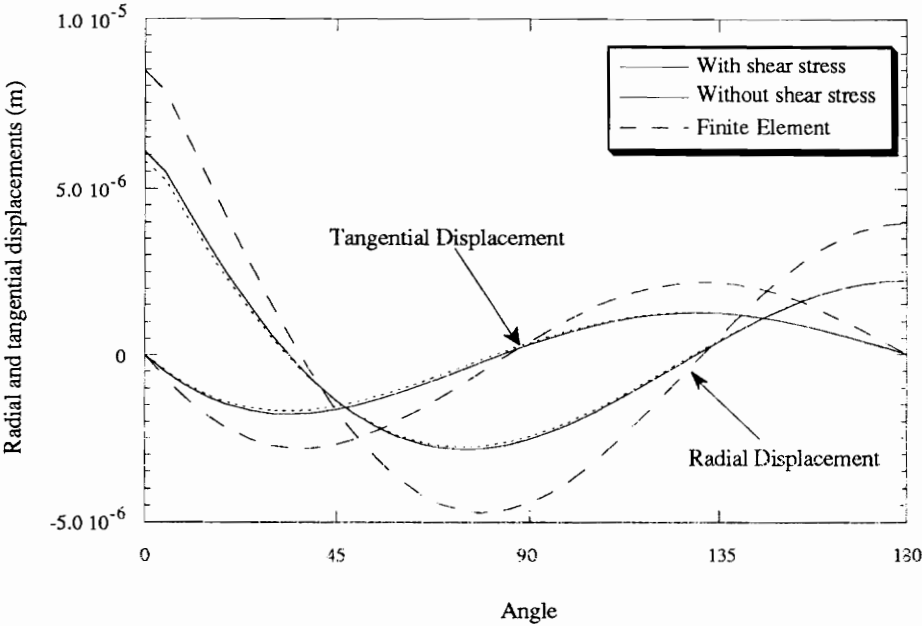


Figure 5.10 Impedance models and finite element displacements under dynamic loading at 5 Hz.

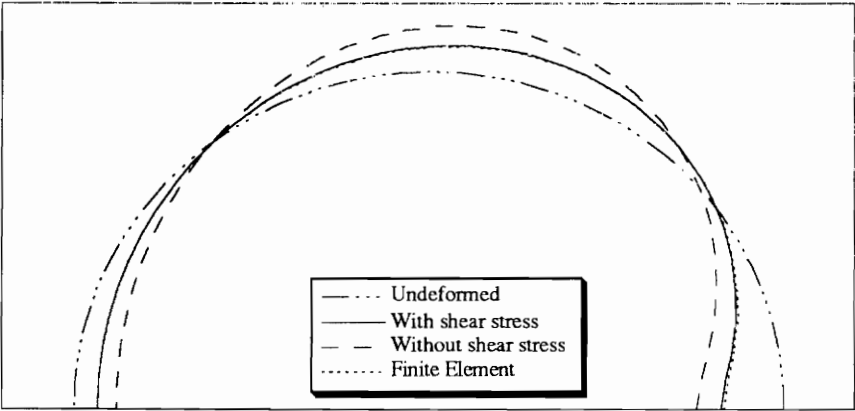


Figure 5.11 Dynamic deformed shape of the impedance models and the finite element model at 5 Hz.

The final step is to look at the response of the ring at higher frequency, i.e., 500 Hz, where the fourth mode is dominant. Figure 5.12 shows the radial and tangential displacement amplitudes. The displacements predicted by the impedance models are still in excellent agreement with the finite element results.

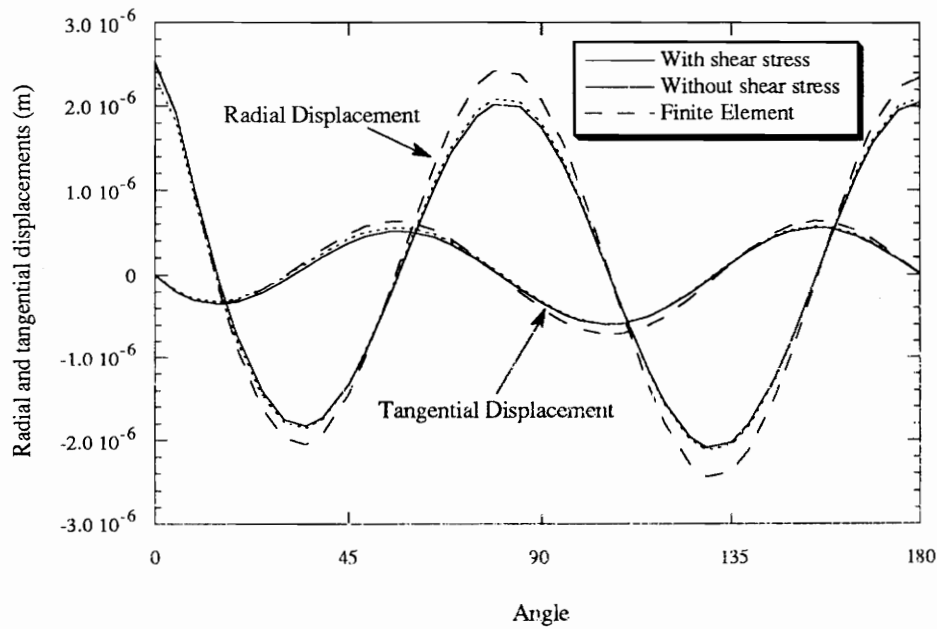


Figure 5.12 Impedance models and finite element displacements under dynamic loading at 500 Hz.

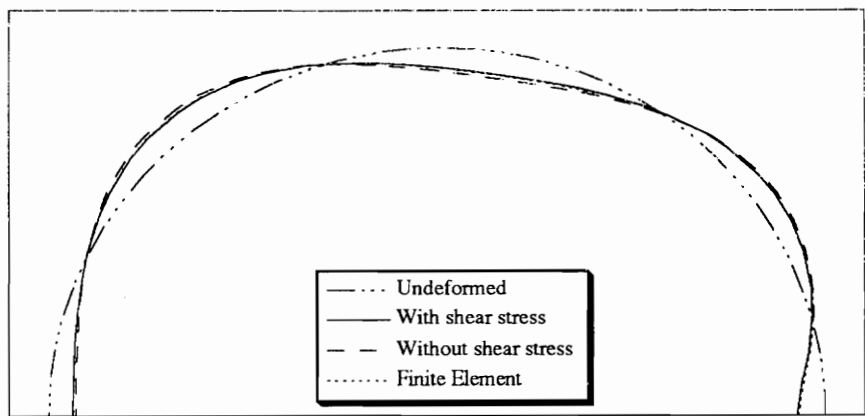


Figure 5.13 Dynamic deformed shape of the impedance models and the finite element model at 500 Hz.

5.6 Conclusions

Two impedance models to represent out-of-phase actuation of induced strain actuators bonded to the surface of a circular ring have been compared. The first impedance model includes the transverse shear stress, while the second model ignores it. Based on the shell governing equations, it was shown that the moment produced by the actuators can be included in the governing equations either as an induced uniform moment on the actuators footprint or as an external line moment on the actuator's edge. Impedance models for ring structures, based on Rayleigh-Ritz and modal expansion, were developed and applied to a particular case. The impedance model ignoring the shear stress resultant showed a significantly different response at low frequencies when compared to the full impedance model. The analytical results were verified using a dynamic finite element analysis with piezoelectric elements available in ANSYS 5.0. The impedance model including the shear stress resultant gives an excellent prediction of the structural response when compared to the finite element model.

Chapter 6

Impedance Modeling of In-Phase Actuation of Actuators Bonded on Ring Structures

Abstract

An impedance model to describe the in-phase actuation of induced strain actuators bonded to the surface of a circular ring has been developed. The essence of the impedance approach is to match the actuator impedance with the structural impedance at the ends of the actuators. This approach enables the model to include the dynamic effects of the system. Impedance modeling is based on the Rayleigh-Ritz method of represent the structural response of shells. The appropriate representation of the loading due to in-phase actuation is discussed. To verify the impedance model, dynamic finite element analysis has been performed using piezoelectric elements available in ANSYS 5.0. A good correlation between the finite element results and the impedance model validates the analytical solution. A comparison between the impedance model and the more conventional static modeling approach is also made. The convergence of the impedance model displacements to the static model displacements at low frequencies further validates the derived impedance model.

6.1 Introduction

Piezoelectric actuators have been used for active shape, vibration, and acoustic control of structures because of their adaptability and light weight. Their ability to be easily integrated into structures makes them very attractive in structural control since all of the moving parts encountered with conventional actuators are eliminated. Structural control is achieved by simply embedding PZT actuators in the structure or bonding them on the surface of the structure. In structural control, the desired deformation in the structure is obtained by the application of localized line forces and moments generated by the expanding or contracting bonded or embedded PZT actuators. In the case of vibration and acoustic control, the piezoelectric actuators

will change the apparent impedance of the structure at the disturbance location, which will reduce the unwanted dynamic effects in the structure.

Previous research performed on PZT-actuated beam and plate structures has led to models describing their response (Crawley and de Luis, 1987; Crawley and Anderson, 1990; Wang and Rogers, 1991; Dimitriadis et al., 1991; Zhou et al., 1994a; Liang et al., 1993b). Other simple but efficient models were also proposed to describe the response of a plate structure to the piezoelectric actuators (Crawley and Lazarus, 1989; Hagood et al., 1991). By simply replacing the PZT actuator with line forces and moments on its edges, very accurate results are achieved even though this type of model is approximate since the mass and stiffness of the actuator is not considered. However, much less research has been performed on structures with curvature. Some experimental work (Fuller et al., 1990) and adaptations of flat structure models to curved structures have been made (Sonti and Jones, 1991; Lester and Lefebvre, 1991). Models based on shell equations have also been proposed (Rossi et al., 1993; Sonti and Jones, 1993; Zhou et al., 1993; Larson and Vinson, 1993b). All these models were developed for out-of-phase actuation of the PZT actuators. Less extensive work has been done on in-phase actuation of shells (see Chapters 3 and 4) (Lester and Lefebvre, 1991; Sonti and Jones, 1993). In-phase actuation refers to the case when the actuators bonded on the top and on the bottom of the structure expand or contract together.

In this chapter, a discussion of the appropriate representation of the equivalent in-phase loading for shells is first done. Then, an impedance model of a circular ring actuated in-phase, based on the Rayleigh-Ritz method, is derived. This is followed by a case study and a finite element verification of the theoretical results.

6.2 In-Phase Equivalent Loading

In chapter 3, the modeling of piezoelectric actuator patches on circular cylinders was considered. When the piezoelectric actuators are actuated in-phase, it is found that the point force model used to represent the actuator creates a rigid body motion since the equivalent line forces are not collinear due to the curvature of the shell (Fig. 6.1). Since the PZT actuators are integrated within the structure, self-equilibrium must be satisfied.

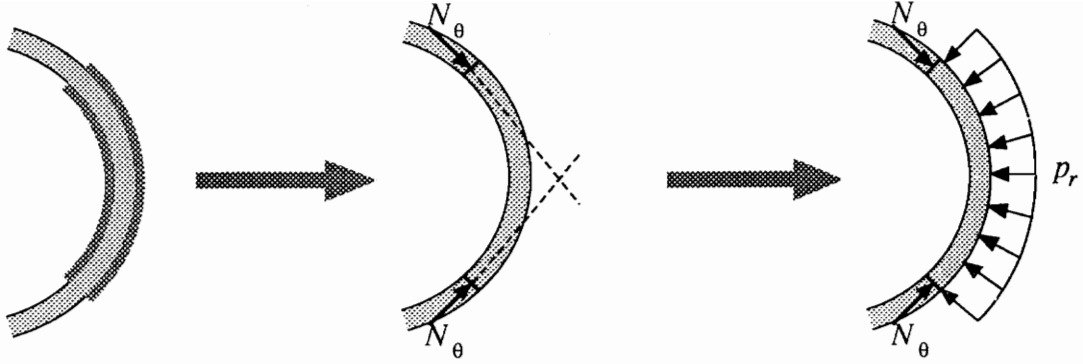


Figure 6.1 Equivalent loading to maintain self-equilibrium of the shell structure.

To eliminate this non-equilibrium state of the structure, a transverse uniform pressure is added (Fig. 6.1). The magnitude of the transverse pressure from simple statics is then:

$$p_r = -\frac{N_\theta}{R}, \quad (6.1)$$

where

$$N_x = N_\theta = \frac{Y_s t_s}{1 - \nu} \frac{2}{2 + \psi} \Lambda \quad (6.2)$$

and

$$\psi = \frac{Y_s t_s}{Y_a t_a}, \quad (6.3)$$

when the Poisson's ratio of the shell and the piezoelectric actuator are assumed to be the same. Y , t , L and R are the Young's modulus, the thickness, the free induced strain and the radius of the ring, respectively, while the subscripts s and a stand for shell and actuator, respectively. If a circular ring is considered, the Poisson's effect disappears since there are no constraints in the axial direction. Thus, for the case of a ring, the Poisson's ratio in equation (6.2) is set to zero. This equivalent loading, used to represent in-phase actuation, is included in the shell governing equations as external loading. Another approach to include the in-phase actuation loading is to consider an induced uniform loading on the actuator footprint.

Using the thin shell theory of a circular cylinder (Soedel, 1976), the equations of motion can be written in terms of the internal shell membrane forces, N_{xx} , $N_{x\theta}$, and $N_{\theta\theta}$, with both the actuator-induced tangential and axial forces, n_x and n_θ , as:

$$\frac{\partial(N_{xx} - n_x)}{\partial x} + \frac{\partial N_{x\theta}}{R\partial\theta} = \rho_s t_s \ddot{u}^o \quad (6.4a)$$

$$\frac{\partial N_{x\theta}}{\partial x} + \frac{\partial(N_{\theta\theta} - n_\theta)}{R\partial\theta} + \frac{1}{R} \left[\frac{\partial M_{x\theta}}{\partial x} + \frac{\partial M_{\theta\theta}}{R\partial\theta} \right] = \rho_s t_s \ddot{v}^o \quad (6.4b)$$

$$\frac{\partial^2 M_{xx}}{\partial x^2} + 2 \frac{\partial^2 M_{x\theta}}{\partial x R \partial \theta} + \frac{\partial^2 M_{\theta\theta}}{(R\partial\theta)^2} - \frac{(N_{\theta\theta} - n_\theta)}{R} = \rho_s t_s \ddot{w}^o, \quad (6.4c)$$

where the discrete induced uniform tangential and axial forces can be written using Heaviside functions:

$$n_x = N_x [H(x - x_1) - H(x - x_2)] [H(\theta - \theta_1) - H(\theta - \theta_2)] \quad (6.5a)$$

$$n_\theta = N_\theta [H(x - x_1) - H(x - x_2)] [H(\theta - \theta_1) - H(\theta - \theta_2)]. \quad (6.5b)$$

The induced uniform tangential and axial forces can be transferred to the right-hand side of the equation:

$$\frac{\partial N_{xx}}{\partial x} + \frac{\partial N_{x\theta}}{R\partial\theta} = \rho_s t_s \ddot{u}^o + \frac{\partial n_x}{\partial x} \quad (6.6a)$$

$$\frac{\partial N_{x\theta}}{\partial x} + \frac{\partial N_{\theta\theta}}{R\partial\theta} + \frac{1}{R} \left[\frac{\partial M_{x\theta}}{\partial x} + \frac{\partial M_{\theta\theta}}{R\partial\theta} \right] = \rho_s t_s \ddot{v}^o + \frac{\partial n_\theta}{R\partial\theta} \quad (6.6b)$$

$$\frac{\partial^2 M_{xx}}{\partial x^2} + 2 \frac{\partial^2 M_{x\theta}}{\partial x R \partial \theta} + \frac{\partial^2 M_{\theta\theta}}{(R\partial\theta)^2} - \frac{N_{\theta\theta}}{R} = \rho_s t_s \ddot{w}^o - \frac{n_\theta}{R} \quad (6.6c)$$

Writing the same shell governing equations, but including the equivalent external loading (axial and tangential line forces (n_x^* and n_θ^*) and uniform radial pressure (p_r^*) (Soedel, 1976):

$$\frac{\partial N_{xx}}{\partial x} + \frac{\partial N_{x\theta}}{R\partial\theta} = \rho_s t_s \ddot{u}^o + n_x^* \quad (6.7a)$$

$$\frac{\partial N_{x\theta}}{\partial x} + \frac{\partial N_{\theta\theta}}{R\partial\theta} + \frac{1}{R} \left[\frac{\partial M_{x\theta}}{\partial x} + \frac{\partial M_{\theta\theta}}{R\partial\theta} \right] = \rho_s t_s \ddot{v}^o + \frac{n_\theta^*}{R} \quad (6.7b)$$

$$\frac{\partial^2 M_{xx}}{\partial x^2} + 2 \frac{\partial^2 M_{x\theta}}{\partial x R \partial \theta} + \frac{\partial^2 M_{\theta\theta}}{(R\partial\theta)^2} - \frac{N_{\theta\theta}}{R} = \rho_s t_s \ddot{w}^o + p_r^*, \quad (6.7c)$$

where the external equivalent loading can be written using Dirac functions:

$$n_x^* = N_x [\delta(x - x_1) - \delta(x - x_2)] [H(\theta - \theta_1) - H(\theta - \theta_2)] \quad (6.8a)$$

$$n_\theta^* = N_\theta [H(x - x_1) - H(x - x_2)] [\delta(\theta - \theta_1) - \delta(\theta - \theta_2)] \quad (6.8b)$$

$$p_r^* = -\frac{N_\theta}{R} [H(x - x_1) - H(x - x_2)] [H(\theta - \theta_1) - H(\theta - \theta_2)]. \quad (6.8c)$$

From equations (6.6) and (6.7), it can be seen that whether induced uniform tangential and axial forces or external equivalent loading is used alone, the equations of motion are the same. Thus, the tangential and axial forces produced by the actuators can be included in the governing equations either as induced uniform membrane forces on the actuators' footprint or as external equivalent loading on the actuators' edges

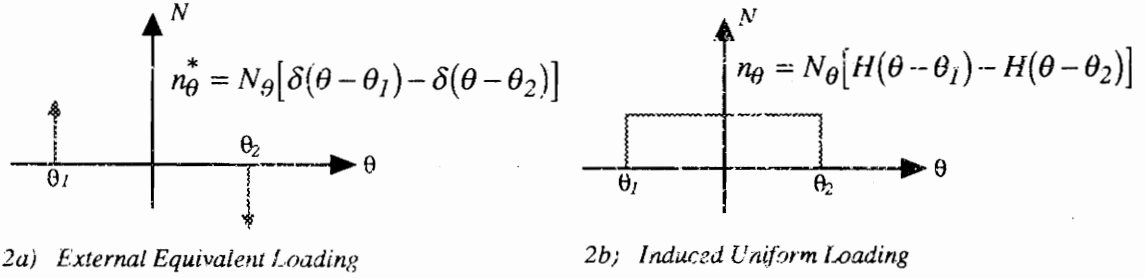


Figure 6.2 Different representations of the loading.

The external equivalent loading can be seen as the pin-force approach, since the actuator is simply replaced by line forces of appropriate magnitude on the actuator edges using Dirac functions (Fig. 6.2a) along with the uniform pressure to maintain self-equilibrium. The induced uniform loading is closely related to the equation derivation proposed by Dimitriadis et al. (1991). The induced uniform tangential and axial forces are not considered to be external and are included in the equilibrium equations in a similar fashion to thermal loading. The induced forces will be uniform over the actuator footprint and will be expressed using Heaviside functions (Fig. 6.2b).

6.3 Impedance Model Derivation

An impedance model of a free floating thin cylindrical ring excited in-phase by a pair of PZT actuators has been derived (Fig. 6.3). The PZT patches are assumed to be perfectly bonded to the structure so that the action of the PZT actuators can be replaced by discrete line forces on

the edges of the actuators. The linear Love-Kirchoff theory (Leissa, 1973; Soedel, 1981) is used since the ring is assumed to be thin and the stress distribution through the thickness of the actuators will be assumed constant.

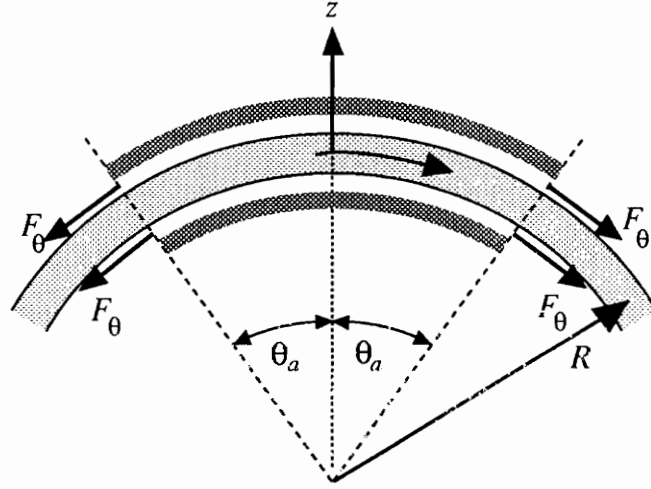


Figure 6.3 One-dimensional ring with bonded pzt actuators actuated in-phase.

The structural impedance is defined on the basis of discrete applied loads and velocities at the ends of the actuator. The mechanical admittance (H) and impedance (Z) can be defined as:

$$F_{\theta} = -Z\dot{v}^{\theta} = -\frac{\dot{v}^{\theta}}{2H}, \quad (6.9)$$

where the minus sign in the previous equation is necessary to take account of the opposite or negative reactions of the structure to the output forces of the actuators and \dot{v}^{θ} and \dot{w}^r are the midplane tangential and radial velocities, respectively. Since there are two actuators, a factor of 2 needs to be included in equation (6.9) for the structural impedance definition.

6.3.1 System Dynamic Modeling

In this section, the dynamic interaction between the actuators and the shell structure is under study. The essence of impedance modeling is to match the structural impedance with the actuator's impedance at its ends; the dynamic actuator force output is thus obtained.

The actuators bonded on the shell are excited in-phase by applying an electric field in the radial polarization direction. Under Love's assumptions for thin shells, the equation of motion of a shell vibrating in the tangential direction can be expressed as:

$$\rho_a \ddot{v}^o(t, \theta) = Y_a^E \frac{\partial \varepsilon_\theta}{R \partial \theta}, \quad (6.10)$$

where ρ_a is the PZT density and Y_a^E is the PZT complex Young's modulus at zero electric field, such that the mechanical dissipation of the actuator can be included.

The piezoelectric actuator patch is thin and has a large radius of curvature with a limited length in the tangential direction. In other words, the actuator's patches are almost flat. These characteristics enable us to simplify the problem by assuming the actuators to be flat and the strain-displacement relation is given by equation (6.11). As a practical matter, for practical cases, the bending of the flat PZT actuator patches on the structure is very limited due to the brittle nature of piezoelectric material.

$$\varepsilon_\theta = -\frac{\partial v^o(t, \theta)}{R \partial \theta} \quad (6.11)$$

Thus, the following equation of motion in the tangential direction will be used:

$$\rho_a \ddot{v}^o(t, \theta) = Y_a^E \frac{\partial^2 v^o(t, \theta)}{R^2 \partial \theta^2}. \quad (6.12)$$

Solving equation (6.12) and assuming harmonic excitation by separating the displacement into time and spatial domain, the tangential displacement response of the actuator is given by:

$$v^o(t, \theta) = [A \sin kR\theta + B \cos kR\theta] e^{i\omega t}, \quad (6.13)$$

where ω is the input angular velocity, and the wave number is given by:

$$k^2 = \omega^2 \frac{\rho_a}{Y_a^E}. \quad (6.14)$$

Using the constitutive equations of the PZT actuator and applying the proper boundary conditions (Rossi et al. 1993; Zhou et al. 1993), the actuator force output of the actuator at θ_a is given by:

$$F_\theta = -2 \frac{Z|_{\theta_a} d_{32} E t_a Y_a^E}{Z|_{\theta_a} + Z_a}, \quad (6.15)$$

where the short-circuit actuator mechanical impedance (Liang et al., 1993b) is:

$$Z_a = \frac{Y_a^E t_a k}{i \omega \tan kR\theta_a}. \quad (6.16)$$

with d_{32} and E being the piezoelectric constant of the actuators and the electric field applied to the actuators, respectively.

At this point, the impedance characteristics of the actuator and the structure have been used to calculate the dynamic tangential force. The actuator impedance is known (equation (6.16)), but the structural impedance remains unknown. The next step is to calculate the structural impedance of a circular cylinder submitted to the equivalent loading of in-phase actuation.

6.3.2 Determination of the Structural Impedance

Using thin shell theory, the equations of motion of a circular ring submitted to the in-phase equivalent loading (Soedel, 1981; Chapter 3) can be written in matrix form:

$$\begin{bmatrix} K \left[\frac{\partial^2}{R^2 \partial \theta^2} \right] + \frac{D}{R^2} \left[\frac{\partial^2}{R^2 \partial \theta^2} \right] & \frac{K}{R} \left[\frac{\partial}{R \partial \theta} \right] - \frac{D}{R} \left[\frac{\partial^3}{R^3 \partial \theta^3} \right] \\ -\frac{K}{R} \left[\frac{\partial}{R \partial \theta} \right] + \frac{D}{R} \left[\frac{\partial^3}{R^3 \partial \theta^3} \right] & -\frac{K}{R^2} - D \left[\frac{\partial^4}{R^4 \partial \theta^4} \right] \end{bmatrix} \begin{Bmatrix} v^o \\ w^o \end{Bmatrix} - \rho_s t_s \begin{Bmatrix} \ddot{v}^o \\ \ddot{w}^o \end{Bmatrix} = \begin{Bmatrix} \frac{\partial n_\theta}{R \partial \theta} \\ -\frac{n_\theta}{R} \end{Bmatrix} \quad (6.17)$$

The bending stiffness is:

$$D = \frac{Y_s t_s^3}{12}, \quad (6.18)$$

and the extensional stiffness is:

$$K = Y_s t_s. \quad (6.19)$$

The Poisson ratio is not present in the stiffnesses expressions due to the one-dimensional state of the ring.

Assuming harmonic excitation of the actuators, the tangential and radial midplane displacements, v^o and w^o , respectively, will thus have the following Rayleigh-Ritz assumed solutions (Meirovitch, 1986):

$$v^o(t, \theta) = \sum_{n=0}^{\infty} V_n \sin(n\theta) e^{i\omega t} \quad (6.20)$$

$$w^o(t, \theta) = \sum_{n=0}^{\infty} W_n \cos(n\theta) e^{i\omega t}. \quad (6.21)$$

Introducing the tangential and radial displacement expressions (equations (6.20) and (6.21)) in the equations of motion (equation (6.17)), a linear system of equations is obtained:

$$[C] \begin{Bmatrix} V_n \\ W_n \end{Bmatrix} = -\frac{2F_\theta \sin(n\theta_a)}{\pi R} \begin{Bmatrix} \frac{1}{l} \\ \frac{1}{n} \end{Bmatrix} \quad (6.22a)$$

where:

$$[C] = \begin{bmatrix} -\frac{D}{R^4}n^2 - \frac{K}{R^2}n^2 + \rho_s t_s \omega^2 & -\frac{D}{R^4}n^3 - \frac{K}{R^2}n \\ -\frac{D}{R^4}n^3 - \frac{K}{R^2}n & -\frac{D}{R^4}n^4 - \frac{K}{R^2} + \rho_s t_s \omega^2 \end{bmatrix} \quad (6.22b)$$

and, for $n=0$,

$$\begin{bmatrix} \rho_s t_s \omega^2 & 0 \\ 0 & -\frac{K}{R^2} + \rho_s t_s \omega^2 \end{bmatrix} \begin{Bmatrix} V_0 \\ W_0 \end{Bmatrix} = \begin{Bmatrix} 0 \\ -\frac{F_\theta \theta_a}{\pi R} \end{Bmatrix}. \quad (6.22c)$$

Solving equation (6.22), the tangential and radial displacements are obtained. The structural admittance can now be determined according to equation (6.9):

$$H = \frac{2i\omega}{\pi R} \sum_{n=1}^{\infty} \left[\frac{\left(\rho_s t_s \omega^2 - \frac{D}{R^4} n^2 (n^2 - 1) \right) \sin^2(n\theta_a)}{|C|} \right]. \quad (6.23)$$

With the structural admittance available, it is now possible to obtain the dynamic actuator force output from equation (6.15) and calculate the structural response to in-phase actuation.

6.4 Theoretical Results

To verify the impedance model, a case study of a circular aluminum ring with G1195 piezoelectric actuator patches was made. The material and geometric properties of the system are shown in Table 6.1. The size of the PZT actuator was kept small enough (10°) to be able to neglect the stiffness and mass loading of the actuators and to satisfy the impedance model assumptions. The results from the static approach were compared to the impedance model.

Table 6.1 *Material and geometric properties of the PZT actuator and the aluminum ring.*

	Aluminum Ring	PZT Actuator
Young's Modulus, Pa	59.5×10^9	63×10^9
Density, kg/m^3	2647	7650
Loss factor	0.006	0.001
Piezo. Coefficient d_{32} , m/V	N/A	-166×10^{-12}
Applied electric field, V/m	N/A	2.625×10^5
Radius, cm Length, °	12.475	10°
Thickness, mm	3	0.23

Figure 6.4 shows the structural and actuator impedance. The lower peaks of the curves correspond to the natural frequencies of the original cylinder, as expected. For this particular case, the dynamic interaction between the actuator and the ring is limited due to the lower input impedance levels of the actuator compared to the impedance levels of the ring. If a thicker actuator is used, the actuator impedance is increased and the dynamic interaction between the actuator and the structure is increased. However, for in-phase actuation, an unreasonable actuator thickness (1 mm), which corresponds to one-third of the shell thickness, is needed to obtain a good interaction (Fig. 6.4).

The actuator output force is shown in Fig. 6.5. The solid line corresponds to the impedance model, and the dotted line is the actuator output force based on the static model. The difference of the force magnitude between impedance and the static model is less than 1% at $w = 0$. At the natural frequencies, the magnitude of the impedance model output force does not increase dramatically. It can thus be concluded that the first natural modes, which are bending modes, are only slightly excited by the in-phase actuation of the shell.

Figures 6.6 and 6.7 show the radial displacement of the ring at 30° and 90° from the actuator, respectively. The natural frequencies of the original structure, obtained from a theoretical approach (Soedel, 1981), match those obtained from the analytical impedance model. The dotted and dashed lines are from the finite element analysis which will be discussed next.

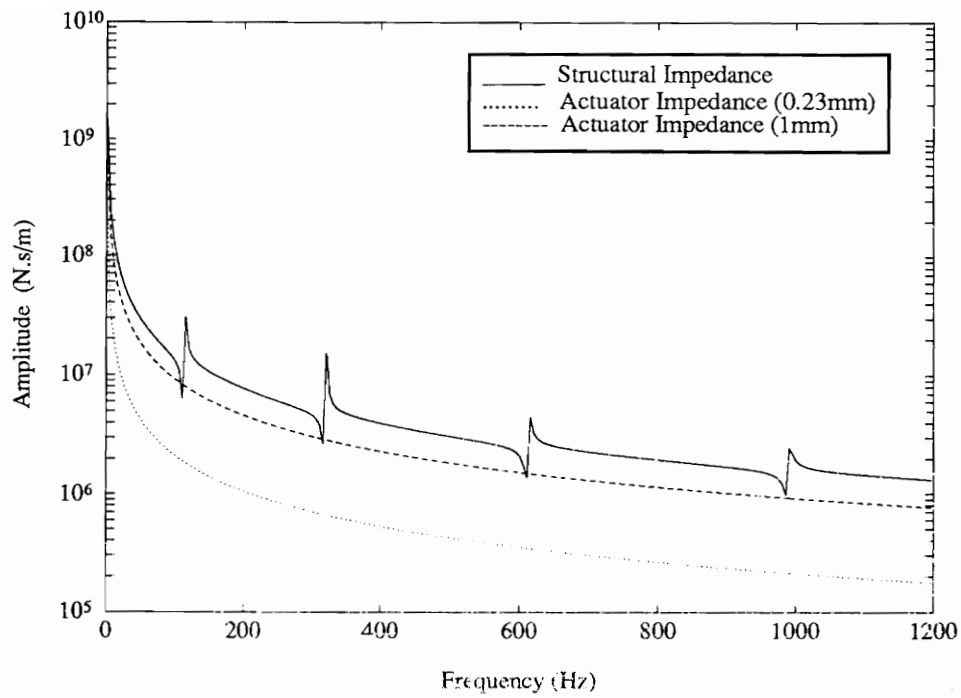


Figure 6.4 Structural and actuator impedance.

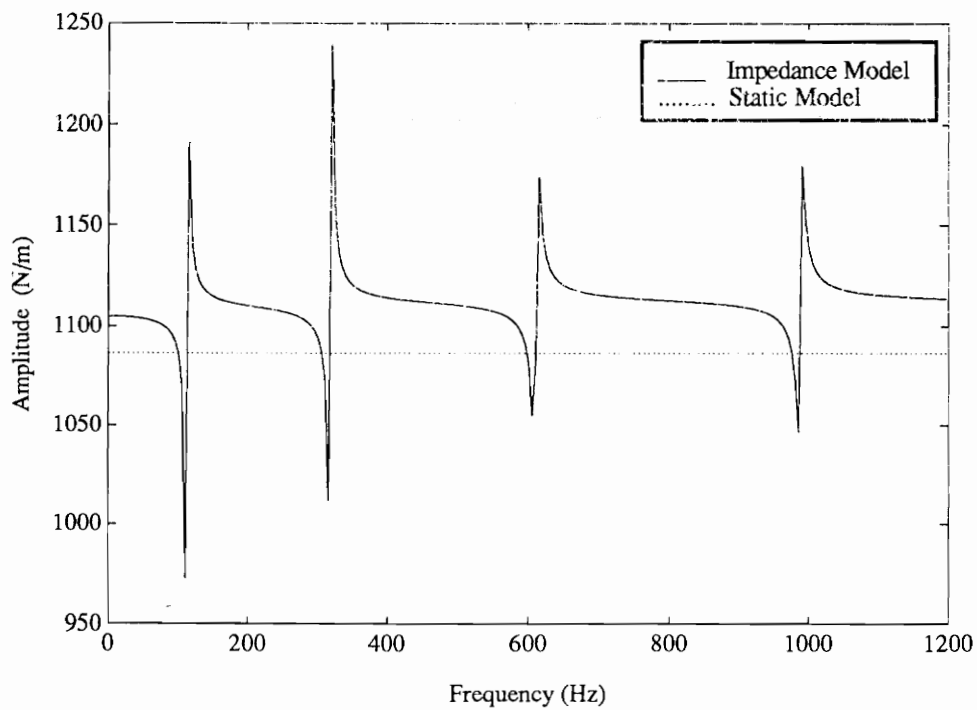


Figure 6.5 Actuator output forces based on the impedance and static models.

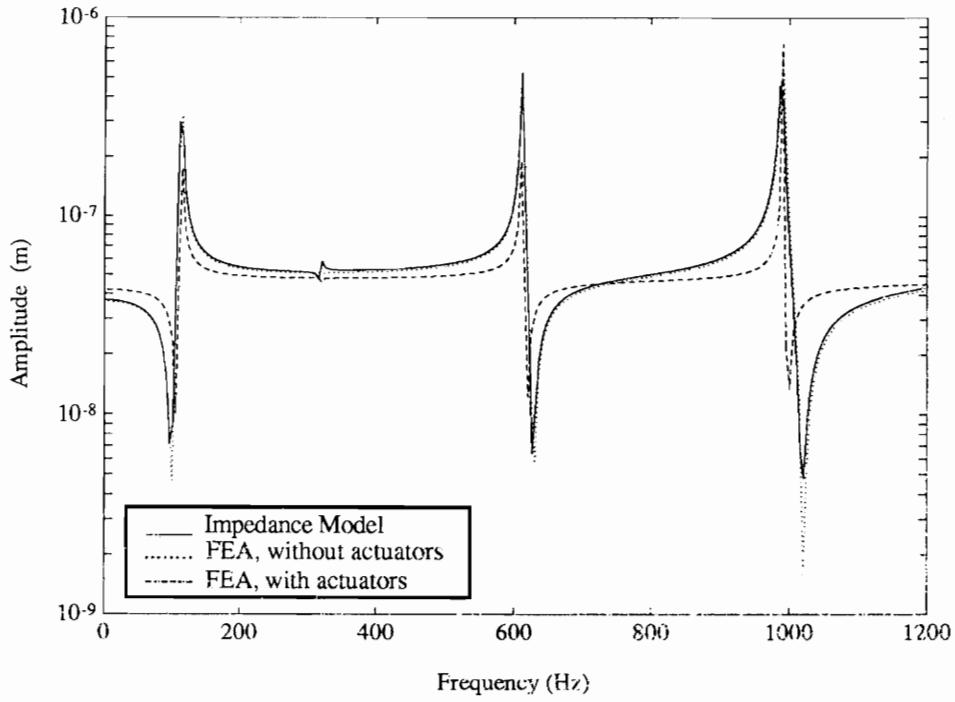


Figure 6.6 Radial displacement frequency response at 30° from the actuator.

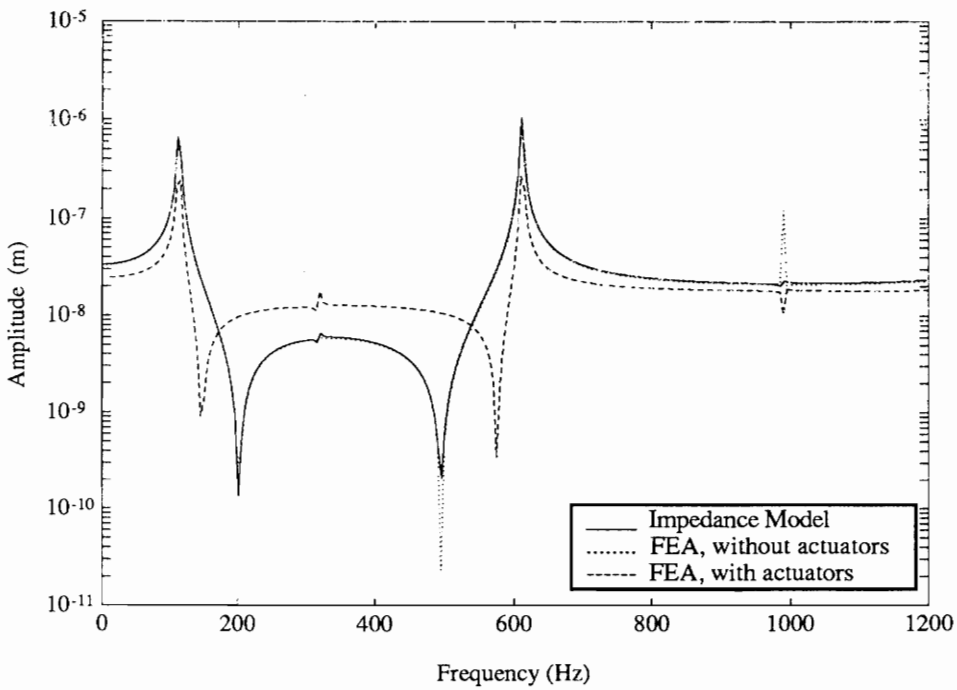


Figure 6.7 Radial displacement frequency response at 90° from the actuator.

6.5 Finite Element Verification

The finite element technique has been used to verify the theoretical impedance model. The dynamic analysis was performed using piezoelectric elements available in ANSYS 5.0. A harmonic electrical field was applied to the piezoelectric elements in two finite element models. The first model does not include the actuators that are bonded to the surface of the shell. Instead, the structure itself in the region of the actuator is modeled with the piezoelectric elements, to which the harmonic electrical field is applied (Fig. 6.8a). The second model includes the piezoelectric actuators on the structure, to which the electrical field is applied (Fig. 6.8b). The theoretical results are expected to match the finite element model without the actuators since the stiffness and mass added by the actuators is not considered in the impedance model. The finite element results including the actuator mass and stiffness should be close to the theoretical predictions due to the small thickness and size of the actuators. For both finite element models, the symmetry of the structure was used to reduce the size of the models. The structure was modeled using plane stress elements and the actuators (with actuator model) or actuator region (without actuator model) were modeled using piezoelectric plane stress elements. Free floating boundary conditions have been used for both models.

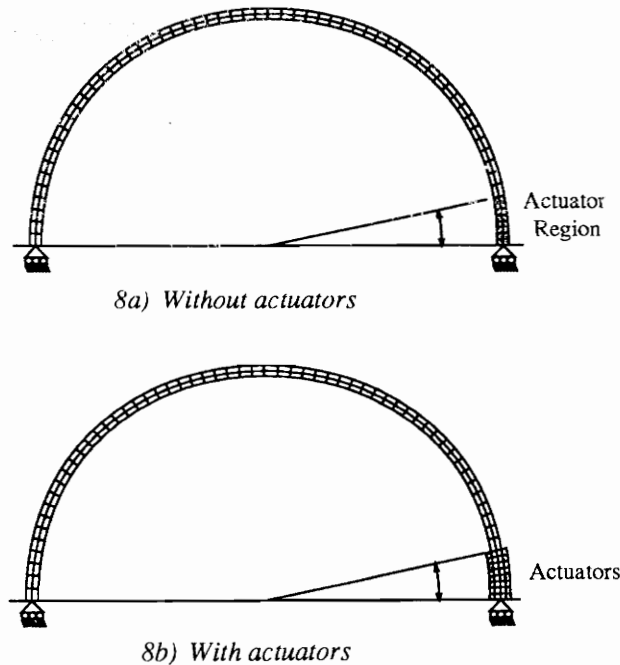


Figure 6.8 Finite element models without and with actuators.

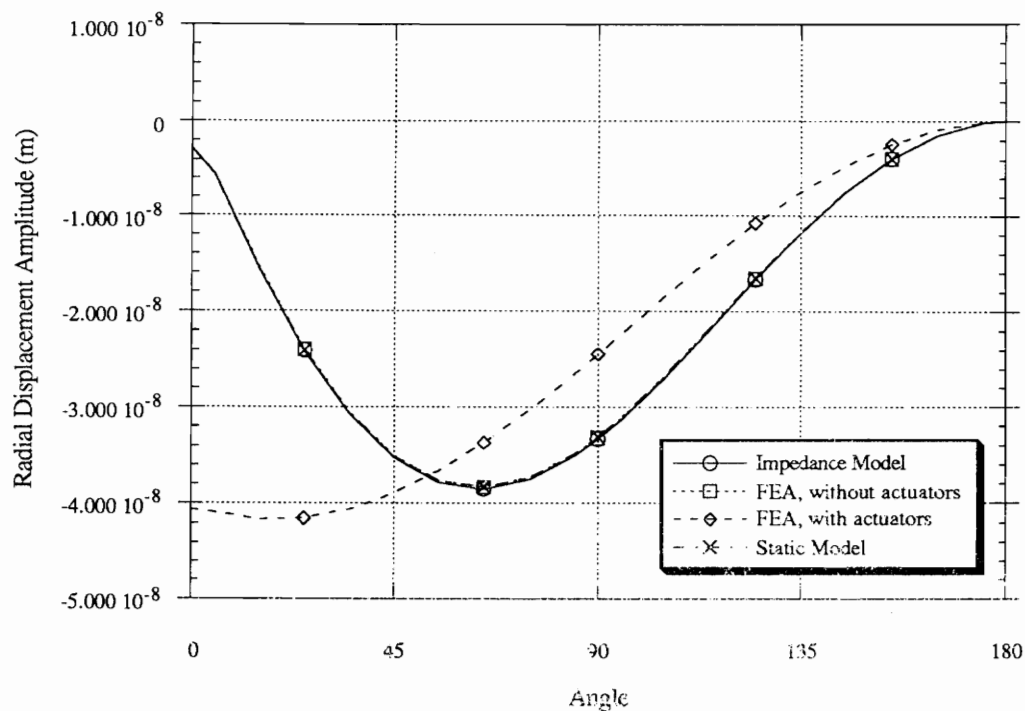


Figure 6.9 Impedance, static and finite element models radial displacement under dynamic loading at 5 Hz.

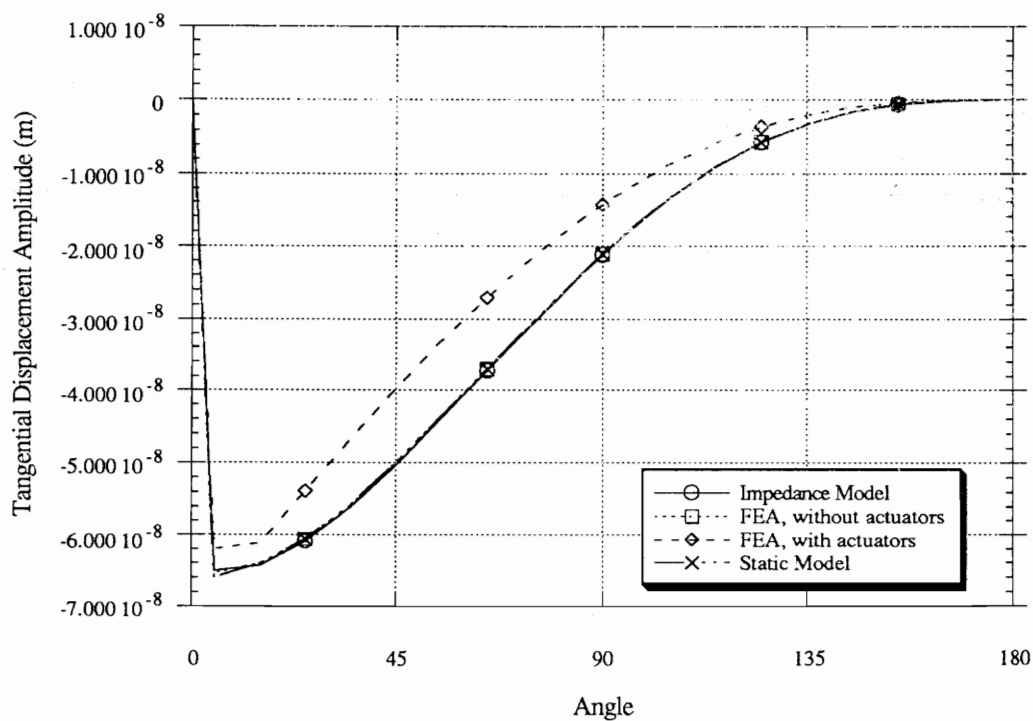


Figure 6.10 Impedance, static and finite element models tangential displacement under dynamic loading at 5 Hz.

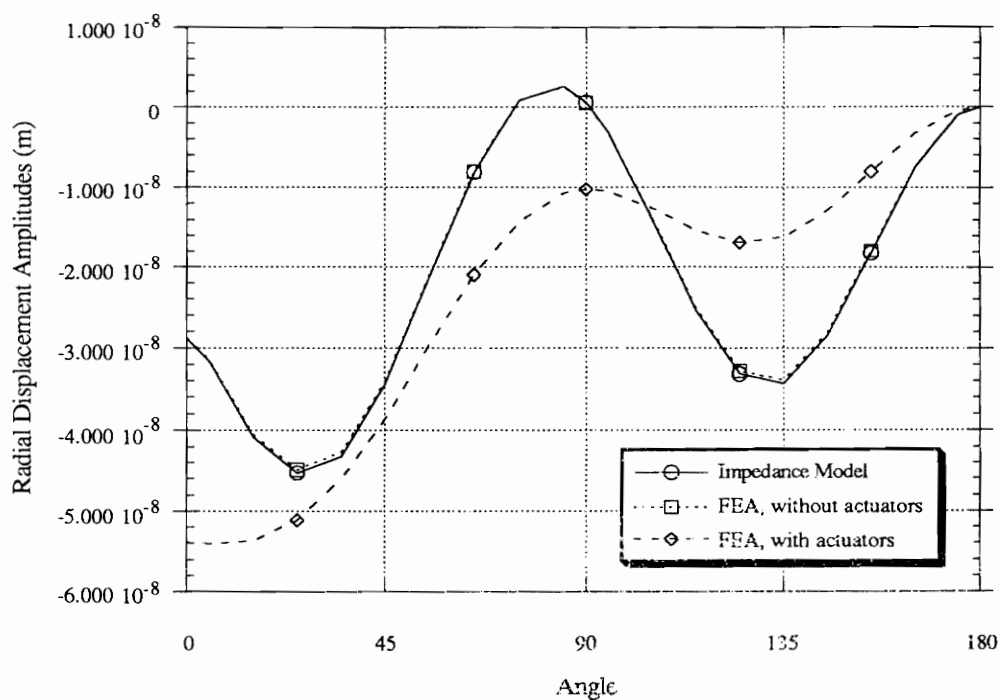


Figure 6.11 Impedance and finite element models radial displacement under dynamic loading at 500 Hz.

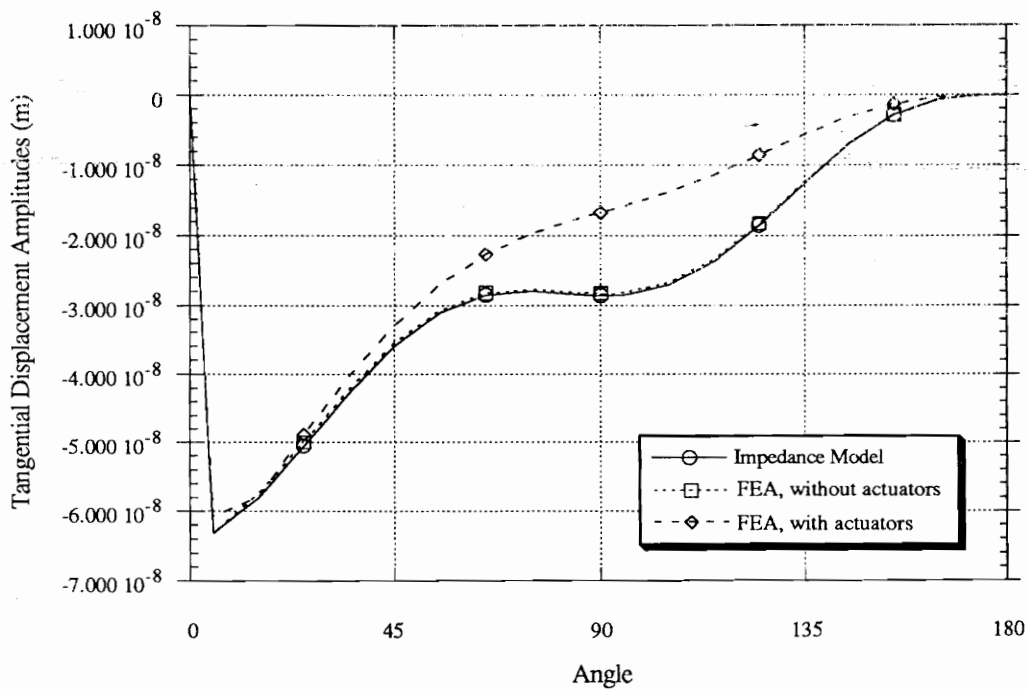


Figure 6.12 Impedance and finite element models tangential displacement under dynamic loading at 500 Hz.

The radial and tangential displacements of the structure at low frequency (5 Hz) are shown in Figures 6.9 and 6.10, respectively. In this figure, it can be observed that the impedance model matches the results of the finite element model without actuators. When the actuator stiffness is included, the displacements do not match the theoretical results. The discrepancies mainly occur in the actuator region where the increased stiffness will reduce the radial displacement amplitude. Nevertheless, the results are close enough to those obtained by the impedance model to validate the theoretical model. At very low frequencies, the dynamic results should converge towards the static results.

The static model for in-phase actuation developed in chapter 3 is also shown in Figures 6.9 and 6.10. It can be seen that the displacement based on the static model matches the displacements based on the impedance model. A coordinate transformation, from free floating to fixed at 180° , was applied to the impedance and finite element models so that it could be compared with the static model.

The structural radial and tangential displacements at 500 Hz, where the fourth mode is dominant, are shown in Figures 6.11 and 6.12, respectively. Once again, the displacements predicted by the impedance model match those obtained with the finite element model without actuators. If the actuator stiffness and mass are included, the displacements are slightly different, but still close enough to the theoretical model to be conclusive.

Finally, the frequency response of the structural radial displacements at 30° and 90° from the actuator are shown in Figures 6.6 and 6.7, respectively. In both cases, the impedance model accurately matches the finite element results without actuators. The differences between the finite element model with actuator mass and stiffness is observed once again.

6.6 Conclusions

An impedance model for the in-phase actuation of induced strain actuators bonded to the surface of a circular ring has been developed. A discussion of the appropriate representation of the loading due to in-phase actuation is presented. It is shown that the in-phase loading can be either included as induced uniform forces on the actuator footprint or as external equivalent loading. To verify the impedance model, two dynamic finite element analyses were performed (with and without actuator mass and stiffness), using piezoelectric elements available in ANSYS 5.0. A good correlation between the impedance model and the finite element results validated the analytical model.

Chapter 7

An Experimental Study of the Actuation Authority of Rings and Shells

Abstract

The in-phase and out-of-phase actuation authority of induced strain actuators bonded to the surface of a shell is compared using previously derived models. In-phase refers to a situation where both actuators bonded on the top and bottom surfaces of the shell are actuated to produce strains in the same direction; out-of-phase refers to opposite direction strains. It is shown that out-of-phase actuation has better authority in exciting the lower order bending modes, while in-phase actuation has better authority in exciting the higher order circumferential modes. In-phase actuation does excite the lower order bending modes through in-plane and out-of-plane displacement coupling, but an order of magnitude lower.

Experimental results of a circular ring actuated in-phase and out-of-phase by a piezoelectric material (PZT) are presented. Different methods of bonding straight actuators on a circular ring are investigated. The effects of segmenting actuators into small strips are studied. Experimental verification of the impedance models is conclusive, particularly for the out-of-phase actuation.

7.1 Introduction

Structural vibration control has always been important in the design of efficient and reliable mechanical systems. Recently, a novel approach using induced strain actuators for such vibrational control has been presented, which can also be extended to acoustic control. Induced strain actuators are particularly interesting because they can be fully integrated in or on the structure itself. By applying forces directly on the structure at critical locations, efficient structural control can be obtained. In vibrational and acoustic control, the undesirable dynamic effects are eliminated by modifying the apparent structural impedance, through the induced strain

actuators. This approach eliminates the moving parts encountered in the bulky shaker-type actuators, which are conventionally used. Such actuators, since they are bonded right on the surface of the structure, do not need a back reaction to function.

When induced strain actuator patches, like piezoelectrics, are symmetrically bonded to the surface on each side of the structure, they generate a set of forces along the edges of the actuators. The two actuators can be activated in-phase or out-of-phase. In-phase actuation refers to the case where both actuators expand and contract together. This type of actuation creates extensional in-plane forces on the structure. Out-of-phase actuation refers to the case when one actuator expands and the other contracts and vice-versa. Bending moments are applied to the structure at the actuator edges when out-of-phase actuation is used. Thus, the same actuator set-up, depending upon the type of actuation used, can generate very different structural actuation and response.

Theoretical studies based on static application of piezoelectric forces and moments on beam structures were proposed by Crawley and De Luis (1987), Crawley and Anderson (1990), Wang and Rogers (1991), and Dimitriadis et al. (1991). Models were also extended to two-dimensional plate structures (Crawley and Lazarus, 1989; Hagood et al., 1991). Adaptations of plate models to shells structures were proposed (Sonti and Jones, 1991; Lester and Lefebvre, 1991). Models based on shell equations have also been proposed (Sonti and Jones, 1993; Larson and Vinson, 1993b; Chapter 4).

Theoretical impedance-based models on the dynamic interaction between the actuators and the structure have also been proposed for beams (Liang et al., 1993b), plates (Zhou et al., 1994a), and shells (Rossi et al., 1993; Zhou et al., 1993; Chapters 5 and 6). The essence of the impedance approach is to match the actuator impedance to the structural impedance at the edges of the actuators. The impedance models are more accurate in the modeling of the structural response due to its dynamic considerations.

Most of the models mentioned above were developed for pure out-of-phase loading, except for the in-phase models presented by Lester and Lefebvre (1991) and in Chapter 6.

All of the theoretical models referred to above were developed independently, without any comparison of the authority of in-phase and out-of-phase actuation. Only Lester and Lefebvre (1991) did such a comparison. However, some drawbacks are present in the modeling proposed by Lester and Lefebvre (1991). No self-equilibrium considerations for the in-phase

actuation were included, and the shell model is a plate adaptation. It is shown in Chapter 3 that special considerations need to be made to eliminate the rigid-body transverse forces inherent to curved structures when in-phase actuation is used. The action of the actuators has to be represented by an equivalent in-plane force and a transverse pressure applied in the region of the actuator patch.

In this chapter, a comparison in the authority of in-phase and out-of-phase actuation for rings is presented. Also, an experimental verification of the impedance models for both in-phase and out-of-phase actuation is presented.

7.2 Impedance Models

The comparison of the in-phase and out-of-phase actuation is based on theoretical impedance models that have been developed in chapters 4 and 5. Only a brief review of those models will be presented. The derived impedance model applies to a free-floating thin circular ring (Fig. 7.1). In the impedance model, the piezoelectric actuators are assumed to be perfectly bonded on the structure and to have the same curvature as the structure. The impedance models were derived using the linear Love-Kirchhoff theory for thin shells.

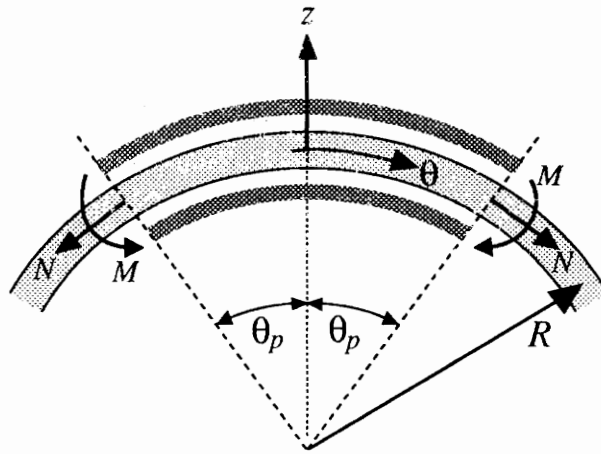


Figure 7.1 One-dimensional ring with bonded PZT actuators actuated in-phase or out-of-phase. The force applied by the actuators at the edge is shown.

The structural impedance is defined on the basis of discrete applied loads and velocities at the ends of the actuators. For in-phase actuation, the mechanical admittance (H_{in}) is defined on the basis of the tangential velocity (\dot{v}) (equation (7.1a)) while for out-of-phase actuation (H_{out}), it

is defined on the basis of rotational velocity ($\dot{\theta}$) (equation (7.1b)). The mechanical impedance (Z) is simply the inverse of the mechanical admittance (H):

$$H_{in} = \frac{\dot{v}}{N} \quad (7.1a)$$

$$H_{out} = \frac{\dot{\theta}}{M}, \quad (7.1b)$$

where the discrete applied in-phase tangential force and out-of-phase moment on the structure are (see Fig. 7.1):

$$N = 2F \quad (7.2a)$$

$$M = (t_a + t_s)F, \quad (7.2b)$$

From the system dynamic modeling between the structure and the actuator, the dynamic actuator force output (F) can be shown to be (Liang et al., 1993b):

$$F = -\frac{Z|_{\theta_p} d_{32} E t_a Y_a^E}{Z|_{\theta_p} + Z_a} \quad (7.3)$$

where the short-circuit actuator mechanical impedance is:

$$Z_a = \frac{Y_a^E t_a k}{i\omega \tan kR\theta_p}, \quad (7.4)$$

and d_{32} , E , Y_a^E , R , t_a and t_s are the piezoelectric constant, the electric field, the actuator Young's modulus, the shell radius, and the thicknesses of the actuator and structure, respectively.

The final step in impedance modeling is to obtain the structural impedance. The Rayleigh-Ritz method is used for the solution of the equations of motion of a circular ring submitted to the in-phase or out-of-phase equivalent loading. Solving the linear system of equations, the structural admittance for in-phase and out-of-phase actuation are, respectively (chapters 4 and 5):

$$H_{in} = \frac{2i\omega}{\pi R} \sum_{n=1}^{\infty} \left[\frac{\left(\rho_s t_s \omega^2 - \frac{D}{R^4} n^2 (n^2 - 1) \right) \sin^2(n\theta_p)}{|C_I|} \right] \quad (7.5a)$$

$$H_{out} = \frac{i\omega}{\pi R^3} \sum_{n=1}^{\infty} \left[\frac{\left[\frac{Kn}{R^2}(n^2 - 1) - \rho_s t_s \omega^2 \right] \sin^2(n\theta_p)}{|C_2|} \right]. \quad (7.5b)$$

The two impedance models for in-phase actuation and out-of-phase actuation have been verified using finite element analysis (Chapters 4 and 5).

7.3 Comparison Of In-Phase And Out-Of-Phase Actuation

A comparison between the in-phase and out-of-phase actuation of a shell structure has been made. The comparison focuses on the structural radial displacements produced by the actuators and on the efficiency to excite the structural resonant modes. These are the most relevant factors needed when vibration and noise control is considered. As a case study, the models were applied to a circular steel ring with G1195 piezoelectric actuator patches, the dimension for which are presented in Table 7.1.

Table 7.1 Material and geometric properties of the PZT actuator and the steel ring.

	Steel Ring	PZT Actuator
Young's Modulus, Pa	190.5×10^9	63×10^9
Density, kg/m ³	7850	7650
Loss factor	0.006	0.001
Piezo. Coefficient d ₃₂ , m/V	N/A	-166×10^{-12}
Applied electric field, V/m	N/A	6.0×10^5
Radius / Length, cm	30.16	3.76
Width, cm	3.175	3.175
Thickness, mm	6.3	0.25

Figure 7.2 shows the structural impedances for both in-phase and out-of-phase actuation. The in-phase impedance has a greater magnitude than the out-of-phase impedance. For comparison, the actuator impedance (dashed curved) is also shown in Figure 7.2. Good actuation authority is obtained when the structural and actuator impedances are of the same order of magnitude. Based on this observation, in-phase actuation will have more limited authority on the structure than out-of-phase actuation. The first six bending modes are shown in Figure 7.2. The

structural resonant frequencies, which are the lower peaks, match the theoretical values given by Soedel (1981). Out-of-phase actuation has a larger impact on the structure at resonant frequencies as opposed to in-phase actuation. Indeed, when the shell is actuated in-phase, the bending modes are only slightly excited through the in-plane/out-of-plane coupling property of shells. However, the in-phase actuation has the capabilities of exciting the higher-frequency circumferential modes, as opposed to out-of-phase actuation.

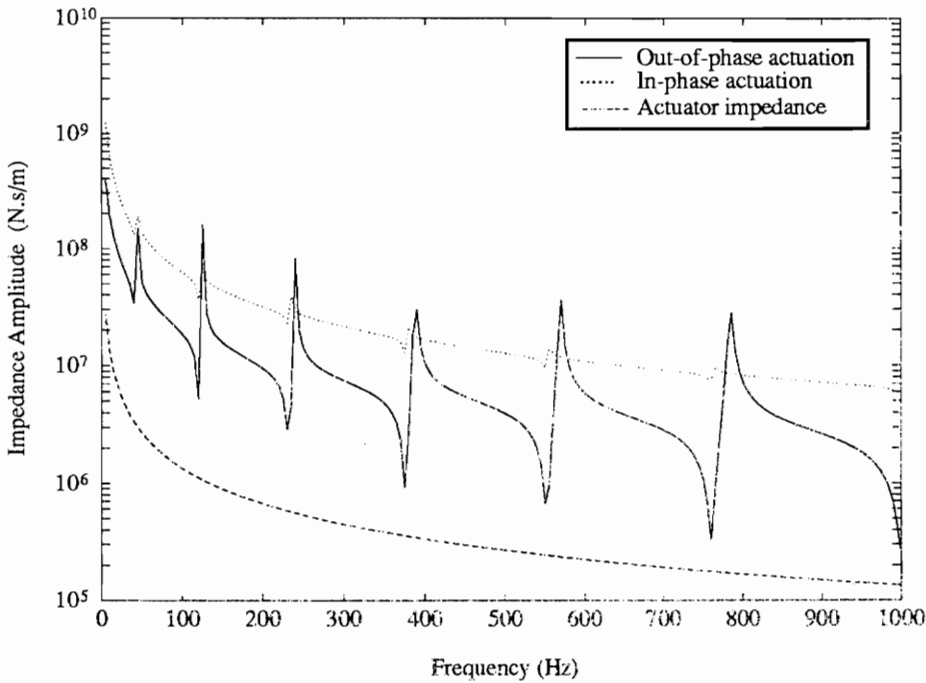


Figure 7.2 Structural impedance for in-phase and out-of-phase actuation.

The radial displacement frequency response at 30° from the actuator is presented in Figure 7.3. The displacements produced by in-phase actuation are an order of magnitude smaller than those obtained by out-of-phase actuation, for the same electrical field applied to the piezoelectric actuators. Unlike in-phase actuation, out-of-phase actuation is very effective in exciting the natural bending modes of the structure. Since the frequency range of interest in structural vibration control is low, out-of-phase actuation is thus more efficient than in-phase actuation for ring structures.

This conclusion can be extended to two-dimensional shells. Based on an impedance model developed for shells (Chapter 8), the response of a shell of same dimension as the ring (Table 7.1) but 75cm long has been calculated. The actuator center is at coordinates ($x=37.5\text{cm}$,

$\theta=0^\circ$). The radial displacement frequency response at ($x=15\text{cm}$, $\theta=30^\circ$) is presented in Figure 7.4. Once again, the displacements produced by in-phase actuation are smaller than those produced by out-of-phase actuation. However, the clear advantage of using out-of-phase over in-phase that was found for one-dimensional rings is not as obvious for two-dimensional shells. The displacement magnitudes are closer to each other, showing a factor of about 5 only for this particular case. Nevertheless, out-of-phase actuation is still more efficient than in-phase actuation.

This conclusion is different from that reported by Lester and Lefebvre (1991). In their paper, a theoretical model based on a static approach was presented for in-phase and out-of-phase actuation. It is stated that in-phase actuation excites the lower bending modes more efficiently than out-of-phase actuation. The reason for this erroneous conclusion is simply the omission of the self-equilibrating pressure that needs to be used for in-phase actuation. Without this extra pressure loading, the shell response will produce erroneous larger displacements. Experiments were performed on a fuselage-type structure, including stiffeners and a floor. This structure is more complex, and thus more difficult to compare to a simply-supported cylinder.

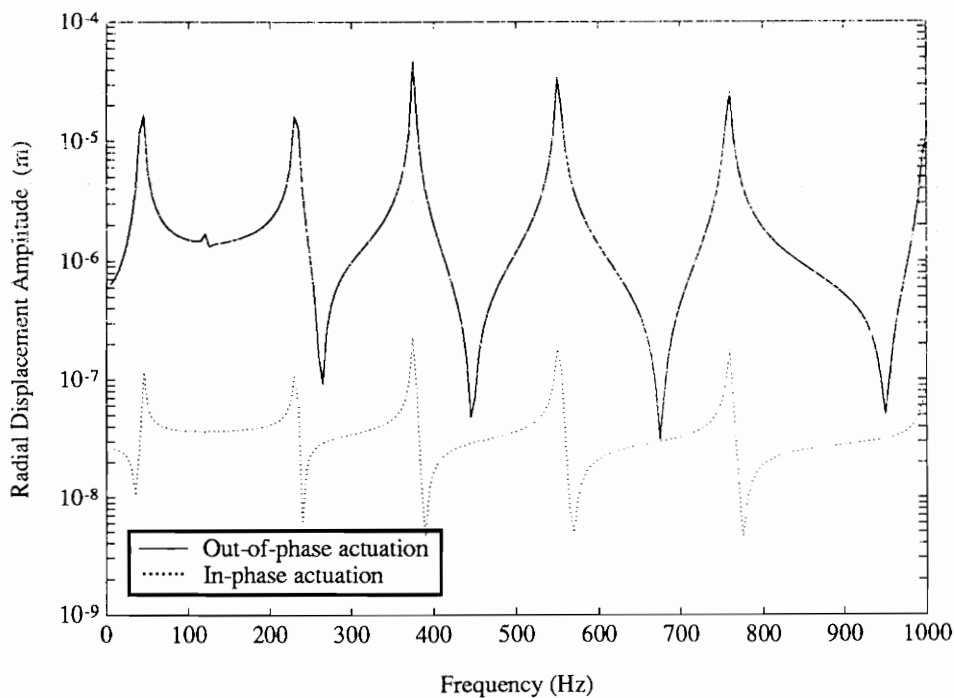


Figure 7.3 Authority comparison of in-phase and out-of-phase actuation for a one-dimensional ring.

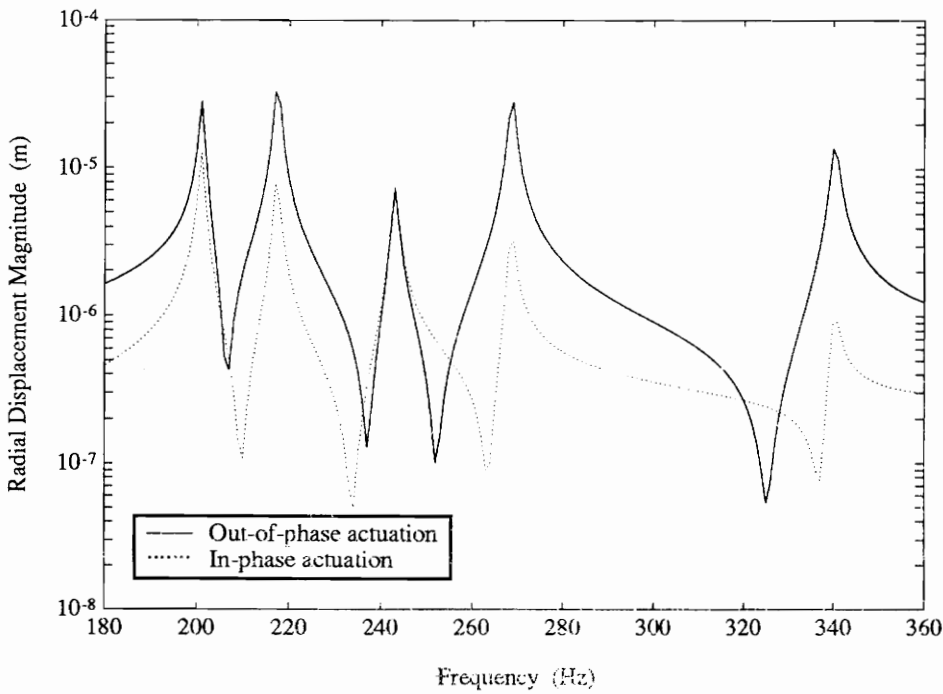


Figure 7.4 Authority comparison of in-phase and out-of-phase actuation for a two-dimensional shell.

7.4 Bonding of Piezoceramic Actuators on Curved Surfaces

Due to their brittle nature, piezoceramic materials can only tolerate a very small curvature before they will break. This creates a problem when actuators need to be used with curved structures. A possible way to obtain a curved piezoceramic actuator is to machine the desired curvature in a thick actuator. This method involves high machining accuracy, only provides limited curvatures, and is expensive. It is also possible to directly fabricate actuators with a curvature, but this is perhaps even more expensive, keeping in mind today's limited market. Thus, there is a need to adapt flat piezoceramic actuators to curved structures.

The most convenient way to apply an actuator on a curved structure is to machine a flat surface on the structure (Fig. 7.5). This provides an easy and inexpensive means of obtaining the desired actuation/sensing. However, this technique is not possible for all situations. For large radius/thickness ratios, the machining of the flat surface can be done without affecting the structural properties of the shell; but, for thin shells, the structural properties can be greatly

modified. Also, the machining of a flat surface can be simply impossible due to the location or the size of the actuator/sensor.

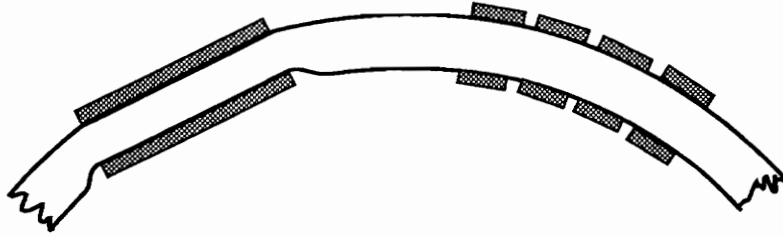


Figure 7.5 *Methods for bonding flat actuators on curved structures.*

An alternative to bonding flat piezoceramic actuators is to cut them into small pieces, and bond them next to each other on the structure (Fig. 7.5). The piezoelectric pieces are bonded as close as possible, but leaving a gap to avoid electrical short circuit. The space between the actuators is small enough to be neglected, so that all pieces can be considered as a single actuator. With a sufficient number of pieces, the actuator could be considered curved. This technique does not involve the machining of the structure and has no limit on the size of the actuator, but has other drawbacks. The first difficulty is the bonding of the actuator itself on the curved surface. For each piece, a non-uniform adhesive layer must be present to accommodate the flatness of each piece (Fig. 7.6). Because of this, it is very difficult to obtain bonding comparable to a flat actuator on a flat surface that will transfer the actuator's induced strain to the structure. A second difficulty is to bond each piece as close as possible to each other, in order to obtain a global uniform patch, but leaving a gap for the electrical insulation. In this technique, it is assumed that each actuator piece will cancel the effect of the adjacent actuator, only producing a global effect on the structure.

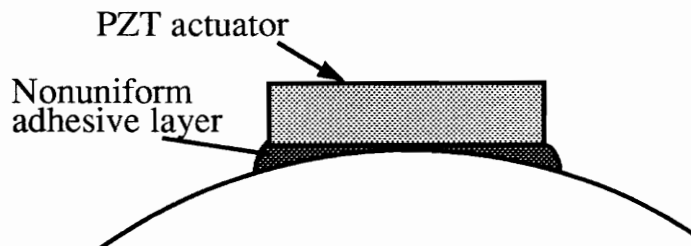


Figure 7.6 *Schematic illustration of a non-uniform adhesive layer accommodating a flat PZT on a curved structure.*

7.5 Experimental Verification

A steel ring actuated in-phase and out-of-phase by surface-bonded PZT actuators was used to experimentally verify the impedance models. The material and geometrical properties of the ring and the actuator used are shown in Table 7.1. The two bonding techniques discussed previously were used. Firstly, a flat surface was machined on the ring. The structural integrity was not affected by the machining process due to the relatively large thickness and radius of the ring and the small actuator patch. Secondly, the actuators were bonded on the curved surface, breaking it into four pieces of 9 mm each and leaving a thin gap between each piece. For the remainder of the chapter, the single piece continuous actuators bonded on the machined flat surface will be referred to as "flat actuators," while the segmented actuators bonded on the curved surface will be referred to as "segmented actuators".

A random signal produced by the WCA Zonic AND and amplified with a Trek 50/750 high voltage power amplifier was applied to the piezoelectric actuators. The ring velocity response was measured using a Polytec laser vibrometer system and data was acquired with WCA Zeta software on a Macintosh Quadra. The experimental set-up is shown in Figure 7.7. The ring was suspended using fishing line to simulate free-floating boundary conditions. Finally, the out-of-plane velocity measurements were done at angles of 30° and 150° from the actuator. The laser vibrometer system is able to measure accurately velocities up to 1 micron/s. The experimental ring was chosen such that the velocities produced by the actuators, which are driven at half of the depoling electrical field, will be large enough to be measured accurately.

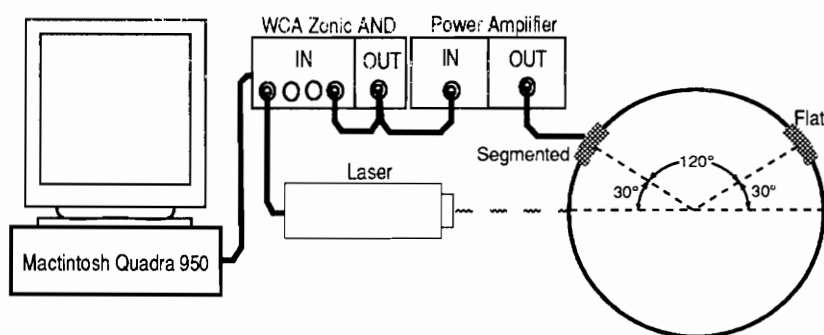


Figure 7.7 Experimental set-up used to measure the out-of-plane velocities of the structure.

The ring's radial frequency response at 30° from the actuator (see Fig. 7.7) subjected to out-of-phase actuation is shown in Figure 7.8. The flat actuators show a better match to the impedance model than the segmented actuators. The segmented actuators produce smaller

displacements than the flat actuators, due to the increased bonding layer thickness and, gaps between each piece, which will reduce the actuators authority on the structure. Nevertheless, both the flat and segmented actuators show a conclusive match with the theoretical impedance model.

The ring's frequency response at the same location due to in-phase actuation is shown in Figure 7.9. In this case, the match between the impedance model and the experimental results is not as conclusive. The differences might be attributed to the actual bonding of the actuators on the curved surface. The theoretical model cannot exactly model the actual experimental set-up, the bonding layer having an impact on the structural response, likewise for the machined flat surface. Taking account of those considerations, the theoretical and experimental results show a good match at the resonant frequencies.

The structural response at 150° from the actuator is not presented since the same conclusions would be drawn.

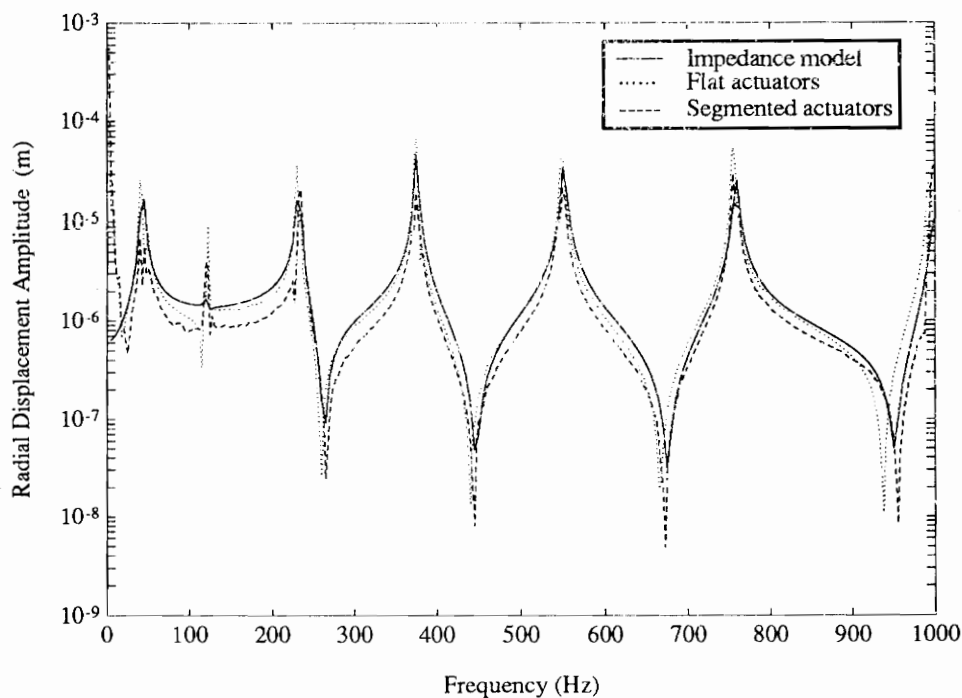


Figure 7.8 Experimental and impedance model ring response to out-of-phase actuation.

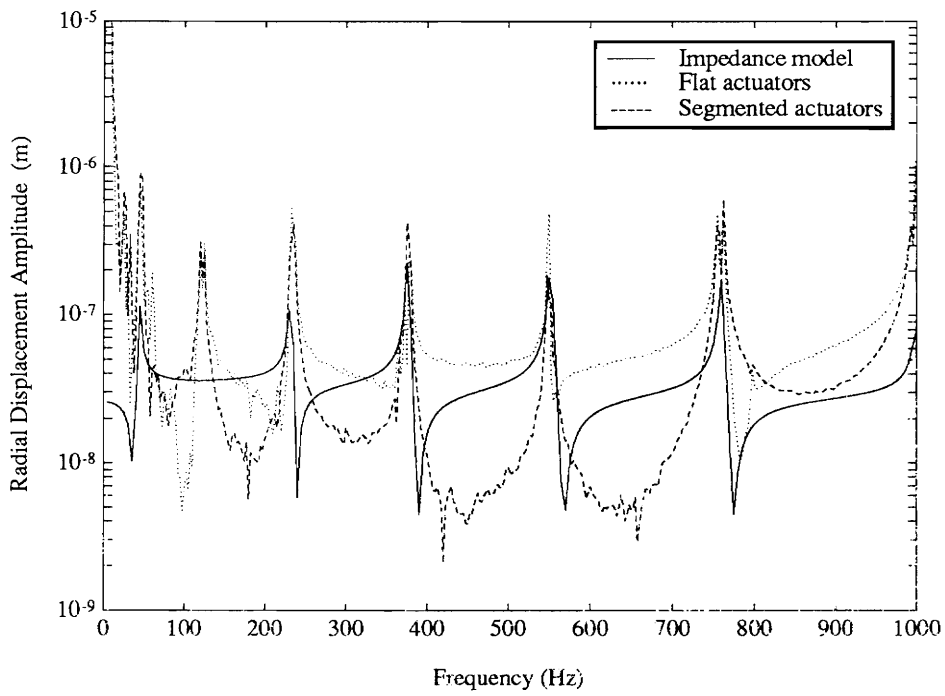


Figure 7.9 *Experimental and impedance model ring response to in-phase actuation.*

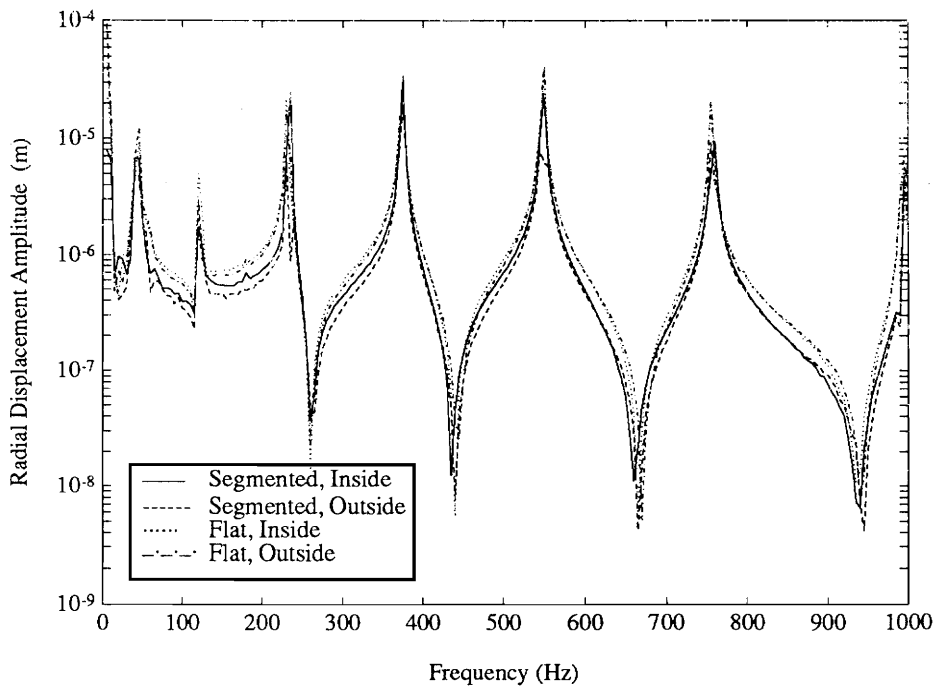


Figure 7.10 *Experimental structural response to actuators bonded on the inside and on the outside of the ring.*

The next figure (Fig. 7.10) shows the structural response if each actuator is excited separately, i.e., a single actuator on the inside of the shell or on the outside of the shell. It can be observed that an actuator bonded on the inside will produce a similar response to an actuator bonded on the outside of the shell, both for the flat and segmented actuators. Once again, the segmented actuators produce smaller displacements than the flat actuators.

7.6 Actuator Response Superposition

A finite element analysis has been performed using the experimental ring dimensions to verify single-side actuation. The model uses piezoelectric elements available in ANSYS 5.0 and is shown in Figure 7.11. The structural response of the ring to inside actuation and outside actuation is presented in Figure 7.12. The structural response of each actuator cannot be considered to be the same, even though only small discrepancies are present. However, for thin shells, the side of the shell on which the actuator is bonded will not have an important impact on the structural response. If the radius is increased to infinity (flat structure), the structural response will be exactly the same.

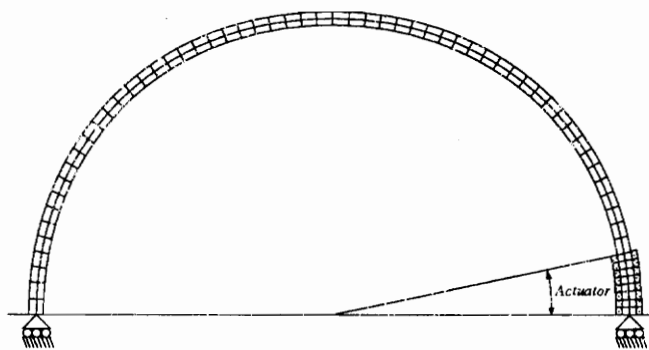


Figure 7.11 *Finite element model using PZT elements.*

The finite element structural response illustrated in figure 7.12 shows an excellent match with the experimental results, as well as with the impedance model results that were presented in Figure 7.10.

The superposition of the response due to a single actuator to get the total in-phase and out-of-phase response is now considered. If the displacements due to the inside actuator are subtracted from the displacements due to the outside actuator, the pure out-of-phase solution is obtained exactly (equation (7.6a)). If the displacements are added, the pure in-phase solution is

also obtained exactly (equation (7.6b)):

$$u_i|_{Outside} - u_i|_{Inside} = u_i|_{Outphase} \quad (7.6a)$$

$$u_i|_{Outside} + u_i|_{Inside} = u_i|_{Inphase} \quad (7.6b)$$

The converse is also true. The structural response of a single actuator bonded on the inside or outside surface of the shell can be obtained from the in-phase and out-of-phase structural responses (equation (7.7)). To a larger extent, any unsymmetrical voltage application on the actuators can be expressed as a linear combination of pure in-phase loading and pure out-of-phase loading:

$$\frac{1}{2}u_i|_{Inphase} + \frac{1}{2}u_i|_{Outphase} = u_i|_{Outside} \quad (7.7a)$$

$$\frac{1}{2}u_i|_{Inphase} - \frac{1}{2}u_i|_{Outphase} = u_i|_{Inside} \quad (7.7b)$$

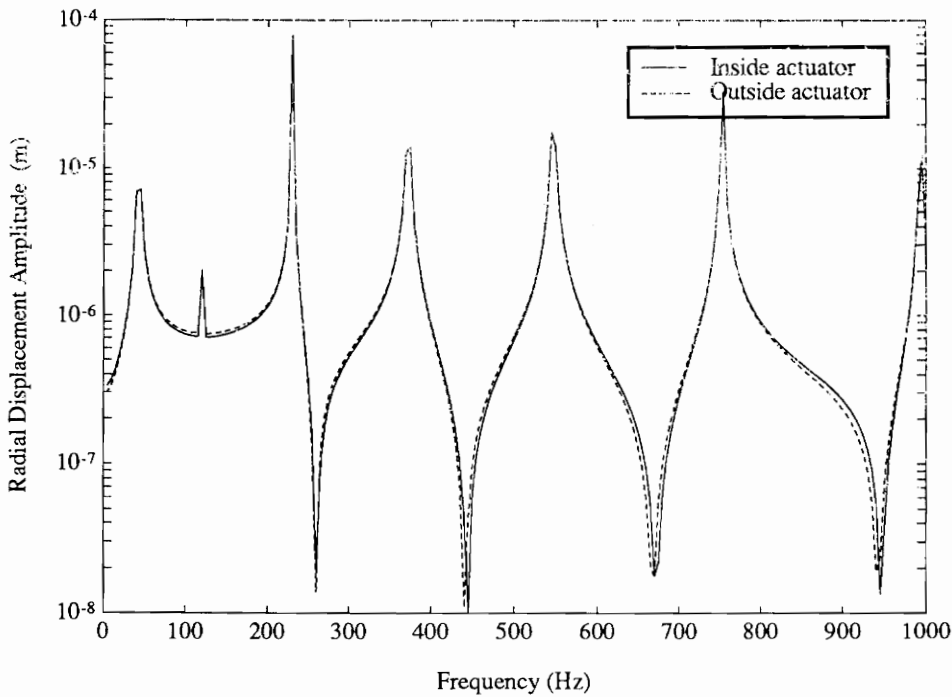


Figure 7.12 Structural response at 30° from the actuators bonded on the inside and on the outside of the ring, using finite element analysis.

7.7 Conclusions

In this chapter, the actuation authorities for different actuation schemes were presented, namely, in-phase and out-of-phase actuation of thin shells. Based on the radial response of the ring, it is shown that in-phase actuation has lesser authority, and out-of-phase actuation has higher authority than in-phase actuation. Also, out-of-phase actuation is more efficient in exciting the lower order bending modes of the ring, while in-phase actuation has the capability of exciting the higher circumferential modes.

The experimental verification of the out-of-phase impedance model was very conclusive. An excellent match between the theoretical and experimental results was observed. However, the match is more difficult for the in-phase actuation case. Greater discrepancies are found due to the smaller displacements involved and to the greater sensitivity to the bonding of the actuators on the structure. Nevertheless, the in-phase actuation experimental results are still similar to the theoretical results, both in shape and magnitude.

Finally, a short discussion on the superposition of the structural responses is presented. It is shown that pure in-phase and pure out-of-phase actuation can be used to model the more general unsymmetric actuator loading, by using simple linear superposition.

Chapter 8

Impedance-Based Modeling of Actuators Bonded to Shell Structures

Abstract

When discrete piezoelectric actuator patches bonded on structures are used for active shape, vibration, and acoustic control, the desired deformation field in the structure is obtained through the application of localized line forces and moments generated by expanding or contracting bonded piezoelectric actuators. An impedance-based model to predict the dynamic response of cylindrical shells subjected to excitation from surface-bonded induced strain actuators is presented. The essence of the impedance approach is to match the actuator impedance with the structural impedance at the ends of the actuators, which will retain the dynamic characteristics of the actuators. A detailed derivation of the actuator and structural impedance is included. It is found that the actuator's output dynamic force in the axial and tangential direction are not equal. Various case studies of a cylindrical thin shell are performed to illustrate the capabilities of the developed impedance model. Out-of-phase actuation is shown to be the most efficient in exciting the lower order bending modes of shell structures. The paper is concluded with a finite element analysis verification of the derived impedance model.

8.1 Introduction

In any mechanical system with moving parts, special attention must be given to reducing vibrations and accompanying noise. If the system cannot be balanced or is subjected to random vibrations, passive or active control of the structure can be considered to reduce vibrations. One way to perform active control is to use shaker type actuators, but this involves many moving parts external to the base structure. By fully integrating the vibration control components within the base structure, self equilibrium of the complete system is insured and simplifies the overall design of the mechanical system. Piezoelectric (PZT), and

other induced strain actuators are one type of actuators which can be easily integrated in the structure. When PZT patches are bonded or embedded in the structure, they apply forces or moments which are concentrated at the edges of the actuator. Using those forces and moments on the structure, the vibrations can be reduced by modifying the apparent structural impedance.

The piezoelectric actuators are often used in pairs, bonded on opposite sides of the structure. By controlling the voltage applied on each actuator it is possible to drive the actuators in-phase (both actuators expanding or contracting together), which creates an extensional deformation of the middle surface or out-of-phase (one actuator expands while the other contracts), which creates bending deformation of the middle surface. In between these two extreme cases, unequal voltage application will create a combination of bending and extension. An actuator bonded only on one side of the structure is the most common case of unsymmetric actuation. Out-of-phase and in-phase actuation will have a different impact on the vibrational response of the structure, out-of-phase actuation being more suitable for exciting the structural bending modes and in-phase being more suitable extensional modes (Chapter 7).

A number of theoretical models have been proposed for out-of-phase actuation of beams (Crawley and de Luis, 1987; Crawley and Anderson, 1990; Wang and Rogers, 1991; Dimitriadis et al., 1991) and plates (Crawley and Lazarus, 1989; Hageod et al., 1988). Other models based on the layered shell theory have also been proposed (Tzou and Gadre, 1989; Jia and Rogers, 1990). For shells actuated with discrete actuator patches, plate models were adapted to shells (Sonti and Jones, 1991; Lester and Lefebvre, 1991) and other models directly based on the shell governing equations (Sonti and Jones, 1993; Larson and Vinson, 1993b; Chapter 4). In all of these models, the actuator output force is computed from static considerations (i.e. local actuator/structural geometric and material properties) and, for vibrational control, the static fixed amplitude actuator forces are simply applied over the whole frequency range of interest.

Impedance models based on the dynamic properties of the actuators and the structure have also been proposed. The essence of the impedance approach is to match the actuator impedance to the structural impedance along the edges of the actuators. Impedance models for out-of-phase actuation have been derived for beams (Liang et al., 1993b), plates (Zhou et al., 1994a), rings (Rossi et al., 1993; Chapter 5), and shells (Zhou et al., 1993). An

impedance model for in-phase actuation of rings has also been proposed (Chapter 6).

Even though unsymmetrical actuation can be represented with simple linear superposition of in-phase and out-of-phase actuation (Chapter 7), no model for such unsymmetrical actuation has been presented yet. In this paper, an impedance-based model of two-dimensional shells subjected to in-phase, out-of-phase, and unsymmetrical actuation is proposed.

8.2 Impedance Model Derivation

An impedance-based model for a simply supported thin cylindrical shell excited with piezoelectric actuator(s) is derived (Fig. 8.1). The impedance model is derived in four major steps: (1) Calculation of the structural impedance at the edges of the actuators using the shell governing equations and the appropriate boundary conditions; (2) Calculation of the actuator impedance; (3) Calculation of the actuator output force based on the structural and actuator impedances interaction; and (4) Application of the frequency-dependent actuator output forces to the shell governing equations previously used to obtain the shell response.

The assumptions used in the following derivation are a perfect bonding of the actuators to the structure, a constant stress distribution through the thickness of the actuators, and a thin shell. Based on these assumptions, the linear Love-Kirchoff shell theory is used. In view of the mechanics through which the forces from the actuator are transferred to the sub-structure, the actuator patches are replaced by discrete line forces and moments along the edges of the footprint of the actuator (Crawley and de Luis, 1988).

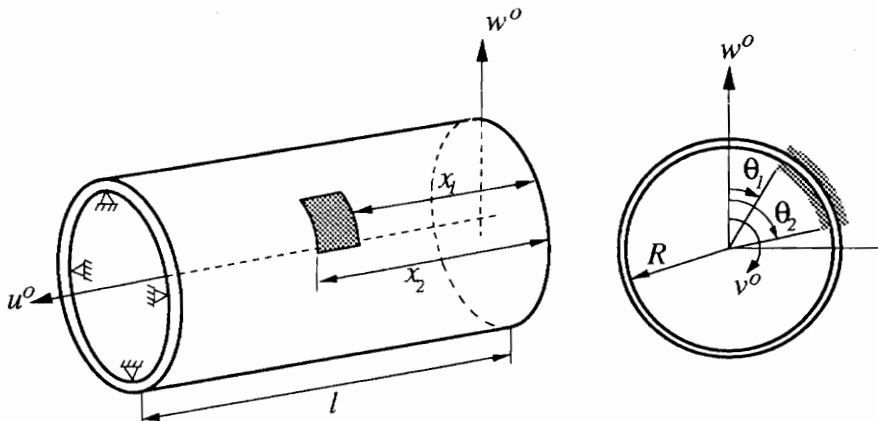


Figure 8.1 Simply supported thin shell with surface bonded actuators.

The pair of piezoelectric actuators can be excited independently if the substructure is not used as a ground and electrical insulation between the actuators and the structure is introduced (Fig. 8.2). This type of bonding allows the pair of actuators to be excited in-phase, out-of-phase, one actuator alone, or unsymmetrically.

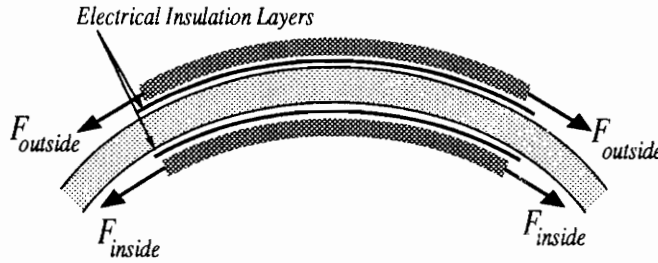


Figure 8.2 Unsymmetric actuation created by electrically insulating the actuators from the structure.

The superposition of the in-phase and out-of-phase actuation structural responses will be used to predict the response due to unsymmetrical actuation. It was shown in Chapter 7 that any unsymmetrical actuation can be expressed as a linear combination of pure in-phase actuation and pure out-of-phase actuation. The appropriate weighting factors for in-phase (ξ^i) and out-of-phase actuation (ξ^o), which are based on the free induced strains (Λ) applied on each actuators, are:

$$\xi^i = \frac{\Lambda_{inside} + \Lambda_{outside}}{2\Lambda_{max}}, \quad (8.1a)$$

$$\xi^o = \frac{-\Lambda_{inside} + \Lambda_{outside}}{2\Lambda_{max}}; \quad (8.1b)$$

where Λ_{max} is the largest of the inside or outside actuator free induced strain. Based on this definition, the free induced strain ratios ξ^i and ξ^o will vary from -1/2 to 1, $\xi^o = 1$ being pure out-of-phase and $\xi^i = 1$ being pure in-phase. The ξ ratios are dependent only on the free induced strain, assuming identical actuators are bonded on both sides of the shell. For cases where the actuators do not have the same thicknesses, the equation derivation becomes more complicated due to different actuator impedances. However, a simple superposition of the structural response to actuators bonded on the inside and on the outside of the shell can still be used to predict the dynamic response using this method.

8.2.1 Determination of the Structural Impedance

The dynamic response of structures can be described through its impedance or admittance. The structural admittance, which is simply the inverse of the impedance, and is defined based on the velocity response of the cylinder at the edges of the piezoelectric actuator, both in the x and the θ directions. Making use of linear superposition, the admittance definition (equation (8.2)) has been separated into two parts: pure in-phase actuation admittance and pure out-of-phase actuation admittance. H_{xx} and $H_{\theta\theta}$ are the direct admittances which directly couple the forces in the x and θ directions, while $H_{x\theta}$ and $H_{\theta x}$ are the cross admittances which couple the input forces in the x and θ directions to the response in the θ and x directions, respectively. In the case of one-dimensional structures, the coupling disappears and the admittance definition simplifies to a single term instead of the 2×2 matrix involved for two dimensional structures.

$$\left(2\dot{u}^o \Big|_{Inphase} - \frac{(t_s + t_a)^2}{2} \frac{\partial \dot{w}^o}{\partial x} \Big|_{Outphase} \right) \Big|_{x=x_2} - \left(2\dot{u}^o \Big|_{Inphase} - \frac{(t_s + t_a)^2}{2} \frac{\partial \dot{w}^o}{\partial x} \Big|_{Outphase} \right) \Big|_{x=x_1} = -(H_{xx}F_x + H_{\theta x}F_\theta) \quad (8.2a)$$

$$\left(2\dot{v}^o \Big|_{Inphase} - \frac{(t_s + t_a)^2}{2} \frac{\partial \dot{w}^o}{R \partial \theta} \Big|_{Outphase} \right) \Big|_{\theta=\theta_2} - \left(2\dot{v}^o \Big|_{Inphase} - \frac{(t_s + t_a)^2}{2} \frac{\partial \dot{w}^o}{R \partial \theta} \Big|_{Outphase} \right) \Big|_{\theta=\theta_1} = -(H_{x\theta}F_x + H_{\theta\theta}F_\theta) \quad (8.2b)$$

where u^o , v^o and w^o are the axial, tangential, and radial midplane displacements, respectively. t is the thickness and subscripts a and s stand for actuator and shell, respectively, and R is the radius of the shell. F_x and F_θ are the actuator output forces in the x and θ directions. In equation (8.2), the minus sign on the right hand side is necessary to indicate that the actuator output forces are equal and opposite to the structural reactions.

The first step of the impedance approach is to calculate the structural impedance of the cylinder, which will be dependent on the actuator's location, the boundary conditions, and the physical properties of the shell. The structural impedance calculations will be based on the modal expansion method. This method is numerically efficient and accurate when the natural modes are available, which is the case for a simply supported shell. The Rayleigh-Ritz method can be used for more complex shell boundary conditions. Using the thin shell

theory of a circular cylinder, the equations of motion including the actuator induced forces and moments are (Soedel, 1981):

$$L_1(u^o, v^o, w^o) - \rho_s t_s \ddot{u}^o = \frac{\partial n_x}{\partial x}, \quad (8.3a)$$

$$L_2(u^o, v^o, w^o) - \rho_s t_s \ddot{v}^o = \frac{\partial n_\theta}{R \partial \theta} + \frac{\partial m_\theta}{R^2 \partial \theta^2}, \quad (8.3b)$$

$$L_3(u^o, v^o, w^o) - \rho_s t_s \ddot{w}^o = -\frac{n_\theta}{R} + \frac{\partial^2 m_x}{\partial x^2} + \frac{\partial^2 m_\theta}{R^2 \partial \theta^2}; \quad (8.3c)$$

where the induced uniform tangential and axial forces can be written using Heaviside functions:

$$n_x = N_x [H(x - x_1) - H(x - x_2)] [H(\theta - \theta_1) - H(\theta - \theta_2)], \quad (8.4a)$$

$$n_\theta = N_\theta [H(x - x_1) - H(x - x_2)] [H(\theta - \theta_1) - H(\theta - \theta_2)], \quad (8.4b)$$

with an in-phase force magnitude of:

$$N_x = 2F_x \xi^i, \quad (8.5a)$$

$$N_\theta = 2F_\theta \xi^i; \quad (8.5b)$$

and where the induced uniform tangential and axial moments can also be written using Heaviside functions:

$$m_x = M_x [H(x - x_1) - H(x - x_2)] [H(\theta - \theta_1) - H(\theta - \theta_2)], \quad (8.6a)$$

$$m_\theta = M_\theta [H(x - x_1) - H(x - x_2)] [H(\theta - \theta_1) - H(\theta - \theta_2)], \quad (8.6b)$$

with an out-of-phase moment magnitude of:

$$M_x = (t_a + t_s) F_x \xi^o, \quad (8.7a)$$

$$M_\theta = (t_a + t_s) F_\theta \xi^o. \quad (8.7b)$$

In the solution of the structural impedance, the actuators' forces are transferred to the midplane of the structure, and the actuators are removed from the structure. It is noted that, at this stage, the actuator output forces F_x and F_θ are still unknown. For a general unsymmetric actuation, the shell will be subjected both to in-plane forces (equations (8.4 and 8.5)) and out-of-plane moments (equations (8.6 and 8.7)) on the edges of the actuators (Fig.

8.3).

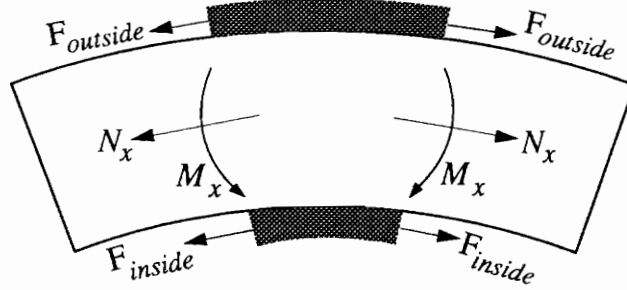


Figure 8.3 Transfer of the actuator's forces to the shell midplane.

Using the modal expansion method, the forced response of the shell is expressed with the following series (Soedel, 1981):

$$u_i(x, \theta, t) = \sum_k p_k U_{ik}(x, \theta) e^{i\alpha t}, \quad (8.8)$$

where p_k is the modal participation factor. For a simply supported cylindrical shell, the axial, tangential, and radial displacements are assumed to be under harmonic loading and may be expressed as:

$$U_{1k} = U_{mnp} = A_{mnp} \cos \alpha x \sin n\theta, \quad (8.9a)$$

$$U_{2k} = V_{mnp} = B_{mnp} \sin \alpha x \sin n\theta, \quad (8.9b)$$

$$U_{3k} = W_{mnp} = C_{mnp} \sin \alpha x \cos n\theta; \quad (8.9c)$$

where $\alpha = \frac{m\pi}{l}$. The subscript p refers to the bending, torsional and extensional modes. Based on the eigenvalue analysis of the system, the Love operators $L_i(u^o, v^o, w^o)$ are obtained, as well as the natural frequencies ω_{mnp} and the displacement ratios A_{mnp}/C_{mnp} and B_{mnp}/C_{mnp} (Soedel, 1981).

$$L_i(u^o, v^o, w^o) = -\rho_s t_s \omega_k^2 U_{ik}. \quad (8.10)$$

Substituting equation (8.10) in equation (8.3), the modal expansion method yields:

$$\ddot{p}_k + \omega_k^2 p_k = F_k e^{i\alpha t}, \quad (8.11)$$

with the forcing function F_k :

$$F_k = F_{mnp} = \frac{I}{\rho_s t_s N_{mnp}} \int_0^{2\pi} \int_0^l \left[\left(\frac{\partial n_x}{\partial x} \right) U_{mnp} + \left(\frac{\partial n_\theta}{R \partial \theta} + \frac{\partial m_\theta}{R^2 \partial \theta} \right) V_{mnp} + \left(-\frac{n_\theta}{R} + \frac{\partial^2 m_x}{\partial x^2} + \frac{\partial^2 m_\theta}{R^2 \partial \theta^2} \right) W_{mnp} \right] R d\theta dx, \quad (8.12)$$

where

$$N_{mnp} = C_{mnp}^2 N_{mnp}^* = \int_0^{2\pi} \int_0^l \left[U_{mnp}^2 + V_{mnp}^2 + W_{mnp}^2 \right] R d\theta dx. \quad (8.13)$$

Solving equation (8.11), the modal participation factor is

$$p_k = \frac{F_k}{\omega_k^2 - \omega^2}. \quad (8.14)$$

At this point, the forced response of the shell under steady state excitation is determined as:

$$u^o(x, \theta, t) = \sum_{p=1}^3 \sum_{m=1} \sum_{n=1} \left\{ \vartheta A_{mnp} / C_{mnp} (S_\theta \cos n\theta - C_\theta \sin n\theta) \cos \alpha x \right\} e^{i\alpha x}, \quad (8.15a)$$

$$v^o(x, \theta, t) = \sum_{p=1}^3 \sum_{m=1} \sum_{n=1} \left\{ \vartheta B_{mnp} / C_{mnp} (S_\theta \sin n\theta + C_\theta \cos n\theta) \sin \alpha x \right\} e^{i\alpha x}, \quad (8.15b)$$

$$w^o(x, \theta, t) = \sum_{p=1}^3 \sum_{m=1} \sum_{n=1} \left\{ \vartheta (S_\theta \cos n\theta - C_\theta \sin n\theta) \sin \alpha x \right\} e^{i\alpha x}; \quad (8.15c)$$

where

$$\vartheta = \frac{R}{\rho_s t_s N_{mnp}^* (\omega_{mnp}^2 - \omega^2)} \left[-\frac{A_{mnp}}{C_{mnp}} (N_x) + \frac{B_{mnp}}{C_{mnp}} \left(\frac{N_\theta}{R\alpha} + \frac{M_\theta}{R^2 \alpha} \right) + \left(\frac{N_\theta}{R\alpha n} + \frac{M_x \alpha}{n} + \frac{M_\theta n}{R^2 \alpha} \right) \right], \quad (8.16a)$$

$$S_\theta = \sin n\theta_1 - \sin n\theta_2, \quad (8.16b)$$

$$C_\theta = \cos n\theta_1 - \cos n\theta_2. \quad (8.16c)$$

Based on the admittance definition (equation (8.2)), the direct structural admittances are:

$$H_{xx} = \frac{1}{R_a} \sum_{p=1}^3 \sum_{m=1} \sum_{n=1} \left\{ \left(\frac{\chi_{in} (A_{mnp} / C_{mnp})^2}{n} + \frac{\chi_{out} \alpha^2}{n} \right) (S_\theta \cos n\theta_o - C_\theta \sin n\theta_o) C_x \right\}, \quad (8.17a)$$

$$H_{\theta\theta} = \frac{1}{l_a} \sum_{p=1}^3 \sum_{m=1}^3 \sum_{n=1}^3 \left\{ \left(\frac{-\chi_{in}(1 + nB_{mnp}/C_{mnp})(B_{mnp}/C_{mnp})}{R\alpha n} + \frac{\chi_{out}n(n + B_{mnp}/C_{mnp})}{R^3\alpha} \right) (S_\theta^2 + C_\theta^2) \sin \alpha x_o \right\}; \quad (8.17b)$$

and the cross admittances are:

$$H_{\theta x} = \frac{1}{l_a} \sum_{p=1}^3 \sum_{m=1}^3 \sum_{n=1}^3 \left\{ \left(\frac{-\chi_{in}(1 + n)(A_{mnp}/C_{mnp})(B_{mnp}/C_{mnp})}{R\alpha n} + \frac{\chi_{out}(n + B_{mnp}/C_{mnp})}{R^2} \right) (S_\theta \cos n\theta_o - C_\theta \sin n\theta_o) C_x \right\}, \quad (8.18a)$$

$$H_{x\theta} = \frac{1}{R_a} \sum_{p=1}^3 \sum_{m=1}^3 \sum_{n=1}^3 \left\{ \left(\frac{\chi_{in}(A_{mnp}/C_{mnp})(B_{mnp}/C_{mnp})}{n} + \frac{\chi_{out}\alpha}{R} \right) (S_\theta^2 + C_\theta^2) \sin \alpha x_o \right\}; \quad (8.18b)$$

where

$$\chi_{in} = -\frac{Ri\omega}{\rho_s t_s} \frac{2\xi^i}{N_{mnp}^*(\omega_{mnp}^2 - \omega^2)} C_x, \quad (8.19a)$$

$$\chi_{out} = -\frac{Ri\omega}{\rho_s t_s} \frac{(t_s + t_a)^2 \xi^o}{2N_{mnp}^*(\omega_{mnp}^2 - \omega^2)} C_x, \quad (8.19b)$$

$$C_x = \cos \alpha x_1 - \cos \alpha x_2, \quad (8.19c)$$

and (x_o, θ_o) are the coordinates of the actuator center. $l_a = x_2 - x_1$ and $R_a = R(\theta_2 - \theta_1)$ are the actuator dimensions in the axial and tangential directions. Finally, the structural impedance along the actuator edges is obtained by inverting the admittance matrix:

$$\begin{bmatrix} Z_{xx} & Z_{x\theta} \\ Z_{\theta x} & Z_{\theta\theta} \end{bmatrix} = \begin{bmatrix} H_{xx} & H_{x\theta} \\ H_{\theta x} & H_{\theta\theta} \end{bmatrix}^{-1}. \quad (8.20)$$

8.2.2 Determination of the Actuator Impedance

With the structural admittance now determined, the next step in the impedance approach is to calculate the actuator impedance and match it to the structural impedance. Making use of the isotropy of the actuator in the 1-1 and 2-2 plane and assuming a thin shell, the Love's equations of motion of the PZT actuator vibrating in the axial and tangential

directions can be expressed as:

$$\rho_a \ddot{u}^o = Y_a^E \frac{\partial \varepsilon_x}{\partial x} , \quad (8.21a)$$

$$\rho_a \ddot{v}^o = Y_a^E \frac{\partial \varepsilon_\theta}{R \partial \theta} ; \quad (8.21b)$$

where ρ_a is the PZT density and Y_a^E is the PZT complex Young's modulus at zero electrical field. The complex Young's modulus is used to include the piezoelectric material's damping.

Under thin shell assumption, the piezoelectric patch is thin with a large radius of curvature. If the actuator patch is small enough, the actuators can be assumed to be flat and the strain-displacement relations for flat structures can be used. This assumption allows us to decouple the radial displacement of the shell from the dynamics of the piezoelectric actuators, i.e.:

$$\begin{Bmatrix} \varepsilon_x \\ \varepsilon_\theta \end{Bmatrix} = \begin{Bmatrix} \frac{\partial u^o}{\partial x} \\ \frac{\partial v^o}{R \partial \theta} \end{Bmatrix} . \quad (8.22)$$

Thus, the equations of motion in the axial and tangential directions for the PZT actuator are:

$$\rho_a \ddot{u}^o = Y_a^E \frac{\partial^2 u^o}{\partial x^2} , \quad (8.23a)$$

$$\rho_a \ddot{v}^o = Y_a^E \frac{\partial^2 v^o}{R^2 \partial \theta^2} . \quad (8.23b)$$

Assuming harmonic excitation by separating the displacements into time and spatial domains, the solution of the equations of motion will give the axial and tangential response of the actuator:

$$u^o(x, t) = [A \sin(kx) + B \cos(kx)] e^{i\alpha t} , \quad (8.24a)$$

$$v^o(\theta, t) = [C \sin(kR\theta) + D \cos(kR\theta)] e^{i\alpha t} ; \quad (8.24b)$$

where ω is the input angular velocity and k is the wave number, which is given by:

$$k^2 = \omega^2 \frac{\rho_a}{Y_a^E} . \quad (8.25)$$

The short-circuit direct input impedances of the piezoelectric actuators in the axial and tangential directions are respectively defined as:

$$Z_{axx} = \frac{Y_a^E t_a k R_a}{i\omega \tan(k l_a)}, \quad (8.26a)$$

$$Z_{a\theta\theta} = \frac{Y_a^E t_a k l_a}{i\omega \tan(k R_a)}, \quad (8.26b)$$

and the short-circuit cross input impedances are:

$$Z_{ax\theta} = \frac{Y_a^E t_a k l_a}{i\omega \tan(k l_a)}, \quad (8.27a)$$

$$Z_{a\theta x} = \frac{Y_a^E t_a k R_a}{i\omega \tan(k R_a)}. \quad (8.27b)$$

Finally, the constitutive equations of the piezoelectric actuator:

$$\begin{Bmatrix} \varepsilon_x \\ \varepsilon_\theta \end{Bmatrix} = \begin{Bmatrix} \frac{\partial u^o}{\partial x} \\ \frac{\partial v^o}{R \partial \theta} \end{Bmatrix} = \begin{bmatrix} 1 & -v_a \\ \frac{Y_a^E t_a R_a}{-v_a} & \frac{Y_a^E t_a l_a}{1} \end{bmatrix} \begin{Bmatrix} F_x \\ F_\theta \end{Bmatrix} + \begin{Bmatrix} d_{31} \\ d_{32} \end{Bmatrix} E, \quad (8.28)$$

where d_{3i} are the piezoelectric constants of the PZT actuators, E is the electrical field and v_a is the actuator's Poisson's ratio.

8.2.3 Structural/Actuator Dynamic Interaction

With the structural and actuator impedances now determined, the third step in the impedance modeling is to consider the structural/actuator dynamic interaction (Fig. 8.4). The interaction between the actuator is taken into account by the equilibrium and compatibility equations, which state the equilibrium of the forces between the actuator and the structure at the actuator edges. Applying the displacement boundary conditions ($u_{x=0} = 0$, $v_{\theta=0} = 0$) (Zhou et al., 1993) to equation (8.28), B and D are found to be zero. The remaining unknowns A and C will be determined using the constitutive equations of the piezoelectric actuator (equation (8.28)) at $x = l_a$ and $\theta = \theta_a$:

$$\begin{bmatrix} k \cos(kl_a) \left(I - \nu_a \frac{Z_{x\theta}}{Z_{ax\theta}} + \frac{Z_{xx}}{Z_{axx}} \right) & k \cos(kR_a) \left(\frac{Z_{\theta x}}{Z_{a\theta x}} - \nu_a \frac{Z_{\theta\theta}}{Z_{a\theta\theta}} \right) \\ k \cos(kl_a) \left(\frac{Z_{x\theta}}{Z_{ax\theta}} - \nu_a \frac{Z_{xx}}{Z_{axx}} \right) & k \cos(kR_a) \left(I - \nu_a \frac{Z_{\theta x}}{Z_{a\theta x}} + \frac{Z_{\theta\theta}}{Z_{a\theta\theta}} \right) \end{bmatrix} \begin{Bmatrix} A \\ C \end{Bmatrix} = \begin{Bmatrix} d_{31} \\ d_{32} \end{Bmatrix} E \quad (8.29)$$

Based on the impedance definition, the dynamic actuator forces output per unit length are:

$$F_x = -\frac{i\omega}{R_a} (A \sin(kl_a) Z_{xx} + C \sin(kR_a) Z_{x\theta}) e^{i\alpha x}, \quad (8.30a)$$

$$F_\theta = -\frac{i\omega}{l_a} (A \sin(kl_a) Z_{\theta x} + C \sin(kR_a) Z_{\theta\theta}) e^{i\alpha x}. \quad (8.30b)$$

Thus, the dynamic actuator force output has been calculated based on the structural impedance.

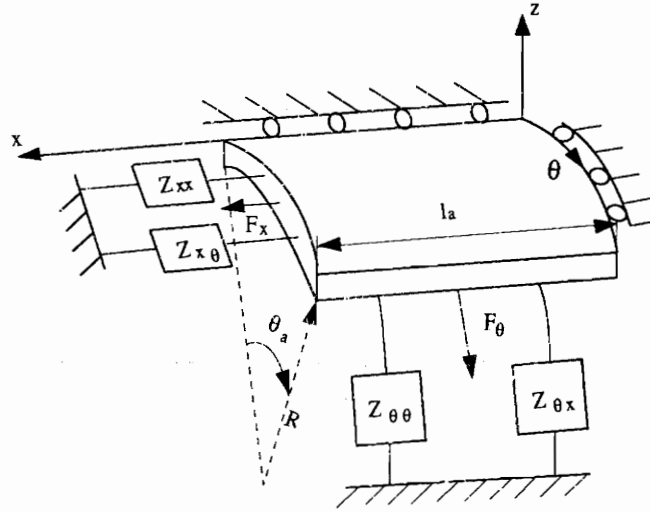


Figure 8.4 Dynamic interaction between the piezoelectric patch and the shell structure represented by mechanical impedance.

8.2.4 Shell Response Calculations

Using the dynamic actuator force output, the shell response can be calculated based on the shell governing equations developed in section 8.2.1. The axial, tangential and radial displacements are given in equation (8.15).

8.3 Theoretical Results

The derived impedance model that was presented in Fig. 8.1 will be applied to the thin cylinder, with dimensions and properties given in Table 8.1. The dimensions were chosen such that the shell is thin and the actuators are small enough not to increase the structural stiffness substantially. The shell is made of aluminum and G1195 piezoelectric actuator patches are used. Various case studies are presented, with a particular attention to pure out-of-phase and to pure in-phase actuation. For comparison purposes, all actuators are always excited with a free induced strain (Λ) of $\pm 1000 \mu\text{strain}$.

Table 8.1 *Material and geometric properties of the PZT actuator and the aluminum shell.*

	Aluminum shell	PZT Actuator
Young's Modulus, Pa	69×10^9	63×10^9
Density, kg/m^3	2700	7650
Poisson's ratio	0.3	0.3
Loss factor	0.006	0.001
Piezo. Coefficient d_{32} , m/V	N/A	-166×10^{-12}
Applied electric field, V/m	N/A	8.20×10^6
Radius / Length, cm	10.65	10°
Width, cm	34	2
Thickness, mm	1.1	0.24

The structural admittance for in-phase actuation is shown in Fig. 8.5. The four peaks corresponds to the first four natural frequencies of the shell, as expected. The reader's attention should be drawn to the cross admittances $H_{x\theta}$ and $H_{\theta x}$. In most cases, one can expect the cross admittances to be equal. However, it can be easily seen that the cross admittances are different both in shape and magnitude, having different antiresonant frequencies. This difference is due to the admittance definition that was used in equation (8.2). In that equation, the admittance definition was based only on F_x and F_θ . However, if a special attention is given to the third equilibrium equation (equation (8.3c)), one will notice the presence of the induced uniform tangential force n_θ . It was previously discussed that this loading term n_q can be viewed as an external transverse pressure load, necessary to maintain the self equilibrium of the shell when actuated in-phase (Chapter 3). If viewed as such, the admittance definition is not only dependent on the forces F_x and F_θ , but also on the radial

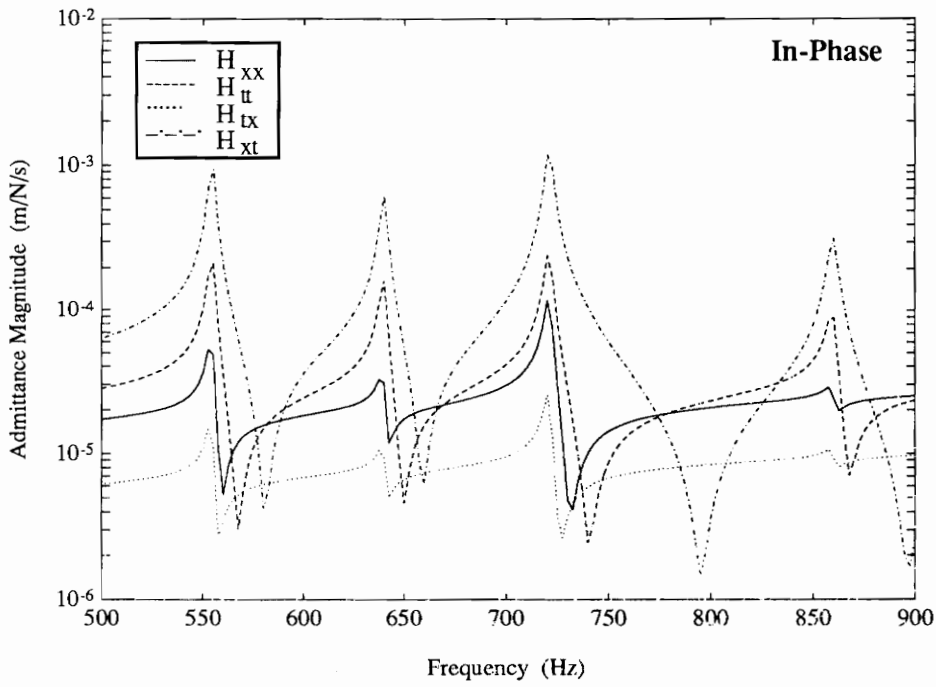


Figure 8.5 Structural admittance for in-phase actuation. Cross admittances are not equal when two dimensional admittance definition is used.

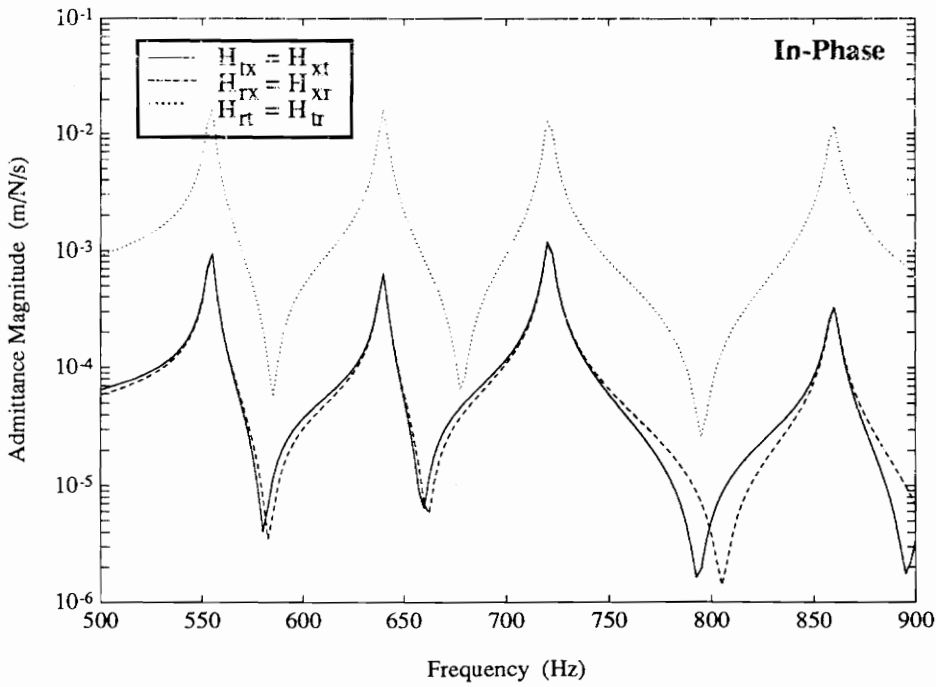


Figure 8.6 Structural cross admittances for in-phase actuation are equal when three dimensional admittance definition is used.

pressure term $-\frac{n_\theta}{R}$. Based on this observation, the admittance for pure in-phase actuation can be defined as a 3×3 matrix:

$$\left(2\dot{u}^o\right)_{Inphase}\bigg|_{x=x_2} - \left(2\dot{u}^o\right)_{Inphase}\bigg|_{x=x_1} = -[H_{xx}F_x + H_{\theta x}F_\theta + H_{rx}F_\theta^*], \quad (8.31a)$$

$$\left(2\dot{v}^o\right)_{Inphase}\bigg|_{\theta=\theta_2} - \left(2\dot{v}^o\right)_{Inphase}\bigg|_{\theta=\theta_1} = -[H_{x\theta}F_x + H_{\theta\theta}F_\theta + H_{r\theta}F_\theta^*], \quad (8.31b)$$

$$2\int_{\theta_1}^{\theta_2} \dot{w}^o d\theta = -[H_{xr}F_x + H_{\theta r}F_\theta + H_{rr}F_\theta^*]; \quad (8.31c)$$

where F_θ^* is the term resulting from radial pressure term. Using this definition, the cross admittances will all be exactly equal, as shown in Fig. 8.6. However, for the purpose of the impedance modeling, it is necessary to lump the radial pressure term F_θ^* with the tangential force F_θ in the admittance definition. This is attributed to the close dependency between the two loads involving F_θ .

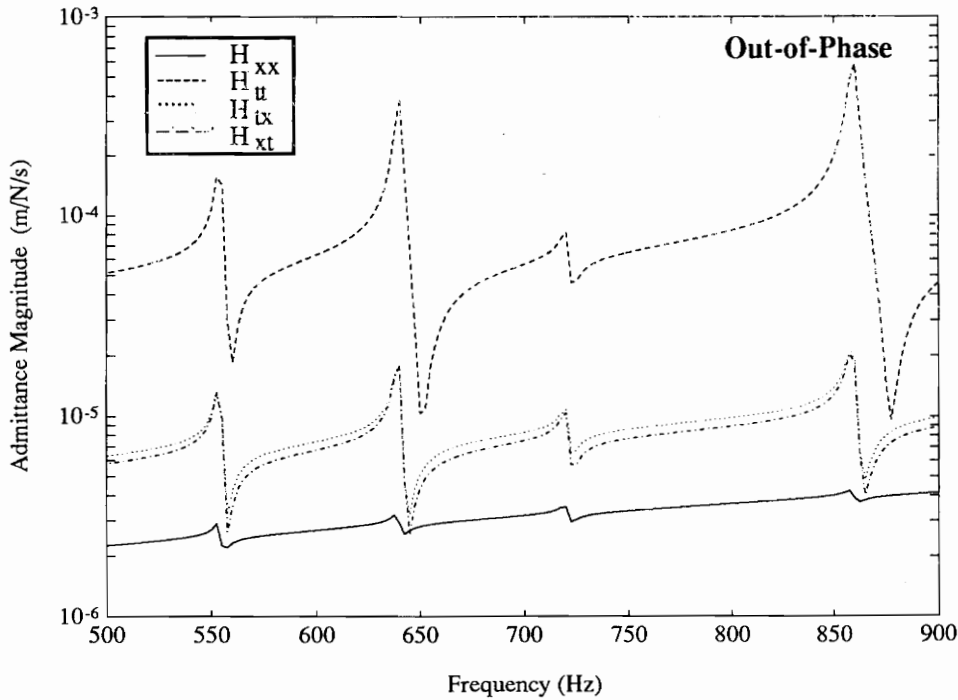


Figure 8.7 Structural admittance for out-of-phase actuation. Slight difference in the cross admittances due to the transverse shear stress included in the equations.

The structural admittance for out-of-phase actuation is shown in Fig. 8.7. Once again, the cross admittances $H_{x\theta}$ and $H_{\theta x}$ are not exactly equal. This time, the difference is due to the transverse shear resultant that is included in the governing equations (Chapter 7). If the shear stress resultant is omitted in the second governing equation, the cross admittances will become equal since the admittances will now have only one dependency on M_θ . For both in-phase and out-of-phase actuation, an increased shell radius will reduce the differences between the cross admittances; and for plates, the cross admittances will be exactly equal. Admittance graphs are not presented for unsymmetric voltages applied to the PZT actuators, since they will be a simple linear combination of the in-phase and out-of-phase admittances.

The in-plane forces created by the in-phase actuation of the piezoelectric patches are shown in Fig. 8.8. In the impedance technique, the force calculations are based on both the actuator and the structural impedances. In Fig. 8.5, the direct admittance in the axial direction is different from the direct admittance in the tangential direction. Thus, if the admittances are different, the dynamic forces produced by the actuators should also be different in the axial and tangential directions. This can be observed in Fig. 8.8. The dashed line, a static model previously developed (Wang and Rogers, 1991), agrees well with the impedance model for the force in the x direction only. However, when this static model or other static models are used, there is no distinction between the two directions and the actuator forces are thus mistakenly assumed to be equal. At the natural frequencies of the structure, the tangential equivalent force developed is larger than the axial equivalent force. This behavior is a simple characteristic of the system, the structural tangential admittance being smaller than the direct axial admittance. The next figure (Fig. 8.9) shows the dynamic equivalent moments produced by pure out-of-phase actuation. The conclusions are similar to those of in-phase actuation, and produced moments of different magnitude in the axial and tangential directions.

The radial displacement response to in-phase and out-of-phase dynamic actuation of the shell at $(x=0.09, \theta=90^\circ)$ is presented in Fig. 8.10. For comparison purposes, the shell response using static modeling⁴ is also presented. The most remarkable characteristic of Fig. 8.10 is the greater authority of out-of-phase actuation when compared to in-phase actuation. The displacements produced by out-of-phase actuation are an order of magnitude larger than the displacements obtained from in-phase actuation. This behavior is predictable based on the admittances plots (Fig. 8.5 and 8.6), since the shell has greater tangential impedance. Thin shells are more sensitive to transverse loading (out-of-phase actuation) than to in-plane

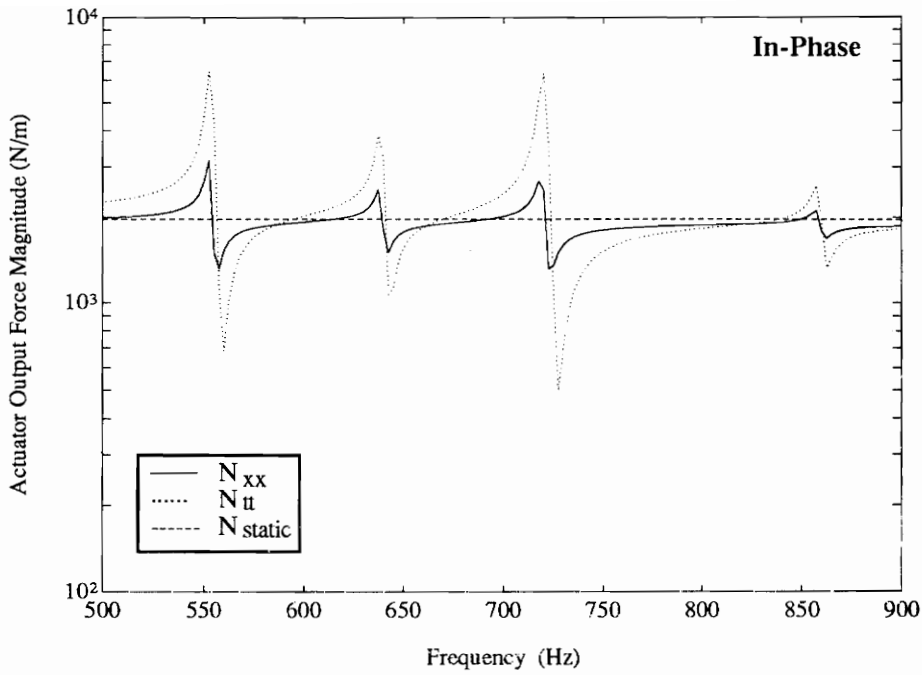


Figure 8.8 Dynamic equivalent forces produced by pure in-phase actuation on the structure are not equal in the axial and tangential directions.

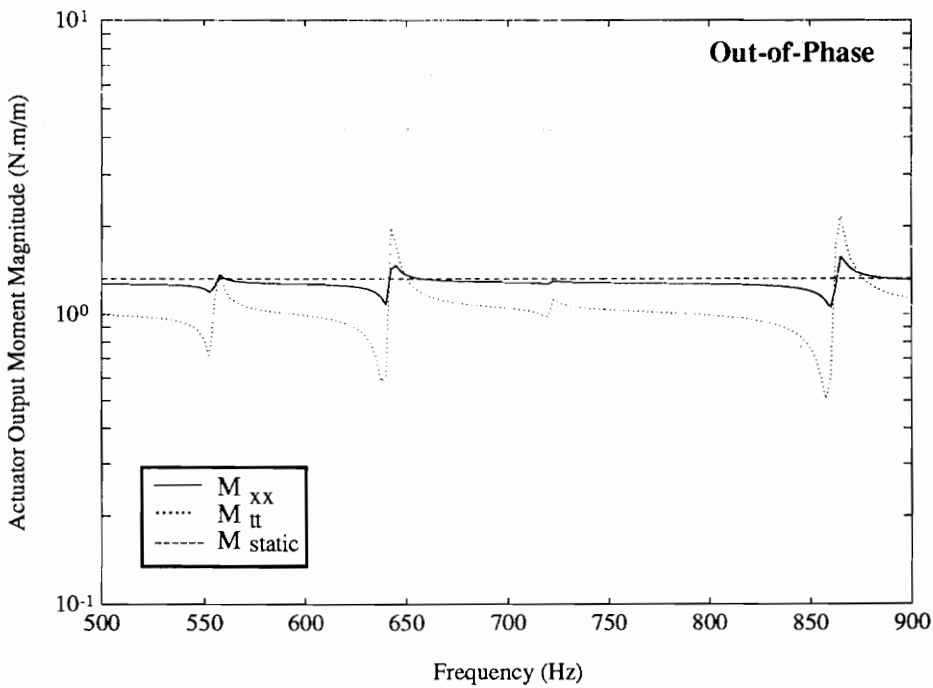


Figure 8.9 Dynamic equivalent moments produced by pure out-of-phase actuation on the structure are not equal in the axial and tangential directions.

loading (in-phase actuation). The transverse natural modes are directly excited when out-of-phase actuation is used, while they are only excited through the in-plane/out-of-plane coupling property of shells when in-phase actuation is used. The resonant frequencies of the shell based on the impedance model are shifted to the right when compared to the resonant frequencies based on the static model. This behavior is due to the increased stiffness of the actuators on the host structure which is included in the impedance model, as opposed to the static model where the actuator stiffness is not included.

In Fig. 8.11, the shell response to a single actuator bonded on the inside and on the outside of the shell at $(x=0.09, \theta=90^\circ)$ is shown. Even though the shell is thin, the shell response is different. The finite element analysis that will be presented in the next section verifies this shell response, as well as the linear combination of pure in-phase and out-of-phase actuation (equation (8.1)) concept to model unsymmetrical actuation. Thus, special considerations should be taken when single sided actuation is used.

A number of other cases were simulated using the impedance model, but only the most relevant information obtained from them will be discussed. Firstly, the stiffness of the actuator has an important impact on the behavior of the system. A thicker actuator will produce higher forces on the host structure, but it will also be more difficult to model the shell response due to the increased non-uniformity of the host structure. Changing the type of actuation material also changes the stiffness of the actuator, e.g. PVDF has a smaller Young's modulus than piezoceramic material, and thus will have a lesser authority on the structure. The size of the actuator patches bonded on the structure also needs to be considered when designing such structures. Another design parameter is the location of the actuator patch on the structure: the mechanical impedance of the structure is dependent on the actuator location and will thus affect the dynamic forces produced by the actuators. At a particular location, the actuator patches will be efficient in exciting some resonant frequencies, while another location will be more efficient at exciting other resonant frequencies. Many cases using different shell and actuator dimensions were considered and all showed better authority when out-of-phase actuation is used.

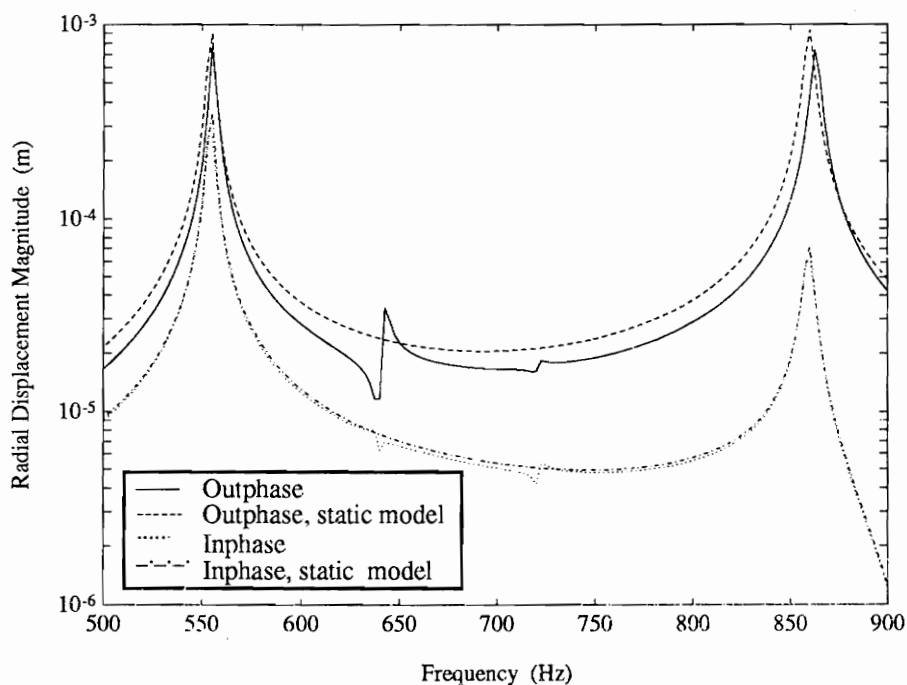


Figure 8.10 The comparison of the structural response between in-phase and out-of-phase actuation shows greater authority for out-of-phase actuation at $(x=0.09, \theta=90^\circ)$.

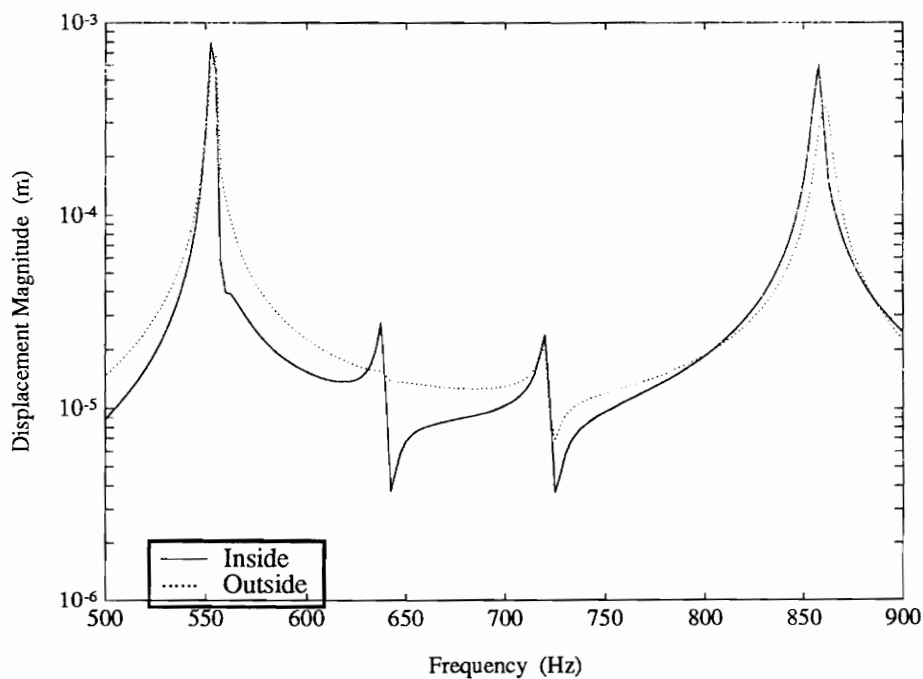


Figure 8.11 Even for thin shells, the structural response to single side actuation (inside and outside patches) is not equal at $(x=0.09, \theta=90^\circ)$.

8.4 Finite Element Verification

To verify the derived impedance model, a finite element analysis of the case study presented in the previous section was carried out. Making use of symmetry, the finite element model consists of only one quarter of the shell, and uses thin shell elements. The actuator patches are also modeled with thin shell elements, and are connected to the shell structure with rigid elements. The finite element analysis will only consider static actuation and will be compared to the impedance model with an excitation frequency of 5 Hz, which is well below the first natural frequency of the shell. This model does not make any assumption on the actuator stiffness or mass. Three different types of loading on the finite element model were considered. Firstly, thermal contraction and/or expansion of the actuators is used to simulate in-phase or out-of-phase actuation. The deformed shapes of the shell under such actuation are presented in Figures 8.12 and 8.13.

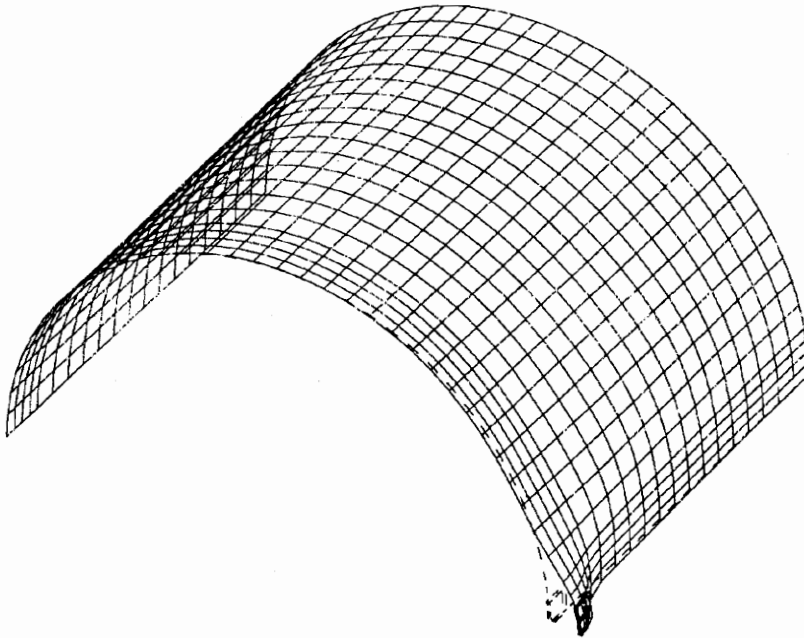


Figure 8.12 Structural response to static in-phase actuation based on finite element analysis.

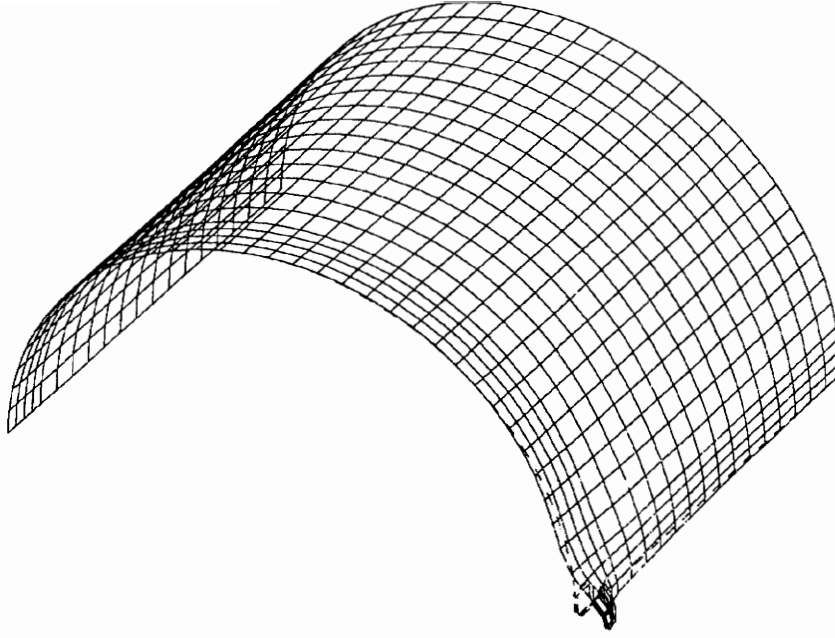


Figure 8.13 *Structural response to static out-of-phase actuation based on finite element analysis.*

The second loading type use line forces and moments, and uniform pressures applied on the elements modeling the shell structure leaving the actuators elements in the model to include their stiffness. The magnitudes of the forces and moments are based on the actuators free expansion and are given by (Chapter 3):

$$N_{\Lambda} = 2 \frac{Y_a^E t_a}{1-\nu} d_{32} E , \quad (8.32a)$$

$$M_{\Lambda} = (t_s + t_a) \frac{Y_a^E t_a}{1-\nu} d_{32} E . \quad (8.32b)$$

The displacements obtained by this second model matches almost exactly the displacements from the thermal loading case, and is thus the appropriate way to apply the loading when the actuators are left on the structure. Finally, the third type of loading also use line forces and moments and uniform pressures applied on the elements modeling the shell structure, but the actuator elements are removed from the model, leaving a uniform structural stiffness. However, for this case the magnitudes of the forces and moments are based on the continuity of the strains at the interface of the shell and the actuators, which is often referred to as the Euler-Bernoulli model, and are given by (Chapter 3):

$$N_{eq} = \frac{Y_s t_s}{1-\nu} \frac{2}{2+\psi} d_{32} E , \quad (8.33a)$$

$$M_{eq} = (t_s + t_a) \frac{Y_s t_s}{1-\nu} \frac{1}{6+\psi + \frac{12}{T} + \frac{8}{T^2}} d_{32} E , \quad (8.33b)$$

where T is the thickness ratio t_s/t_a . The deformed shape based on this loading is the same as the two previous cases, but differs in magnitude. This magnitude difference comes from the assumptions made in the derivation of the equivalent forces and moments applied to the shell. In the equation derivation, the boundary conditions are assumed to be free. When shells are considered, the structure is a closed body and does not have free boundary conditions, since stresses will be present in the whole shell. The same phenomena occurs for simpler structures such as beams (Chaudhry and Rogers, 1993). When the beam is simply supported, the boundary conditions will be free and the equivalent loading based on the Euler-Bernoulli method will give accurate results. If the boundary conditions are changed to clamped, the assumed stress free boundary condition in the equation derivation is no longer valid and will produce errors in the magnitude of the structural displacements. In Figures 8.14 and 8.15, the displacements of the shell at $x=0.09$ based on the two loading types are presented. It can be easily seen from the displacements that the deformed shape is similar, but differs in the magnitude.

The final step in this paper is to directly compare the impedance model at 5 Hz with the static finite element model. For both in-phase and out-of-phase actuation, the radial displacements based on the impedance model match the finite element results in shape, but not in magnitude (Figs. 8.14 and 8.15). In the impedance modeling, the actuator stiffness is included in the calculations of the actuator forces output. At that point of the modeling, no assumptions have been made either on the mass or the stiffness of the actuators. When the displacements are calculated using the dynamic actuator forces, the displacement equations (equation (8.15)) are based on a uniform shell stiffness, not including the increased mass or stiffness due to the actuators. Neglecting the actuator stiffness will reduce the stiffness of the integrated system, and thus produce larger impedance model displacements seen in the last two figures. The discrepancies between the impedance model and the finite element analysis will reduce with decreasing actuator size and thickness.

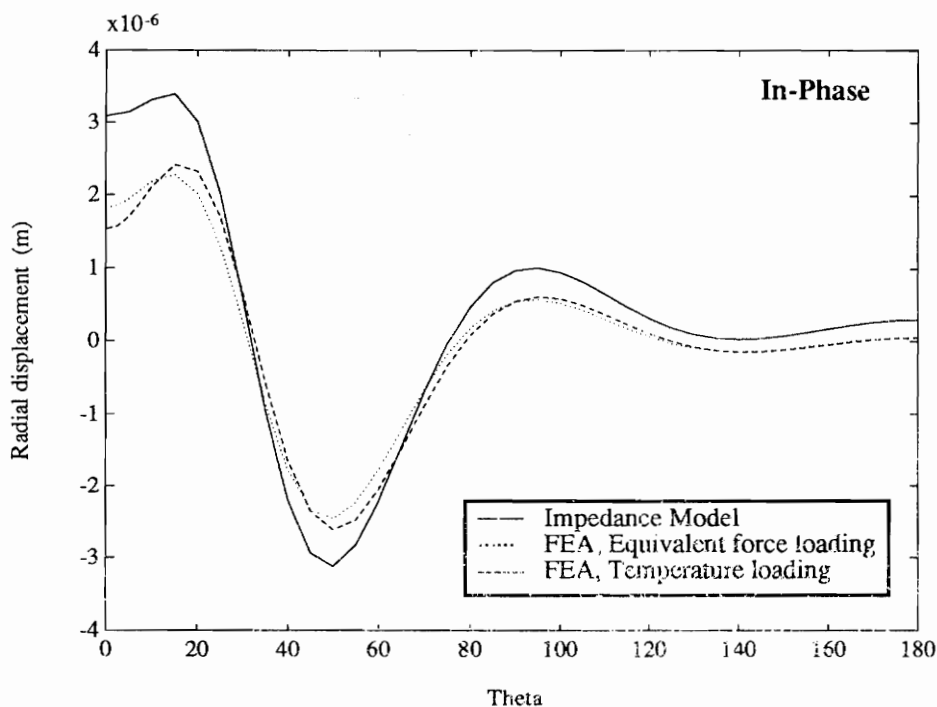


Figure 8.14 Comparison of the displacements of the static finite element model and the impedance model at 5 Hz for out-of-phase actuation at $x=0.09$.

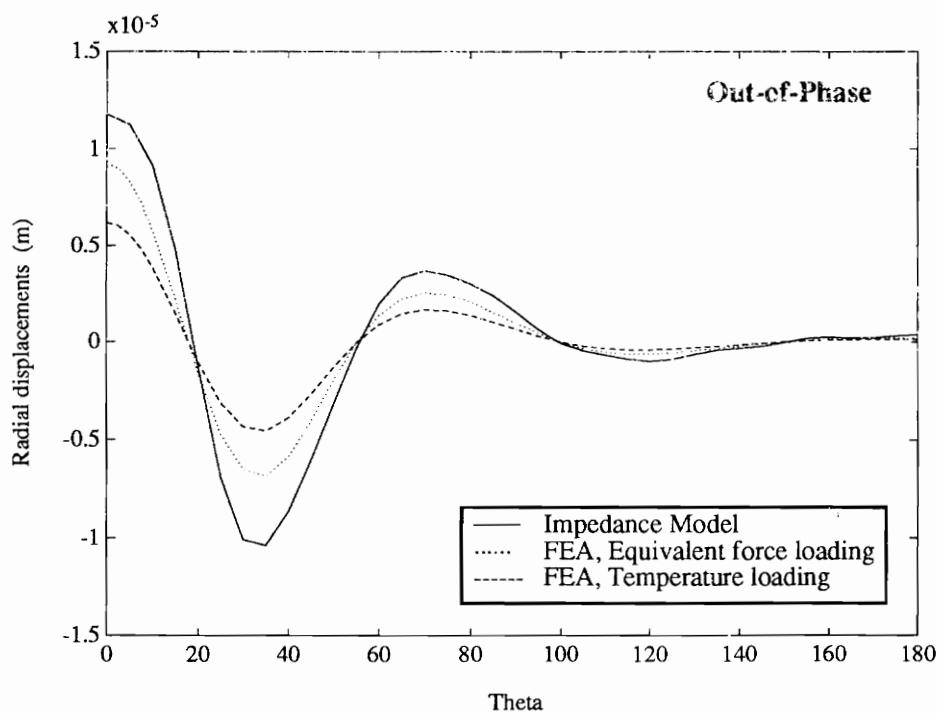


Figure 8.15 Comparison of the displacements of the static finite element model and the impedance model at 5 Hz for in-phase actuation at $x=0.09$.

8.5 Conclusions

In this chapter, an impedance-based model to predict the dynamic response of cylindrical shells subjected to excitation from surface-bonded induced strain actuators was presented. The strength of the impedance model over the conventional static approach is the inclusion of the dynamic interaction between the induced strain actuators and the host structure. In its derivation, the impedance model includes the actuator mass and stiffness for a more accurate representation of the actual system. The impedance model also considers the different shell stiffnesses in the axial and tangential directions. Doing so, it was found that the actuators' dynamic forces in the axial and tangential direction are not equal and are frequency dependent. However, in the shell response calculations the actuator mass and stiffness are neglected to simplify the shell governing equations, and thus will over-predict the displacements. Out-of-phase actuation is shown to be more efficient than in-phase actuation in exciting the lower order bending modes of shell structures. The impedance-based model for low frequencies was validated by a static finite element analysis.

Chapter 9

Conclusions and Recommendations

9.1 Conclusions

In this dissertation, an impedance-based model to predict the dynamic response of shells actuated with surface-bonded induced strain actuators was presented. General basis for the induced strain actuation of shell structures were first introduced. Then, the impedance model was derived for pure out-of-phase actuation and pure in-phase actuation of one-dimensional rings, followed with a generalization to unsymmetric actuation of two-dimensional shells. Finite element analysis and experimental work were performed and compared to the derived impedance model. The strength of the impedance model over the conventional static approach is the inclusion of the dynamic interaction between the induced strain actuators and the host structure. Because of its dynamic characteristics, the impedance modeling approach is the appropriate tool to be used in the vibrational and acoustical control of structures.

The principal conclusions of this dissertation are:

- Based on Donnell's theory, the expressions to represent the actuator forces and moments for shell structures are found to be the same as those obtained for plates. However, due to the curvature of the shell, the representation of the in-phase actuation with an equivalent in-plane line force applied along the edge of the actuator results in the application of erroneous rigid-body transverse forces. To avoid these rigid body forces, a method to represent the in-phase actuation with a system of self-equilibrating forces must be applied. Thus, the action of the actuator should be represented by an equivalent in-plane force and a transverse distributed pressure applied in the region of the actuator patch.
- A discussion of the appropriate representation of the loading due to out-of-phase actuation and in-phase actuation was presented. For out-of-phase actuation, the loading can be represented in the shell governing equations either as an induced

uniform moment over the footprint of the actuators or as an external line moment at the ends of the actuators. For in-phase actuation, the loading can be represented in the shell governing equations either as induced uniform forces on the actuator footprint or as a combination of external tangential forces at the ends of the actuators and an external uniform transverse pressure over the footprint of the actuators.

- The transverse shear stress resultant has an important impact in the modeling of out-of-phase actuation. If the shear stress resultant is neglected in the governing equations, a significantly different response at low frequencies from the full impedance model is obtained. The impedance model including the shear stress resultant gives an excellent prediction of the structural response when compared to the dynamic finite element model.
- The impedance model for the in-phase actuation of induced strain actuators bonded to the surface of a circular ring has a good correlation with the dynamic finite element results.
- Linear superposition of pure in-phase and pure out-of-phase actuation can be used to model the more general unsymmetric actuator loading.
- The actuators' dynamic forces in the axial and tangential direction are not equal because the impedance model considers different shell stiffnesses in the axial and tangential directions, as it should be.
- In-phase actuation has lesser authority on shell structures than out-of-phase actuation. Also, out-of-phase actuation is more efficient in exciting the lower order bending modes of the shell because in-phase actuation only excite the bending modes through in-plane and out-of-plane displacement coupling, while out-of-phase actuation excite the bending modes directly. On the other hand, in-phase actuation has the capability of exciting the higher circumferential and axial modes, as opposed to out-of-phase actuation.
- The experimental verifications used to validate the impedance model were conclusive. An excellent match for out-of-phase actuation was obtained, with a more difficult match for in-phase actuation. The larger discrepancies are found due to the smaller displacements involved and to the greater sensitivity to the bonding of the actuators

on the structure. Nevertheless, the in-phase actuation experimental results are still similar to the theoretical results, both in shape and magnitude.

- Various finite element models were used and compared to the derived impedance model. When the actuator mass and stiffness are neglected in the finite element model, an perfect agreement with the impedance model is obtained. However, if the actuator stiffness is considered in the finite element model, the analytical model only gives a good approximation of the shell's deformed shape. In the impedance approach, the actuator mass and stiffness are included in the derivation of the dynamic equivalent actuator forces, but are neglected in the final shell response calculations .
- The piezoelectric elements available in ANSYS 5.0 are an efficient mean to dynamic analysis of induced strain actuated structures.

In summary, two important messages to remember: (i) the plate models can not be used to model curved structures; (ii) the impedance approach should always be used when induced strain actuators are excited harmonically. Using the conventional static-based introduces many assumptions, which will results in important modeling errors.

9.2 Recommendations

In this dissertation, a complete impedance model for simply supported circular cylindrical thin shells was presented. This work have limitations for practical applications because of the targeted shell structure used in the modeling derivation. To extend the reach of this work, a few recommendations on possible future work are suggested:

- Experimentation on two dimensional shells could be done to verify the accuracy of the dynamic response obtained from the impedance model. In present work, the two dimensional impedance model was only verified using a static finite element analysis. This verification was found satisfactory since the dynamic characteristics were verified for one dimensional rings. Further verification of the two dimensional impedance model could also be done using the full version of ANSYS 5.0 (the academic version available at CIMSS has limited number of elements).

- Based on the impedance model, a coupled electro-mechanical model for shell structures could be easily derived. Such model would provide important information on the power consumption of the induced strain actuators and the energy transfer in electro-mechanical system.
- Extend the two dimensional impedance model to a larger array of boundary conditions, such as clamped-clamped, free-free, cantilever, etc... However, some difficulties may arise in the choice of the appropriate shape functions to model the shell deformation for some boundary conditions. Numerical methods such as the Rayleigh-Ritz solution could be used to solve for the system parameters. In this work, only simply-supported boundary conditions were used.
- Extend the two dimensional impedance model to open shells and curved panels. Such structures are solved from the same governing equations as closed shells, but uses different boundary conditions.
- Extend the derivation of the impedance modeling to more general shells, i.e., anisotropic shells, composite shells, elliptic cylinders or shells with double curvatures. This extended model could be based on the layered shell theory. In this work, the impedance model derivation was limited to circular cylindrical shells.
- Investigate the possibility to apply the derived impedance model to more complex structures like aircraft fuselage and submarine hulls. These complex structures contains nonuniform properties due to the presence of stiffeners, floors, and windows that will greatly complicate modeling of the structural response to induced strain actuation. The goal of this investigation would be to determine if the same conclusions obtained for simple shells can be translated to more complex structures, conclusions like better authority of out-of-phase actuation over in-phase actuation and better efficiency of out-of-phase actuation in exciting the lower order bending modes.

Bibliography

- [1] Accorsi, M.L., 1993, "Mechanics of Adaptive Materials Using the Eigenstrain Finite Element Method," *Proceedings, ASME Winter Annual Meeting Adaptive Structures Symposium*, New Orleans, LA, AD-Vol. 35, ASME Technical Publishing, New-York, NY, pp. 203-207.
- [2] Agarwal, S.K., Tong, D., and Nagaraja, K., 1994, "Control of Shapes of Elastic Plates Using Embedded Piezoelectric Actuators," *Proceedings, SPIE Conference on Smart Structures and Materials*, Orlando, FL, Vol. 2190, SPIE Publishing, Bellingham, WA, pp. 463-470.
- [3] Babu, G.L., and Hanagud, S., 1990, "Delamination in Smart Composite Structures: A parametric Study on Vibrations," *Proceedings, AIAA/ASME/ASCE/AHS/ASC 30th Structures, Structural Dynamics and Materials Conference*, Long Beach, CA, AIAA Publishing, Washington, DC, pp. 2417-2426.
- [4] Bailey, T.B., and Hubbard, J.E., 1985, "Distributed Piezoelectric-Polymer Active Vibration Control of a Cantilever Beam," *Journal of Guidance Control and Dynamics*, Vol. 8, No. 5, pp. 605-611.
- [5] Birman, V., 1992, "Theory of Geometrically Nonlinear Composite Plates with Piezoelectric Stiffeners," *Proceedings, ASME Winter Annual Meeting*, Anaheim, CA, DSC-Vol. 38, ASME Technical Publishing, New-York, NY, pp.231-237.
- [6] Cao, W., 1993, "Nonuniform Surface Deformation of Piezoelectric Composites and the Effect of Surface Plates," *Proceedings, ASME Winter Annual Meeting*, New Orleans, LA, AD-Vol. 35, ASME Technical Publishing, New-York, NY, pp. 197-201.
- [7] Cao, W., Zhang, Q., and Cross, L.E., 1992, "Theoretical Study of the Static Performance of Piezoelectric Ceramic-Polymer Composites with 1-3 Connectivity," *Journal of Applied Physics*, Vol. 72, pp. 5814-5821.
- [8] Cao, W., Zhang, Q., and Cross, L.E., 1993, "Theoretical Study of the Static Performance of Piezoelectric Ceramic-Polymer Composites with 2-2 Connectivity," *IEEE Transactions on Ultrasonics, Ferroelectrics and Frequency Control*, Vol. 40, pp. 103-109.

- [9] Carman, G.P., and Reichik, B., 1994, "Modeling of Laminated Plates Containing Elastic Nonlinear Actuators," *Proceedings, SPIE Conference on Smart Structures and Materials*, Orlando, FL, Vol. 2190, SPIE Publishing, Bellingham, WA, pp. 142-152.
- [10] Cawley, J.D., 1991, "Introduction to Ceramic-Metal Joining," *Proceedings, TMS Fall Meeting, Ceramic-Metal Joining Symposium*, Detroit, MI, pp. 3-11.
- [11] Chandrashekhara, K., and Agarwal, A.N., 1993, "Dynamic Modeling of Piezoelectric Plates Using Finite Element Method," *Proceedings, SPIE Conference on Smart Structures and Materials*, Albuquerque, NM, Vol. 1917, SPIE Publishing, Bellingham, WA, pp. 451-460.
- [12] Chaudhry, Z., and Rogers, C.A., 1992, "Enhanced Structural Control with Discretely Attached Induced Strain Actuators," *Proceedings, AIAA/ASME/ASCE/AHS/ASC 33rd Structures, Structural Dynamics and Materials Conference*, Dallas, TX, AIAA Publishing, Washington, DC, pp. 548-555.
- [13] Chaudhry, Z., and Rogers, C.A., 1993, "Performance and Optimization of Induced Strain Actuated Structures Under the Action of External Loads," *Proceedings, AIAA/ASME/ASCE/AHS/ASC 34th Structures, Structural Dynamics and Materials Conference*, La Jolla, CA, AIAA Publishing, Washington, DC, pp. 3475-3484.
- [14] Chaudhry, Z., and Rogers, C.A., 1994, "The Pin-Force Model Revisited", *Journal of Intell. Mater. Syst. and Struct.*, Vol. 5, No. pp. 347-354.
- [15] Crawley, E.F., and Anderson, E.H., 1990, "Detailed Models of Piezoceramic Actuation of Beams," *Journal of Intell. Mater. Syst. and Struct.*, Vol. 1, No. 1, pp. 4-25.
- [16] Crawley, E.F., and de Luis, J., 1987, "Use of Piezoelectric Actuators as Elements of Intelligent Structures," *AIAA Journal*, Vol. 25, No. 10, pp. 1373-1385.
- [17] Crawley, E.F., and Lazarus, K.B., 1989, "Induced Strain Actuation of Isotropic and Anisotropic Plate," *AIAA Journal*, Vol. 29, No. 6, pp. 944-951.
- [18] Crawley, E.F., 1993, "Intelligent Structures: A Technology Overview and Assessment," pp. 6.1-6.16.
- [19] Davidson, R., 1990, "The Current Status and Future Prospects of Smart Composites," *ESA Symposium on Space Applications of Advanced Structural Materials*, Noordwijk, Netherlands, pp. 429-436.

- [20] De Salvo, G.J. and Swanson, J.A., 1979, *ANSYS User's Manual*, Swanson analysis systems, Houston, PA.
- [21] Detwiler, D.T., Shen, M.H., and Venkayya, V.B., 1994, "Two-Dimensional Finite Element Analysis of Composite Plates Containing Distributed Piezoelectric Actuators and Sensors," pp. 451-460.
- [22] Diehl, G.W., and Cudney, H.H., 1994, "The Effects of Shaped Piezoceramic Actuators on the Excitation of Beams," *Proceedings, AIAA/ASME/ASCE/AHS/ASC 35th Structures, Structural Dynamics and Materials Conference, Adaptive Structures Forum*, Hilton Head, SC, AIAA Publishing, Washington, DC, pp. 270-278.
- [23] Dimitriadis, E.K., Fuller, C.R., and Rogers, C.A., 1991, "Piezoelectric Actuators for Distributed Vibration Excitation of Thin Plates," *Journal of Vibration and Acoustics*, Vol. 113, pp. 100-107.
- [24] Fanson, J.L., and Caughey, T.K., 1987, "Positive Position Feedback Control for Large Space Structures," *Proceedings, AIAA/ASME/ASCE/AHS/ASC 28th Structures, Structural Dynamics and Materials Conference*, Monterey, CA, AIAA Publishing, Washington, DC, pp. 588-598.
- [25] Fleischer, M., Stein, D., and Meixner, H., 1989, "New Type of Piezoelectric Ultrasonic Motor," *IEEE Transactions on Ultrasonics, Ferroelectrics, and Frequency Control*, Vol. 36, No. 6, pp. 614-619.
- [26] Fuller, C.R., Snyder, S., Hanson, C. and Silcox, R., 1990, "Active Control of Interior Noise in Model Aircraft Fuselages using Piezoceramic Actuators," *Proceedings of the AIAA 13th Aeroacoustic Conference*, Vol. 90-3922, Tallahassee, FL, October 22-24.
- [27] Goto, H., and Sasaoka, T., 1988, "Virtual Micro Positioning System using PZT Actuators," *Bulletin of Japanese Society of Precision Engineering*, Vol. 22, No. 4, pp. 277-282.
- [28] Ha, S.K., and Chang, F.K., 1990, "Finite Element Modeling of Response of Laminated Composites with Embedded Piezoelectric Actuators," *Proceedings, AIAA/ASME/ASCE/AHS/ASC 31st Structures, Structural Dynamics and Materials Conference*, Long Beach, CA, AIAA Publishing, Washington, DC, pp. 2323-2330.

- [29] Ha, S.K., Keilers, C., and Chang, F.K., 1991, "Analysis of Laminated Composites Containing Distributed Piezoelectric Ceramics," *J. of Intell. Mater. Syst. and Struct.*, Vol. 2, No. 1, pp. 59-71.
- [30] Ha, S.K., Keilers, C., and Chang, F.K., 1992, "Finite Element Analysis of Composite Structures Containing Distributed Piezoceramic Sensors and Actuators," *AIAA Journal*, Vol. 30, No. 3, pp. 772-780.
- [31] Hagood, N.W., and Bent, A.A., 1993, "Development of Piezoelectric Fiber Composites for Structural Actuation," *Proceedings, AIAA/ASME/ASCE/AHS/ASC 33rd Structures, Structural Dynamics and Materials Conference*, La Jolla, CA, AIAA Publishing, Washington, DC, pp. 3625-3638.
- [32] Hagood, N.W., Chung, W.H., and von Flotow, A., 1990, "Modeling of Piezoelectric Actuator Dynamics for Active Structural Control," *Proceedings, AIAA/ASME/ASCE/AHS/ASC 31st Structures, Structural Dynamics and Materials Conference*, Long Beach, CA, AIAA Publishing, Washington, DC, pp. 2242-2256.
- [33] Hagood, N.W., Crawley, E.F., de Luis, J., and Anderson, E.H., 1988, "Development of Integrated Components for Control of Intelligent Structures," *American Control Conference*, Atlanta, GA, pp. 1890-1896.
- [34] Hagood, N., Kindel, R., Ghandi, K., and Gaudenzi, P., 1993, "Improving Transverse Actuation of Piezoceramics using Interdigitated Surface Electrodes," *Proceedings, SPIE Conference on Smart Structures and Materials*, Orlando, FL, Vol. 2190, SPIE Publishing, Bellingham, WA, pp. 341-352.
- [35] Hwang, W.S., and Park, H.C., 1993, "Finite Element Modeling of Piezoelectric Sensors and Actuators," *AIAA Journal*, Vol. 31, No. 5, pp. 930-937.
- [36] Inman, D.J., 1990, "Control/Structure Interaction: Effects of Actuator Dynamics," *Mechanics and Control of Large Flexible Structures*, edited by J.L. Junkins, AIAA, Inc., Washington, DC, pp. 507-533.
- [37] Im, S. and Alturi, S.N., 1989, "Effects of a Piezo-Actuator on a Finitely Deformed Beam Subjected to General Loading," *AIAA Journal*, Vol. 27, No. 12, pp. 1801-1807.
- [38] Jia, J., and Rogers, C.A., 1990, "Formulation of a Laminated Shell Theory Incorporating Embedded Distributed Actuators," *Journal of Mechanical Design*, Vol. 112, pp. 596-604.

- [39] Jones, R.M., 1975, *Mechanics of Composite Materials*, Scripta book company, Washington.
- [40] Kannan, K.S., and Dasgupta, A., 1994a, "A Non-Linear Finite Element Scheme for Modeling the Magnetoelastic response of Magnetostrictive Structures," *Proceedings, SPIE Conference on Smart Structures and Materials*, Orlando, FL, Vol. 1917, SPIE Publishing, Bellingham, WA, pp. 182-193.
- [41] Kannan, K.S., and Dasgupta, A., 1994b, "Finite Element Scheme for Modeling the Magnetoelastic Response of Magnetostrictive Smart Structures," *Proceedings, Second International Conference on Intelligent Materials*, Williamsburg, VA, Technomic Publishing Co., Lancaster, PA, pp. 719-730.
- [42] Kannan, K.S., and Dasgupta, A., 1994c, "Finite Element Modeling of Multi-Functional Composites With Embedded Magnetostrictive Devices," *Proceedings, ASME Winter Annual Meeting Adaptive Structures Symposium*, Chicago, IL, AD-Vol. 45, ASME Technical Publishing, New-York, NY, pp. 21-28.
- [43] Kaweicki, G., and Smith, W.P., 1994, "Piezoelectric Actuator Capable of Inducing Torsional and Bending Control Loads with No Structural Coupling," *Proceedings, AIAA/ASME/ASCE/AHS/ASC 35th Structures, Structural Dynamics and Materials Conference, Adaptive Structures Forum*, Hilton Head, SC, AIAA Publishing, Washington, DC, pp. 49-56.
- [44] Kim, S.J., and Jones, J.D., 1991a, "Optimal Design of Piezoactuators for Active Noise and Vibration Control," *AIAA Journal*, Vol. 29, No. 12, pp. 2047-2053.
- [45] Kim, S.J., and Jones, J.D., 1991b, "Optimization of Piezo-Actuator/Substructure Coupling for Active Noise and Vibration Control," *Proceedings, Recent Advances in Active Control of Sound and Vibration*, Blacksburg, VA, Technomic Publishing Co., Lancaster, PA, pp. 78-94.
- [46] Kim, S.J., and Jones, J.D., 1991c, "Semi-Active Control of a Composite Beam Using Embedded Piezoelectric Actuators," *Proceedings, ASME Winter Annual Meeting*, Atlanta, GA, AD-Vol. 24, ASME Technical Publishing, New-York, NY, pp.131-138.
- [47] Kim, S.J., and Jones, J.D., 1991d, "A Study of Actuators for the Active Control of Distributed Elastic Systems," *Proceedings, NOISE-CON 91*, Tarrytown, NY, pp. 283-290.

- [48] Kim, S.J., and Jones, J.D., 1992, "Effects of Piezo-Actuator Delamination on the Performance of Active Noise and Vibration Control Systems," *Proceedings, ASME Winter Annual Meeting*, Anaheim, CA, DSC-Vol. 38, ASME Technical Publishing, New-York, NY, pp. 213-221.
- [49] Kim, S.J., Sonti, V.R., and Jones, J.D., 1993, "Equivalent Forces and Wavenumber Spectra of Shaped Piezoelectric Actuators," *Proceedings, Second Conference on Recent Advances in Active Control of Sound and Vibration*, Blacksburg, VA, Technomic Publishing Co., Lancaster, PA, pp. 216-227.
- [50] Kumada, A., 1985, "A Piezoelectric Ultrasonic Motor," *Japanese Journal of Applied Physics*, Vol. 24, pp. 739-741.
- [51] Kurosawa, M., and Ueha, S., 1991, "Hybrid Transducer Type Ultrasonic Motor," *IEEE Transactions on Ultrasonics, Ferroelectrics, and Frequency Control*, Vol. 38, No. 2, pp. 89-92.
- [52] Kurosawa, M., Yamada, H., and Ueha, S., 1988, "Hybrid Transducer Type Ultrasonic Linear Motor," *Japanese Journal of Applied Physics*, Vol. 28, pp. 158-160.
- [53] Larson, P.H., and Vinson, J.R., 1993a, "On the Analysis of Adaptive Shell Structures Employing Piezoelectric Materials," *Proceedings, 8th Annual Conference of the American Society for Composites*, Cleveland, OH, Technomic Publishing Co., Lancaster, PA.
- [54] Larson, P.H., and Vinson, J.R., 1993b, "The Use of Piezoelectric Materials in Curved Beams and Rings," *Proceedings, ASME Winter Annual Meeting Adaptive Structures Symposium*, New Orleans, LA, AD-Vol. 35, ASME Technical Publishing, New-York, NY, pp. 277-285.
- [55] Lee, C.K., 1989, "Laminated Piezopolymer Plates for Torsion and Bending Sensors and Actuators," *Journal of Acoustical Society of America*, Vol. 85, pp. 2432-2439.
- [56] Lee, C.K., 1990, "Theory of Laminated Piezoelectric Plates for the Design of Distributed Sensors/Actuators. Part I: Governing Equations and Reciprocal Relationships," *J. of Acoustical Society of America*, Vol. 87, No. 3, pp. 1144-1158.
- [57] Lee, S-W.R., 1994, "On the Sensing and Actuation of Clamped Elliptic Piezoelectric Laminates," *Proceedings, ASME Winter Annual Meeting*, Chicago, IL, AD-Vol. 45, ASME Technical Publishing, New-York, NY, pp. 275-279.

- [58] Lee, S-W.R., and Sun, C.T., 1994, "Bending/Twisting/Shearing Actuation and Sensing of Laminated Composites Beams with Piezopolymer Film," *Proceedings, 8th CIMTED International Conference*, Techna Publishers, Faenza, Italy.
- [59] Leissa, A. W., 1973, "Vibrations of shells", NASA.
- [60] Lester, H.C., and Lefebvre, S., 1991, "Piezoelectric Actuator Models for Active Vibration Control of Cylinders," *Proceedings, Recent Advances in Active Noise and Vibration Control*, Blacksburg, VA, Technomic Publishing Co., Lancaster, PA, Vol. 3, pp. 3-26.
- [61] Liang, C., and Rogers, C.A., 1989, "Behavior of Shape Memory Alloy Actuators Embedded in Composites," *Proceedings, 7th International Conference on Composite Materials*, Beijing, China, Pergamon Press, Elsford, NY, pp. 475-482.
- [62] Liang, C., Sun, F.P. and Rogers, C.A., 1992, "Investigation of the Energy Transfer and Consumption of Adaptive Structures," *Proceedings, IEEE Ultrasonics Conference*, Tucson, AZ, IEEE Publishing, New-York, NY
- [63] Liang, C., Sun, F.P. and Rogers, C.A., 1993a, "Dynamic Output Characteristics of Piezoceramic Actuators", *Proceedings, SPIE Conference on Smart Structures and Materials*, Albuquerque, NM, Vol. 1917, SPIE Publishing, Bellingham, WA, pp.
- [64] Liang, C., Sun, F.P., and Rogers, C.A., 1993b, "An Impedance Method for Dynamic Analysis of Active Material Systems," *Proceedings, AIAA/ASME/ASCE/AHS/ASC 34th Structures, Structural Dynamics and Materials Conference*, La Jolla, CA, AIAA Publishing, Washington, DC, pp. 3587-3599.
- [65] Liang, C., Sun, F.P., and Rogers, C.A., 1993c, "Coupled Electro-Mechanical Analysis of a Piezoelectric Ceramic Actuator Driven Systems - Determination of the Actuator Power Consumption and System Energy Transfer", *Proceedings, SPIE Conference on Smart Structures and Materials*, Albuquerque, NM, Vol. 1917, SPIE Publishing, Bellingham, WA, pp. 286-298.
- [66] Lin, M.W., Abatan, O., and Rogers, C.A., 1994, "Application of Commercial Finite Element Codes for the Analysis of Induced Strain-Actuated Structures," *Proceedings, Second International Conference on Intelligent Materials*, Williamsburg, VA, Technomic Publishing Co., Lancaster, PA, pp. 846-855.

- [67] Lin, M.W., and Rogers, C.A., 1992a, "Analysis of a Beam Structure with Induced Strain Actuators Based on an Approximated Linear Shear Stress Field," *Proceedings, Recent Advances in Active Noise and Vibration Control*, Blacksburg, VA, Technomic Publishing Co., Lancaster, PA, pp. 363-376.
- [68] Lin, M.W., and Rogers, C.A., 1992b, "Formulation of a Beam Structure with Induced Strain Actuators Based on an Approximated Linear Shear Stress Field," *Proceedings, AIAA/ASME/ASCE/AHS/ASC 33rd Structures, Structural Dynamics and Materials Conference*, Dallas, TX, AIAA Publishing, Washington, DC, pp. 896-904.
- [69] Lin, M.W., and Rogers, C.A., 1993, "Modeling of the Actuation Mechanism in a Beam Structure with Induced Strain Actuators," *Proceedings, AIAA/ASME/ASCE/AHS/ASC 34th Structures, Structural Dynamics and Materials Conference*, La Jolla, CA, AIAA Publishing, Washington, DC, pp. 3608-3617.
- [70] Lin, M.W., and Rogers, C.A., 1994a, "Bonding Layer Effects on the Actuation Mechanism of an Induced Strain Actuator/Substructure System," *Proceedings, SPIE Conference on Smart Structures and Materials*, Orlando, FL, Vol. 2190, SPIE Publishing, Bellingham, WA, pp. 658-670.
- [71] Lin, M.W., and Rogers, C.A., 1994b, "A Mechanical Approach to Interfacial Stress Alleviation in an Integrated Induced Strain Actuator/Substructure System," *Proceedings, AIAA/ASME/ASCE/AHS/ASC 35th Structures, Structural Dynamics, and Materials Conference. Adaptive Structures Forum*, Hilton Head, SC, AIAA Publishing, Washington, DC, pp. 422-428.
- [72] Lin, M.W., and Rogers, C.A., 1994c, "Induced Strain Actuation on a Beam Structure Subjected to External Loads," *Proceedings, SPIE Conference on Smart Structures and Materials*, Orlando, FL, Vol. 2190, SPIE Publishing, Bellingham, WA, pp. 671-681.
- [73] Masters, A.R., and Jones, J.D., 1991, "Optimal Design of Piezo-Actuators in a Layered Composite Structure for Active Noise and Vibration Control," *Proceedings, ASME Winter Annual Meeting*, Atlanta, GA, AD-Vol. 24, ASME Technical Publishing, New-York, NY, pp. 123-129.
- [74] Masters, A.R., and Jones, J.D., 1993, "Basic Design for Embedded Piezo-Actuators in a Layered Composite Structure," *Proceedings, SPIE Conference on Smart Structures and Materials*, Albuquerque, NM, Vol. 1917, SPIE Publishing, Bellingham, WA, pp. 329-340.

- [75] Meirovitch, L., 1986, *Elements of vibration analysis*, McGraw-Hill Inc, New-York.
- [76] Mitchell, J.A., 1992, "The effects of Embedded Piezoelectric Layers in Composite Cylinders and Applications," Master of Science Thesis, Virginia Polytechnic Institute and State University, Blacksburg, VA.
- [77] Mitchell, J.A., and Reddy, J.N., 1993, "Study of the Effect of Embedded Piezoelectric Layers in Composite Cylinders," *Proceedings, SPIE Conference on Smart Structures and Materials*, Albuquerque, NM, Vol. 1917, SPIE Publishing, Bellingham, WA, pp. 440-450.
- [78] Mollenhauer, D.H., 1992, "Induced Strain of Actuation of Surface Bonded and Embedded Piezoceramic Patches," Master of Science Thesis, Virginia Polytechnic Institute and State University, Blacksburg, VA.
- [79] Natori, M., Shibayama, Y., and Sekine, K., 1988, "Active Accuracy Adjustment of Reflectors through the Change of Element Boundary," *Proceedings, AIAA/ASME/ASCE/AHS/ASC 30th Structures, Structural Dynamics and Materials Conference*, Mobile, AL, AIAA Publishing, Washington, DC, pp. 1514-1521.
- [80] Newton, D., Garcia, E., and Horner, G.C., 1994, "Development of a Linear Piezoelectric Motor," *Proceedings, AIAA/ASME/ASCE/AHS/ASC 35th Structures, Structural Dynamics and Materials Conference, Adaptive Structures Forum*, Hilton Head, SC, AIAA Publishing, Washington, DC, pp. 101-106.
- [81] Niedermann, P., Emch, R., and Descouts, P., 1988, "Simple Piezoelectric Translation Device," *Rev. Science and Instrumentation*, Vol. 59, No. 2, pp. 368-369.
- [82] Ohnishi, O., Myohga, O., Uchikawa, T., Tamegai, M., Inoue, T., and Takahashi, S., 1989, "Piezoelectric Ultrasonic Motor using Longitudinal Torsional Composite Vibration of a Cylindrical Resonator," *Proceedings, IEEE Ultrasonics Symposium*, Montreal, Canada, IEEE Publishing, New-York, NY, pp. 739-743.
- [83] Onders, J.P., and Naganathan, N.G., 1994, "Investigation of Strain Transfer in a Smart Structure Adhesive Joint," *Proceedings, SPIE Conference on Smart Structures and Materials*, Orlando, FL, Vol. 2190, SPIE Publishing, Bellingham, WA, pp. 634-646.
- [84] Pai, P.F., Nayfeh, A.H., and Oh, K., 1992a, "A Nonlinear Theory of Laminated Piezoelectric Plates," *Proceedings, AIAA/ASME/ASCE/AHS/ASC 33rd Structures,*

Structural Dynamics and Materials Conference, Dallas, TX, AIAA Publishing, Washington, DC, pp. 577-585.

- [85] Pai, P.F., Nayfeh, A.H., and Oh, K., 1992b, "A Refined Nonlinear Model of Piezoelectric Plates," *Proceedings, Recent Advances in Adaptive and Sensory Materials and their Applications*, Blacksburg, VA, Technomic Publishing Co., Lancaster, PA, pp. 331-342.
- [86] Park, C., and Chopra, I., 1994, "Modeling Piezoceramic Actuation of Beams in Torsion," *Proceedings, AIAA/ASME/ASCE/AHS/ASC 35th Structures, Structural Dynamics and Materials Conference, Adaptive Structures Forum*, Hilton Head, SC, AIAA Publishing, Washington, DC, pp. 438-450.
- [87] Park, C., Walz, C., and Chopra, I., 1993, "Bending and Torsion Models of Beams with Induced Strain Actuators," *Proceedings, SPIE Conference on Smart Structures and Materials*, Albuquerque, NM, Vol. 1917, SPIE Publishing, Bellingham, WA, pp. 192-216.
- [88] Robbins, D.H., and Reddy, J.N., 1991, "Analysis of Piezoelectrically Actuated Beams Using a Layer-Wise Displacement Theory," *Computers & Structures*, Vol. 41, No. 2, pp. 265-279.
- [89] Robbins, D.H., and Reddy, J.N., 1993, "Modeling of Actuators in Laminated Composite Structures," *Proceedings, SPIE Conference on Smart Structures and Materials*, Albuquerque, NM, Vol. 1917, SPIE Publishing, Bellingham, WA, pp. 485-496.
- [90] Rogers, C.A., 1992, "Intelligent Material Systems: The Dawn of a New Materials Age," *Journal of Intell. Mater. Syst. and Struct.*, Vol. 4, No. 1, pp. 4-14.
- [91] Rossi, A., Liang, C. and Rogers, C.A., 1993, "Impedance Modeling of Piezoelectric Actuator-Driven Systems: an Application to Cylindrical Ring Structures", *Proceedings, AIAA/ASME/ASCE/AHS/ASC 34th Structures, Structural Dynamics and Materials Conference*, La Jolla, CA, AIAA Publishing, Washington, DC, pp. 3618-3624.
- [92] Schadegrodt, G., and Salomon, B., 1990, "The Piezo Traveling Wave Motor -- A New Element in Actuation," *Control Engineering*, pp. 10-18.

- [93] Shah, D.K., Chan, W.S., Joshi, S.P., and Subramanian, S., 1990, "Analysis of Laminates with Embedded Piezoelectric Layers," *Proceedings, ASME Winter Annual Meeting*, Dallas, TX, AD-Vol. 19, ASME Technical Publishing, New-York, NY, pp. 19-24.
- [94] Shah, D.K., Chan, W.S., and Joshi, S.P., 1993a, "Finite Element Analysis of Plates with Piezoelectric Layers," *Proceedings, AIAA/ASME/ASCE/AHS/ASC 34th Structures, Structural Dynamics and Materials Conference*, La Jolla, CA, AIAA Publishing, Washington, DC, pp. 3189-3197.
- [95] Shah, D.K., Joshi, S.P., and Chan, W.S., 1993b "Structural Response of Plates with Piezoceramic Layers," *Proceedings, SPIE Conference on Smart Structures and Materials*, Albuquerque, NM, Vol. 1917, SPIE Publishing, Bellingham, WA. pp. 428-439.
- [96] Shah, D.K., Joshi, S.P., and Chan, W.S., 1993c "Comparison of Embedded and Surface Mounted Piezoelectric Actuators," *Proceedings, ASME Winter Annual Meeting Adaptive Structures Symposium*, New Orleans, LA, AD-Vol. 35. ASME Technical Publishing, New-York, NY, pp. 237-245.
- [97] Singh, D.A., and Vizzini, A.J., 1993, "Structural Integrity of Composite Laminates with Interlaced Piezoceramic Actuators," *Proceedings, SPIE Conference on Smart Structures and Materials*, Albuquerque, NM, Vol. 1917, SPIE Publishing, Bellingham, WA, pp. 473-484.
- [98] Smith, W.P., and Kaweicki, G., 1992, "Twist and Torque Generating in Thin-Walled Composite Members using Piezoelectric Elements," *Proceedings, 7th Technical Conference of the American Society of Composites*, University Park, PA, Technomic Publishing Co., Lancaster, PA.
- [99] Soedel, W., 1976, "Shells and Plates Loaded by Dynamic Moments with Special Attention to Rotating Point Moments", *J. of Sound and Vibration*, Vol. 48 (2), pp. 179-188.
- [100] Soedel, W., 1981, *Vibrations of Plates and Shells*, Marcel and Decker Inc, New-York.
- [101] Sonti, V. R., and Jones, J. D., 1991, "Active Vibration Control of Thin Cylindrical Shells Using Piezo-Electric Actuators", *Proceedings, Recent Advances in Active Noise and Vibration Control*, Blacksburg, VA, Technomic Publishing Co., Lancaster, PA, pp. 27-38.

- [102] Sonti, V.R., and Jones, J.D., 1993, "Curved Piezo-Actuator Models for Active Vibration Control of Cylindrical Shells", *Proceedings, Meeting of the Acoustical Society of America*, Ottawa, Canada.
- [103] Subramania, S., Liang, C., and Rogers, C.A., 1993, "A Computer Implementation of the Static and Dynamic Analysis of Induced Strain Actuated Beams," *Proceedings, 2nd Conference on Recent Advances in Active Control of Sound and Vibration*, Blacksburg, VA, Technomic Publishing Co., Lancaster, PA, pp. 240-251.
- [104] Sun, W., 1993, "Modeling of Flexible Piezoelectric Laminates," *Proceedings, SPIE Conference on Smart Structures and Materials*, Albuquerque, NM, Vol. 1917, SPIE Publishing, Bellingham, WA, pp. 497-507.
- [105] Sung, C.C., Varadan, V.V., Bao, X.Q., and Varadan, V.K., 1990, "Active Control of Torsional Vibration using Piezoceramic Sensors and Actuators," *Proceedings, AIAA/ASME/ASCE/AHS/ASC 30th Structures, Structural Dynamics and Materials Conference*, Long Beach, CA, AIAA Publishing, Washington, DC, pp. 2317-2322.
- [106] Tzou, H.S., and Bao, Y., 1993, "Modeling of Thick Composite Piezoelectric Shell Transducer Laminates," *Proceedings, ASME Winter Annual Meeting Adaptive Structures Symposium*, New Orleans, LA, AD-Vol. 35, ASME Technical Publishing, New-York, NY, pp. 269-276.
- [107] Tzou, H.S., Bao, Y., and Ye, R., 1994, "A Theory on Nonlinear Piezothermoelastic Shell Laminates," *Proceedings, SPIE Conference on Smart Structures and Materials*, Orlando, FL, Vol. 2190, SPIE Publishing, Bellingham, WA, pp. 206-214.
- [108] Tzou, H.S., and Fu, H.Q., 1994a, "A Study on Segmentation of Distributed Piezoelectric Sensors and Actuators: Part I – Theoretical Analysis," *J. of Sound and Vibrations*, Vol. 172, No. 2, pp. 247-259.
- [109] Tzou, H.S., and Fu, H.Q., 1994b, "A Study on Segmentation of Distributed Piezoelectric Sensors and Actuators: Part II – Experimental Verifications," *J. of Sound and Vibrations*, Vol. 172, No. 2, pp. 261-275.
- [110] Tzou, H.S., and Gadre, M., 1989, "Theoretical Analysis of a Multi-Layered Thin Shell Coupled with Piezoelectric Shell Actuators for Distributed Vibration Control," *J. of Sound and Vibrations*, Vol. 132, No. 3, pp. 433-450.

- [111] Tzou, H.S., and Tseng, C.I., 1990, "Distributed Dynamic Identification and Controls of Flexible Shells: Theory and Finite Element Development," *Proceedings, AIAA/ASME/ASCE/AHS/ASC 31st Structures, Structural Dynamics and Materials Conference*, Long Beach, CA, AIAA Publishing, Washington, DC, pp. 2265-2273.
- [112] Tzou, H.S., and Ye, R., 1994, "Analysis of Laminated Piezoelectric Shell Systems with C⁰ Piezoelectric Triangle Finite Elements," *Proceedings, ASME Winter Annual Meeting Adaptive Structures Symposium*, Chicago, IL, AD-Vol. 45, ASME Technical Publishing, New-York, NY, pp. 113-124.
- [113] Tzou, H.S., and Zhong, J.P., 1991, "Adaptive Piezoelectric Shell Structures: Theory and Experiments," *Proceedings, AIAA/ASME/ASCE/AHS/ASC 32nd Structures, Structural Dynamics and Materials Conference*, Baltimore, MD, AIAA Publishing, Washington, DC, pp. 2290-2296.
- [114] Wada, B., Fanson, J.L., and Crawley, E.F., 1990, "Adaptive Structures," *Journal of Intell. Mater. Syst. and Struct.*, Vol. 1, No. 2, pp. 157-174.
- [115] Walker, J.G., Liang, C., and Rogers, C.A., 1993, "Finite Element Analysis of Adhesively-Bonded Piezoceramic Patches Implementing Modeling Techniques and Design Considerations to Reduce Critical Stresses," *Proceedings, AIAA/ASME/ASCE/AHS/ASC 34th Structures, Structural Dynamics and Materials Conference*, La Jolla, CA, AIAA Publishing, Washington, DC, pp. 3244-3249.
- [116] Wang, B.T., and Rogers, C.A., 1991a, "Laminate Plate Theory for Spatially Distributed Induced Strain Actuators," *Journal of Composite Materials*, Vol. 25, pp. 433-452.
- [117] Wang, B.T., and Rogers, C.A., 1991b, "Modeling of Finite Length Spatially Distributed Induced Strain Actuators for Laminate Beams and Plates," *Journal of Intell. Mater. Syst. and Struct.*, Vol. 2, No. 1, pp. 38-58.
- [118] Wetherhold, R.C., and Wang, J., 1994, "Laminate Bending and Twisting Actuation using Piezoelectric Laminae," *Proceedings, ASME Winter Annual Meeting*, Chicago, IL, AD-Vol. 45, ASME Technical Publishing, New-York, NY, pp. 93-99.
- [119] Zhou, S., Liang, C., and Rogers, C.A., 1993, "Impedance Modeling Of Two Dimensional Piezoelectric Actuators Bonded On A Cylinder", *Proceedings, ASME Winter Annual Meeting Adaptive Structures Symposium*, New Orleans, LA, AD-Vol. 35, ASME Technical Publishing, New-York, NY, pp. 247-255.

- [120] Zhou, S., Liang, C., and Rogers, C.A., 1994a, "A Dynamic Model of a Piezoelectric Actuator Driven Thin Plate", *Proceedings, SPIE Conference on Smart Structures and Materials*, Orlando, FL, Vol. 2190, SPIE Publishing, Bellingham, WA, pp. 550-562.
- [121] Zhou, S.W., Liang, C., and Rogers, C.A., 1994b, "Dynamic Design and Stress Characteristics of Integrated Piezoelectric Patch Actuators," *Proceedings, Second International Conference on Intelligent Materials*, Williamsburg, VA, Technomic Publishing Co., Lancaster, PA, pp.1360-1374.
- [122] Zhuang, Y., and Baras, J.S., 1992, "Distributed Control of a Timoshenko Beam," *Proceedings, Third International Conference on Adaptive Structures*, San Diego, CA, Technomic Publishing Co., Lancaster, PA, pp. 216-227.

Appendix A

List of Publications

Chapter 3

Chaudhry, Z., Lalande, F. and Rogers, C.A., 1994, "Modeling of Induced Strain Actuator Patches", *Proceedings, SPIE Conference on Smart Structures and Materials*, Orlando, FL, Vol. 2190, SPIE Publishing, Bellingham, WA, pp. 563-570; and accepted in the *Journal of the Acoustical Society of America*.

Chapter 4

Lalande, F., Chaudhry, Z. and Rogers, C.A., 1994a, "Modeling Considerations for In-Phase Actuation of Actuators Bonded to Shell Structures", *Proceedings, AIAA/ASME/ASCE/AHS /ASC 35th Structures, Structural Dynamics and Materials Conference, Adaptive Structures Forum*, Hilton Head, SC, AIAA Publishing, Washington, DC, pp. 429-437; and accepted in the *AIAA Journal*.

Chapter 5

Lalande, F., Chaudhry, Z. and Rogers, C.A., 1994b, "Comparison of Different Impedance-Based Models for Out-of-Phase Actuation of Actuators Bonded on Ring Structures", *Proceedings, Second International Conference on Intelligent Materials*, Williamsburg, VA, Technomic Publishing Co., Lancaster, PA, pp. 771-782.

Chapter 6

Lalande, F., Chaudhry, Z. and Rogers, C.A., 1994c, "Impedance Modeling of In-Phase Actuation of Actuators Bonded on Ring Structures", *Proceedings, ASME Winter Annual Meeting, Adaptive Structures Forum*, Chicago, IL, AD-Vol. 45, ASME Technical Publishing, New-York, NY, pp. 193-200.

Chapter 7

Lalande, F., Chaudhry, Z. and Rogers, C.A., 1995a, "Comparison Of In-Phase And Out-Of-Phase Induced Strain Actuation Of Shells: An Experimental Verification," *Proceedings, AIAA/ASME/ASCE/AHS/ASC 36th Structures, Structural Dynamics and Materials Conference, Adaptive Structures Forum*, New Orleans, LA, AIAA Publishing, Washington, DC, in press.

Combination of Chapters 5, 6, and 7

Lalande, F., Chaudhry, Z. and Rogers, C.A., "Impedance-Based Modeling of Induced Strain Actuators Bonded on Ring Structures," submitted to the *Journal of Sound and Vibrations*.

Chapter 8

Lalande, F., Chaudhry, Z. and Rogers, C.A., 1995b, "Impedance Modeling of Actuators Bonded on Shell Structures," *Proceedings, SPIE Conference on Smart Structures and Materials*, San Diego, CA, SPIE Publishing, Bellingham, WA, in press; and submitted to the *Journal of Intelligent Material Systems and Structures*.

Vita

Frederic Lalande was born in Montreal, Canada on August 7, 1968. He graduated from Mont-de-la-Salle High School in June 1985 and from Montmorency College in May 1987 with a degree in Applied Sciences. He then began his bachelor degree in Mechanical Engineering at Ecole Polytechnique de Montreal, which he completed in May 1991. After completing his Master degree in Mechanical Engineering at Stanford University in June 1992, he registered to Doctorate program in Mechanical Engineering at Virginia Polytechnic Institute and State University .

A handwritten signature in black ink, reading "Frederic Lalande". The signature is written in a cursive style with a large, stylized 'F' and 'L'.